

User Documentation for Cycle 1: MID-INFRARED INSTRUMENT (MIRI)

This PDF was last updated on February 12, 2018.
For the most current information, visit
<https://jwst-docs.stsci.edu>
and use on-line documentation.



STScI | SPACE TELESCOPE
SCIENCE INSTITUTE

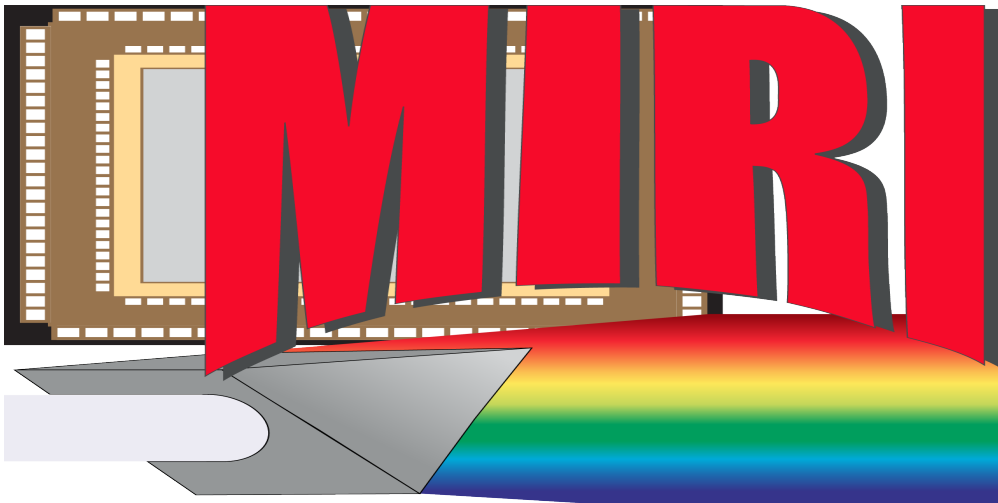
[HELP DESK](#)
[SITE MAP](#)
[JWST WEBSITE](#)

[REPORT WEBSITE PROBLEMS](#)



1. Mid-Infrared Instrument, MIRI	2
1.1 MIRI Overview	5
1.2 MIRI Observing Modes	11
1.2.1 MIRI Imaging	12
1.2.2 MIRI Coronagraphic Imaging	18
1.2.3 MIRI Low-Resolution Spectroscopy	22
1.2.4 MIRI Medium-Resolution Spectroscopy	29
MIRI MRS Simultaneous Imaging	36
1.3 MIRI Instrumentation	40
1.3.1 MIRI Optics and Focal Plane	41
1.3.2 MIRI MRS Field	48
1.3.3 MIRI Filters and Dispersers	52
1.3.4 MIRI Coronagraph Masks	58
1.3.5 MIRI Spectroscopic Elements	62
1.3.6 MIRI Detector Overview	69
MIRI Detector Readout Overview	73
MIRI Detector Readout Slow	75
MIRI Detector Readout Fast	77
MIRI Detector Performance	79
MIRI Detector Subarrays	83
1.4 MIRI Operations	88
1.4.1 MIRI Target Acquisition Overview	89
MIRI Imaging Target Acquisition	90
MIRI Coronagraphic Imaging Target Acquisition	91
MIRI LRS Slit Target Acquisition	97
MIRI MRS Target Acquisition	101
MIRI Bright Source Imaging Target Acquisition	103
MIRI LRS Slitless Target Acquisition	104
1.4.2 MIRI Dithering Overview	108
MIRI Imaging Dithering	109
MIRI Coronagraph Imaging Dithering	121
MIRI LRS Dithering	122
MIRI MRS Dithering	124
MIRI MRS Dedicated Sky Observations	131
1.4.3 MIRI Mosaics Overview	133
MIRI Imaging Mosaics	134
MIRI LRS Mosaics	137
MIRI MRS Mosaics	138
1.4.4 MIRI Time Series Observations	142
MIRI Imaging TSOs	143
MIRI LRS TSOs	145
1.5 MIRI Predicted Performance	147
1.5.1 MIRI Bright Source Limits	148
1.5.2 MIRI Sensitivity	151

Mid-Infrared Instrument, MIRI



The JWST Mid-Infrared Instrument (MIRI) provides imaging and spectroscopic observing modes from 4.9 to 28.8 μm ([Wright et al. 2015](#), [Rieke et al. 2015](#)). These wavelengths can be utilized for studies including, but not limited to: direct imaging of young warm exoplanets and spectroscopy of their atmospheres; identification and characterization of the first galaxies at redshifts $z > 7$; and analysis of warm dust and molecular gas in young stars and proto-planetary disks.

To achieve these goals MIRI offers a very broad range of observing [modes](#), including:

- [imaging](#)
- [low-resolution slitted and slitless spectroscopy](#)
- [medium-resolution integral field unit \(IFU\) spectroscopy](#)
- [coronagraphy](#)

External MIRI links and documents

MIRI "Encyclopedia"

[Rieke, G. et al. 2015, PASP, 127, 584](#)

The Mid-Infrared Instrument for the James Webb Space Telescope, I: Introduction
PDF, Univ. of Arizona

[Wright, G.S. et al. 2015, PASP, 127, 595](#)

Cycle 1 Call for Proposals

The Mid-Infrared Instrument for the James Webb Space Telescope, II: Design and Build
[PDF, Univ. of Arizona](#)

[Bouchet, P. et al. 2015, PASP, 127, 612](#)

The Mid-Infrared Instrument for the James Webb Space Telescope, III: MIRIM, The MIRI Imager
[PDF, Univ. of Arizona](#)

[Kendrew, S. et al. 2015, PASP, 127, 623](#)

The Mid-Infrared Instrument for the James Webb Space Telescope, IV: The Low-Resolution Spectrometer
[PDF, Univ. of Arizona](#)

[Boccaletti, A. et al. 2015, PASP, 127, 633](#)

The Mid-Infrared Instrument for the James Webb Space Telescope, V: Predicted Performance of the MIRI Coronagraphs
[PDF, Univ. of Arizona](#)

[Wells, M. et al. 2015, PASP, 127, 646](#)

The Mid-Infrared Instrument for the James Webb Space Telescope, VI: The Medium Resolution Spectrometer
[PDF, Univ. of Arizona](#)

[Rieke, G. H. et al. 2015, PASP, 127, 665](#)

The Mid-Infrared Instrument for the James Webb Space Telescope, VII: The MIRI Detectors
[PDF, Univ. of Arizona](#)

[Ressler, M. E. et al. 2015, PASP, 127, 675](#)

The Mid-Infrared Instrument for the James Webb Space Telescope, VIII: The MIRI Focal Plane System
[PDF, Univ. of Arizona](#)

[Glasse, A. et al. 2015, PASP, 127, 686](#)

The Mid-Infrared Instrument for the James Webb Space Telescope, IX: Predicted Sensitivity
[PDF, Univ. of Arizona](#)

[Gordon, K. D. et al. 2015, PASP, 127, 696](#)

The Mid-Infrared Instrument for the James Webb Space Telescope, X: Operations and Data Reduction
[PDF, Univ. of Arizona](#)

External MIRI websites

[STScI MIRI Website](#)

[UK Astronomy Technology Centre; The Royal Observatory, Edinburgh MIRI Site](#)

[University of Arizona MIRI Site](#)

[NASA MIRI Site](#)

[European Space Agency \(ESA\) MIRI Site](#)

Lectures

[JWST Community Lecture Series - The Mid-Infrared Instrument \(MIRI\) for JWST \(G. Rieke\)](#)

Other documents

[JWST Pocket Guide](#)

[JWST technical documents](#)

Acknowledgements

MIRI development was an equal collaboration between European and US partners.

The MIRI optical system was built by a consortium of European partners from Belgium, Denmark, France, Germany, Ireland, the Netherlands, Spain, Sweden, Switzerland, and the United Kingdom. They were led by Gillian Wright, the European Principal Investigator, and Alistair Glasse, Instrument Scientist.

EADS-Astrium (now [Airbus Defence and Space](#)) provided the project office and management. The full instrument test was conducted at [Rutherford Appleton Laboratory](#).

The [Jet Propulsion Laboratory](#) (JPL) provided the core instrument flight software, the detector system, including infrared detector arrays obtained from Raytheon Vision Systems, collaborated with Northrop Grumman Aerospace Systems on the cooler development and test, and managed the US effort.

The JPL Instrument Scientist is Michael Ressler and the MIRI Science Team Lead is George Rieke.

MIRI Overview

The JWST [Mid-Infrared Instrument \(MIRI\)](#) provides imaging and spectroscopic observing modes from 4.9 to 28.8 μm .

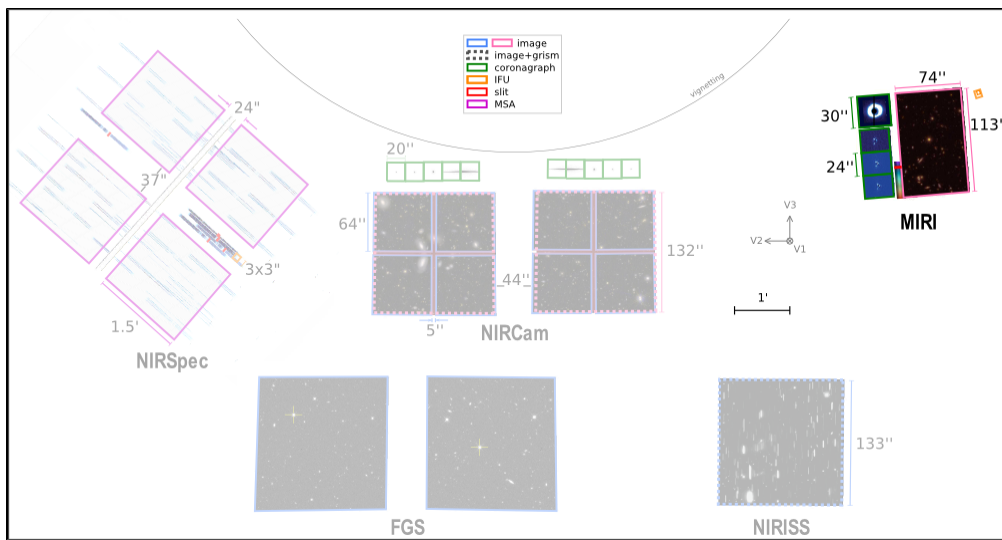
Introduction

The JWST Mid-Infrared Instrument (MIRI) provides imaging and spectroscopic observing modes from 4.9 to 28.8 μm ([Wright et al. 2015](#), [Rieke et al. 2015](#)). These wavelengths can be utilized for studies including, but not limited to: direct imaging of young warm exoplanets and spectroscopy of their atmospheres; identification and characterization of the first galaxies at redshifts $z > 7$; and analysis of warm dust and molecular gas in young stars and proto-planetary disks.

To achieve these goals MIRI offers a very broad range of observing [modes](#), including:

- [imaging](#)
- [low-resolution slitted and slitless spectroscopy](#)
- [medium-resolution integral field unit \(IFU\) spectroscopy](#)
- [coronagraphy](#)

Figure 1. JWST MIRI field of view in the telescope focal plane



Observational capabilities

MIRI offers 4 different observing modes, including (1) [imaging](#) with 9 photometric bands, (2) [coronagraphic imaging](#) with 4 different filters, (3) [low-resolution spectroscopy](#) with a slit or slitless configuration, and (4) [medium-resolution spectroscopy](#) with 4 different IFUs. Each mode has its own template in the [Astronomer's](#)

[Proposal Tool \(APT\)](#). Note that MIRI can also be used effectively for [parallel observations](#) with other instruments.

Table 1. Properties of MIRI observing modes

Observing mode	Wavelength coverage (μm)	Field of view or slit size (arcsec)	Pixel scale ("/pixel)	Resolving power $R = \lambda/\Delta\lambda$	FWHM	Comment
Imaging	5–28	74 \times 113	0.11	n/a	2 pix @ 6.25 μm	Subarrays available FWHM = 2 pix \times ($\lambda/6.25 \mu\text{m}$) for $\lambda > 6.25 \mu\text{m}$
4QPM coronagraphic Imaging	10.65, 11.4, 15.5	24 \times 24	0.11	n/a	2 pix @ 6.25 μm	
Lyot coronagraphic Imaging	23	30 \times 30	0.11	n/a	2 pix @ 6.25 μm	
Low-resolution spectroscopy	5–12	0.51 \times 4.7 (slit size)	0.11	\sim 100 @ 7.5 μm	2.6 pix @ 7.7 μm	Slit or slitless modes
Medium-resolution spectroscopy	4.9–28.8	3.9 to 7.7	0.196–0.273	\sim 1550–3250	2 pix @ 6.2 μm	FWHM = 0.314" \times ($\lambda/10 \mu\text{m}$) for $\lambda > 8 \mu\text{m}$

Optical elements

Imager

The major optical elements in the [MIRI Imager](#) include an 18-station [filter wheel](#), [coronagraphic masks](#), and a single 1k \times 1k pixel [mid-infrared detector](#).

Filter wheel: The 18-station [filter wheel](#) includes [imaging filters](#), LRS prism, and [coronagraphic filters](#).

Coronagraphic masks: In addition to a classical [Lyot coronagraph](#) at the telescope [focal plane](#)

, MIRI incorporates the **4-quadrant phase mask coronagraph technology** (4QPM; Rouan et al. 2000) to provide the smallest possible inner working angle (IWA) of $\sim 1\lambda/D$ at 10–16 μm .

Slit: In addition to the coronagraphic masks, the LRS slit is also located at the telescope focal plane.

Detectors: In contrast to other JWST instruments, which use HgCdTe infrared detector arrays, MIRI uses 3 arsenic-doped silicon (Si:Ar) IBC arrays, each with $1\text{K} \times 1\text{K}$ pixels. The MIRI detectors were developed specifically for JWST sensitivity requirements; MIRI, being most sensitive to thermal background of all the JWST instruments, is also the coldest instrument, actively cooled to its operating temperature of 7 K by a cryocooler. Since the cryocooler uses a two-stage closed-cycle design, there is no expendable cryogen.

Figure 2. Optical elements and optical path for the MIRI imager

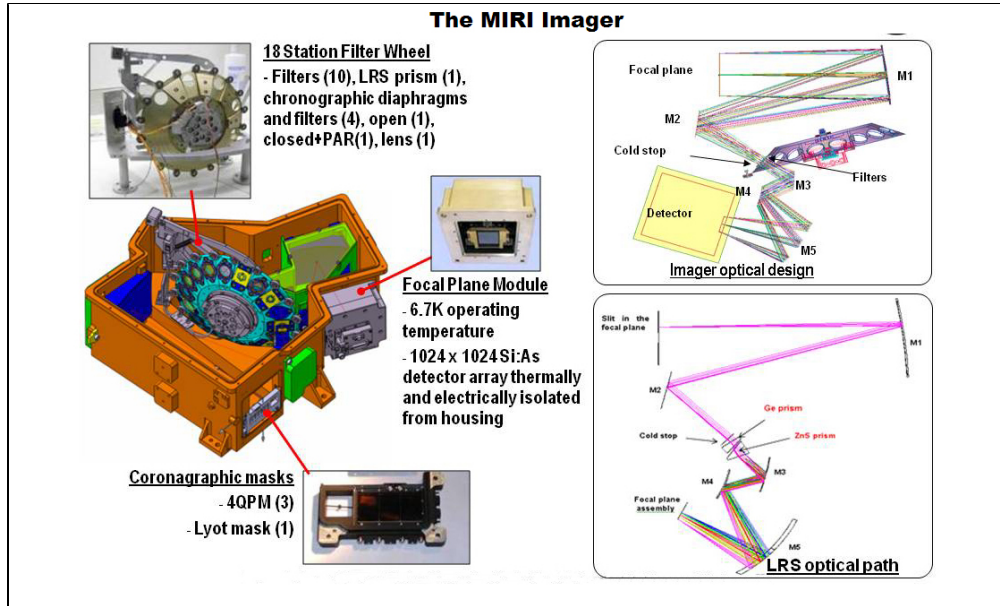


Figure 3. MIRI imaging filter curves

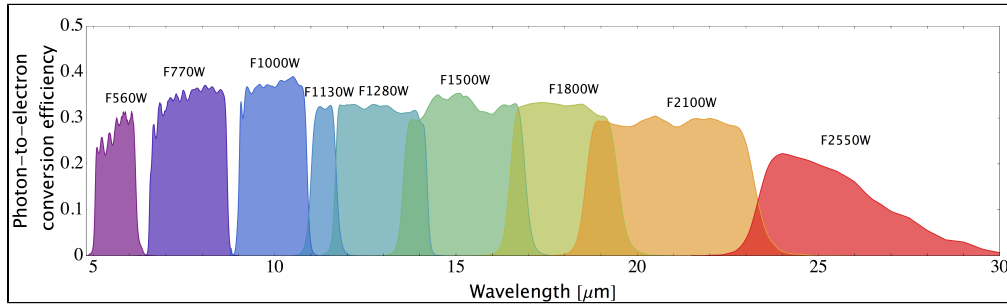
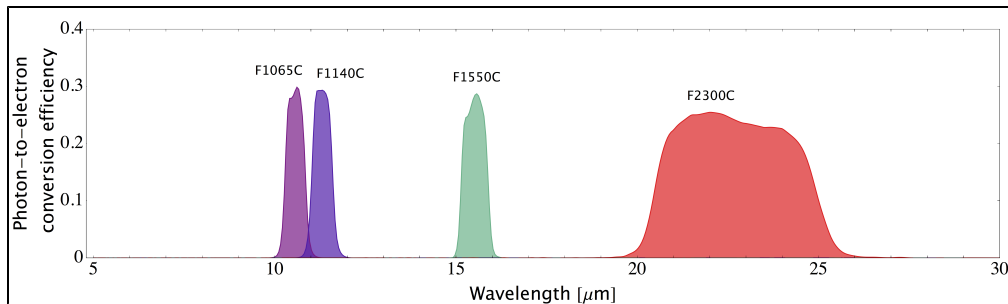


Figure 4. MIRI coronagraphic imaging filter curves



Medium-resolution spectrometer (MRS)

The major optical elements in the **MRS** include 2 gratings/dichroic wheels and 4 integral field units (**IFUs**). The MRS also has 2 mid-infrared detectors of the same type used in the imager.

Figure 5. Optical elements and optical path for the MIRI MRS

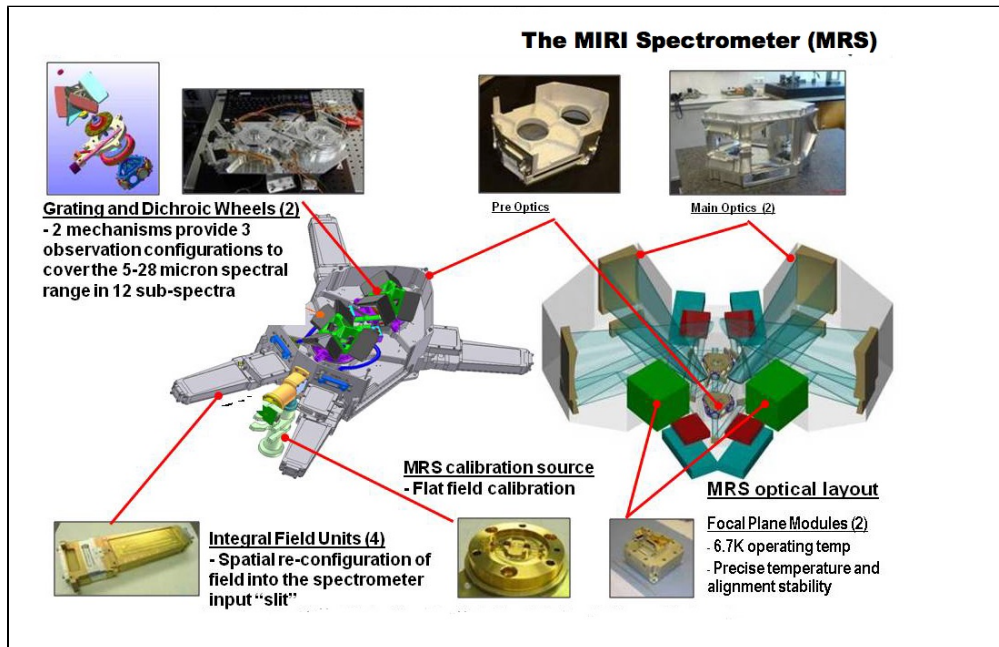
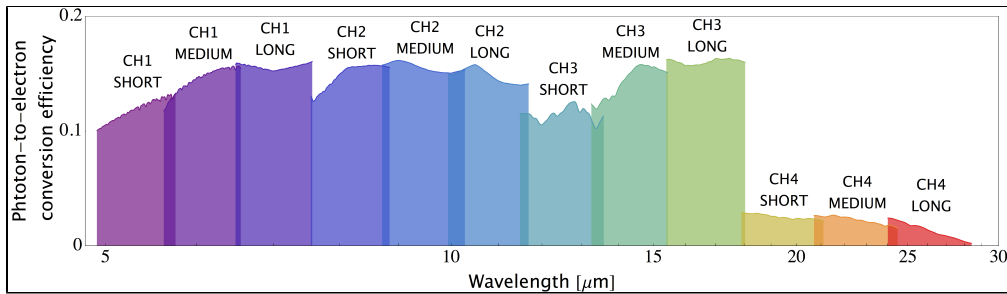


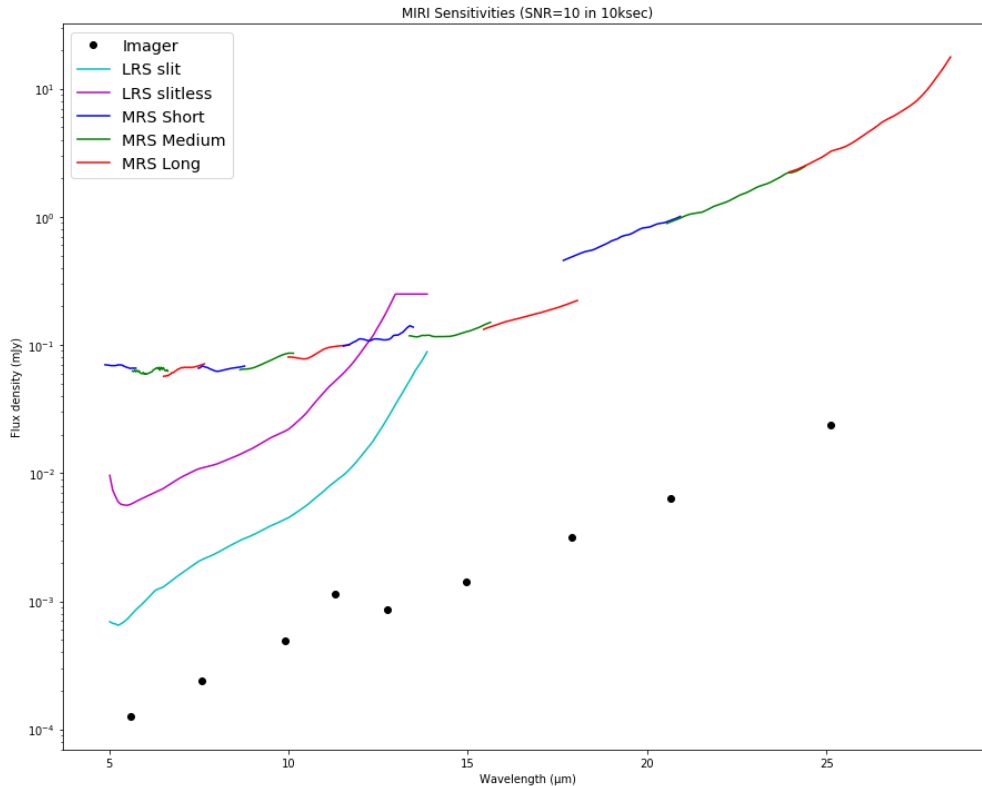
Figure 6. MIRI MRS IFU channels



Sensitivity and performance

Glasse et al. (2015) summarize the approximate sensitivities and saturation limits for various modes obtained from laboratory testing. Observers preparing MIRI proposals should use the JWST ETC to obtain detailed performance estimates (jwst.etc.stsci.edu). Up-to-date information on the use and applicability of the ETC can be found on the [ETC website](#) and in the [ETC Documentation](#).

Figure 7. MIRI sensitivity plot for various instrument modes



MIRI sensitivity plot for MRS (in colors), LRS (in black), and imager (in circles) configurations, corresponding to 10 in a 10,000 s on-source integration time.

Data calibration and analysis

Coming soon ...

References

[Glasse, A. et al., 2015, PASP, 127, 686](#)

The Mid-Infrared Instrument for the James Webb Space Telescope, IX: Predicted Sensitivity

[Updated version](#)

[Rieke, G. et al. 2015, PASP, 127, 584](#)

The Mid-Infrared Instrument for the James Webb Space Telescope, I: Introduction

[Updated version](#)

[Rouan, D. et al. 2000, PASP, 112, 1479](#)

The Four-Quadrant Phase-Mask Coronagraph. I. Principle

[Wright, G.S. et al. 2015, PASP, 127, 595](#)

The Mid-Infrared Instrument for the James Webb Space Telescope, II: Design and Build

[Updated version](#)

[JWST technical documents](#)

MIRI Observing Modes

JWST's Mid-Infrared Instrument (MIRI) has four observing modes: [imaging](#), [coronagraphic imaging](#), [low-resolution spectroscopy](#), and [medium-resolution spectroscopy](#).

The JWST [Mid-Infrared Instrument \(MIRI\)](#) provides imaging and spectroscopic observing modes from 5 to 28.5 μm that correspond to [templates](#) in the [Astronomer's Proposal Tool \(APT\)](#):

- [Imaging](#): Field of view is up to 74" \times 113" with filters ranging from 5.6 to 25.5 μm .
- [Low-resolution spectroscopy](#): Slitted and slitless modes are available from 5 to 12 μm . Slitless modes are currently only available for time-series observations (TSOs).
- [Medium-resolution spectroscopy](#): Integral field unit (IFU) spectroscopy is available from 4.9 to 28.8 μm .
- [Coronagraphic imaging](#): Four individual coronagraphs are available, one of which is based on the classic design of [Lyot](#) and three of which are based on 4-quadrant phase masks (4QPM).

Table 1. Properties of MIRI observing modes

Observing mode	Wavelength coverage (μm)	Field of view or slit size (arcsec)	Pixel scale ("/pixel)	Resolving power $R = \lambda/\Delta\lambda$	FWHM	Comment
Imaging	5-28	74 \times 113	0.11	n/a	2 pix @ 6.25 μm	Subarrays available FWHM = 2 pix \times $(\lambda/6.25 \mu\text{m})$ for $\lambda > 6.25 \mu\text{m}$
4QPM coronagraphic Imaging	10.65, 11.4, 15.5	24 \times 24	0.11	n/a	2 pix @ 6.25 μm	
Lyot coronagraphic Imaging	23	30 \times 30	0.11	n/a	2 pix @ 6.25 μm	
Low-resolution spectroscopy	5-12	0.51 \times 4.7 (slit size)	0.11	\sim 100 @ 7.5 μm	2.6 pix @ 7.7 μm	Slit or slitless modes
Medium-resolution spectroscopy	4.9-28.8	3.9 to 7.7	0.196-0.273	\sim 1550-3250	2 pix @ 6.2 μm	FWHM = $0.314'' \times (\lambda/10 \mu\text{m})$ for $\lambda > 8 \mu\text{m}$

MIRI Imaging

The imaging mode for JWST's [Mid-Infrared Instrument \(MIRI\)](#) offers 9 broadband filters from 5.6 to 25.5 μm in a 74" \times 113" FOV at 0.11"/pixel plate scale.

Introduction

Parent page: [MIRI Observing Modes](#)

See also: [MIRI Imaging Template APT Guide](#)

For imaging, the MIRI imager offers [9 broadband filters](#) covering wavelengths from 5.6 to 25.5 μm over an unobstructed 74" \times 113" field of view, and a detector plate scale of 0.11"/pixel ([Bouchet et al. 2015](#)). The MIRI imaging mode also supports the use of detector subarrays for bright targets, as well as a variety of dither patterns that could improve sampling at the shortest wavelengths, remove detector artifacts and cosmic ray hits, and facilitate self-calibration. The [Astronomer's Proposal Tool \(APT\)](#) can be used to design mosaic observations to image larger fields.

This mode is not for [coronagraphic imaging](#).

Basic performance

Main article: [MIRI Predicted Performance](#)

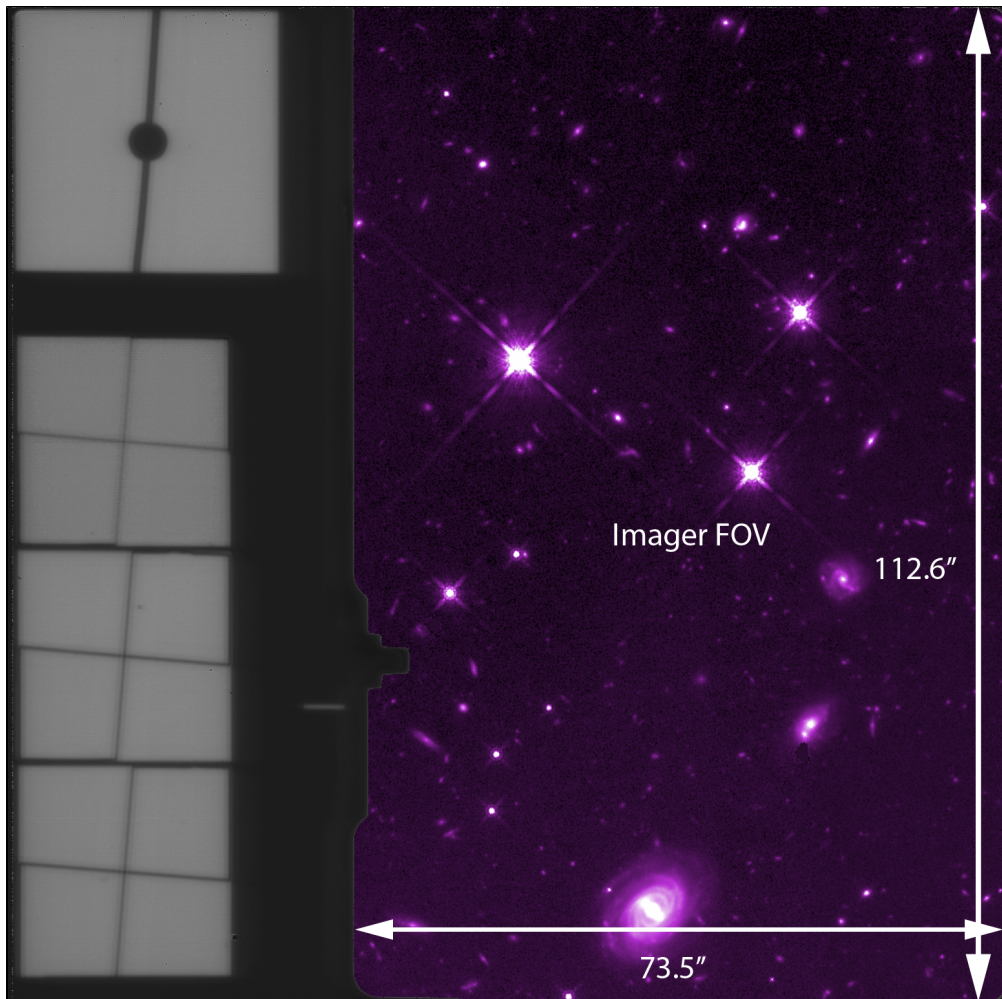
See also: [MIRI Sensitivity](#), [MIRI Bright Source Limits](#)

Imaging with MIRI is diffraction limited in all filters, with Strehl ratios in excess of 90%, although the detector plate scale of 0.11"/pixel slightly undersamples the PSF at the F560W band.

MIRI imaging sensitivity is [background](#) limited in all the imaging bands (unless one takes short integrations): astronomical background limited at wavelengths $< 11 \mu\text{m}$ and telescope background (primary mirror and sunshield) limited at wavelengths $> 11 \mu\text{m}$.

Observers will be able to specify settings for 4 primary MIRI imaging parameters: (1) [filters](#), (2) dithering pattern, (3) choice of subarray, and (4) [detector read out modes](#) and [exposure time](#) (via the number of frames and integrations).

Figure 1. The MIRI imaging FOV



Specific sections of the MIRI imager focal plane are used for imaging, coronagraphic imaging, and low-resolution spectroscopy modes. The imaging mode FOV takes up a large section to the right of the imager focal plane.

Imaging filters

Main article: [MIRI Filters and Dispersers](#)

All of the MIRI filters available for scientific imaging are broadband ($\lambda/\Delta\lambda \sim 5$), except for F1130W, which is narrower ($\lambda/\Delta\lambda \sim 16$) to isolate the 11.3 μm PAH emission feature. They are designed to cover the full wavelength range without significant gaps in wavelength coverage.

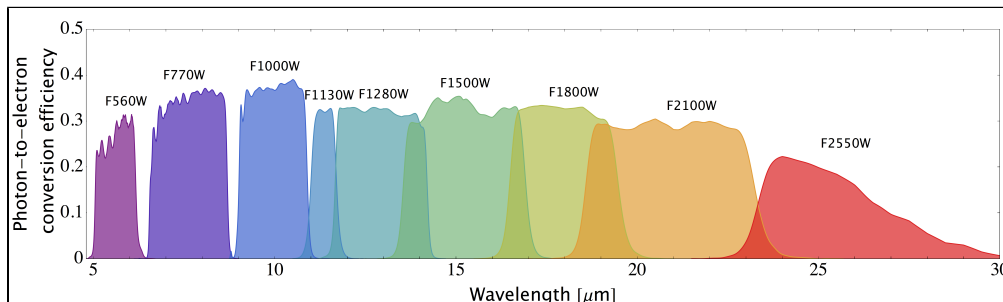
Table 1. MIRI filter properties

Filter name	λ_0 (μm)	$\Delta\lambda$ (μm)	FWHM (arcsec)	Point source detection limit ¹ (μJy)	Extended source detection limit ¹ (μJy arcsec ⁻²)	Comment
F560W	5.6	1.2	0.22	0.182	0.22	Broadband Imaging
F770W	7.7	2.2	0.25	0.276	0.26	PAH, broadband imaging
F1000W	10.0	2.0	0.32	0.592	0.53	Silicate, broadband imaging
F1130W	11.3	0.7	0.36	1.465	1.2	PAH, broadband imaging
F1280W	12.8	2.4	0.41	0.945	0.83	Broadband imaging
F1500W	15.0	3.0	0.48	1.618	0.93	Broadband imaging
F1800W	18.0	3.0	0.58	3.881	1.9	Silicate, broadband imaging
F2100W	21.0	5.0	0.67	7.550	3.3	Broadband imaging
F2550W	25.5	4.0	0.82	26.959	9.1	Broadband imaging

¹ Signal/noise = 10 for 10^4 s on-source integration time.

² Saturation based on 13% of flux falling within the brightest pixel for lambda $\lambda \leq 8$ μm and $13\% \times (8 \text{ μm}/\lambda)^2$ for lambda $\lambda > 8$ μm.

Figure 2. MIRI imaging filter bandpasses



Click on the image for a larger view.

Dithering performance

Main article: [MIRI Imaging Dithering](#)

See also: [MIRI Dithering Overview](#)

MIRI operations offers several options for imaging dithers. There are multiple reasons for an observer to use

dithers, some of which are unique to MIRI imaging.

- Dithering allows for the removal of bad pixels and for improving the resolution of undersampled images. For MIRI imaging, only the F560W band produces undersampled images of point sources.
- Dithering by a distance larger than a few times the PSF width on a timescale of a few minutes is necessary to self-calibrate detector gain variations and drifts since detector drifts grow larger with increasing signal.
- At longer wavelengths, when the telescope [background](#) dominates the noise, dithering is needed to track temporal variations in the telescope background.

Multiple dither patterns are available to support different science strategies (e.g., deep imaging, snapshots, improved PSF sampling) and different target morphologies (e.g., point, compact and extended sources). They're also available for use with predefined detector subarrays.

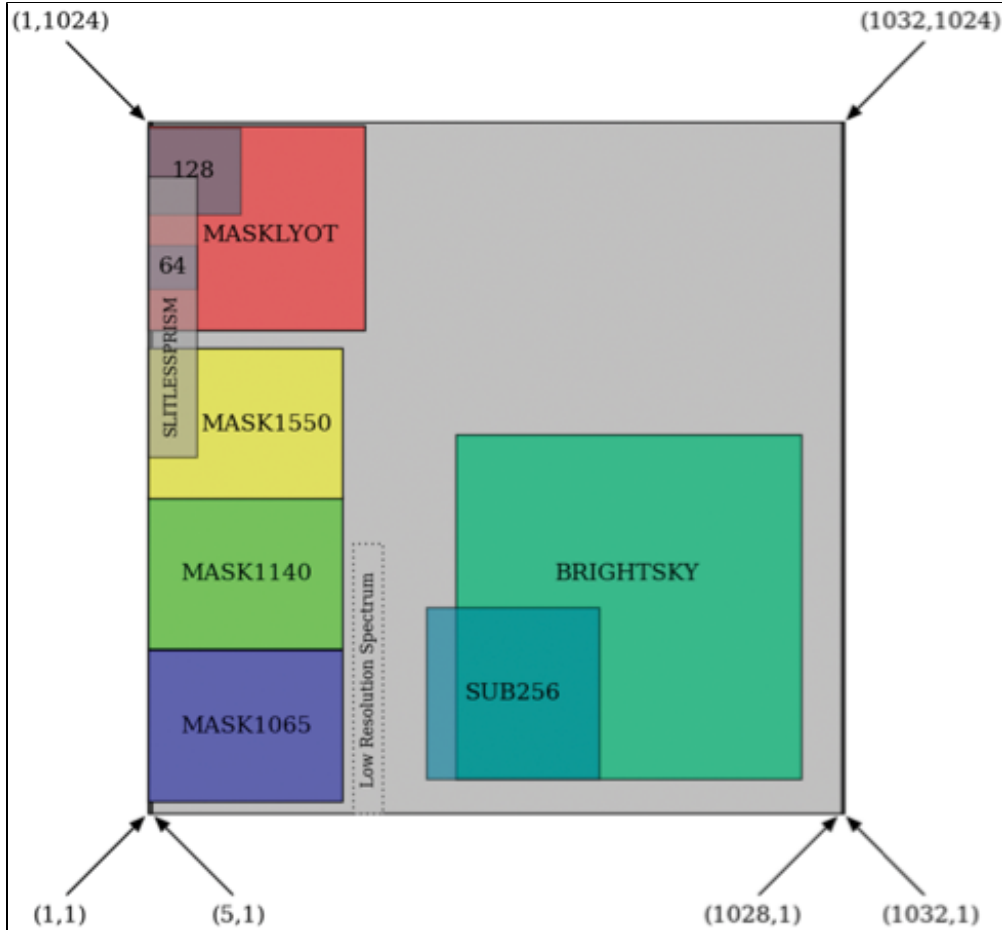
As with the other near-infrared instruments, MIRI dither specifications can be conceptually separated into large- and small-scale dithers. Large-scale dithers are intended to handle self-calibration and large scale gain variations. Since there is only one imaging MIRI detector, dithers are not required to cover gaps, as is the case for [NIRCam](#). Small-scale dithers are needed to improve image quality when the native plate scale undersamples the PSF. For MIRI, only the F560W PSF is undersampled. The F770W PSF is Nyquist sampled and all other filters lead to oversampled PSFs.

Subarrays

Main article: [MIRI Detector Subarrays](#)

MIRI imaging supports a small pre-defined set of [subarrays](#) for imaging bright sources or bright backgrounds without saturating the detector. The MIRI imaging detector creates subarrays using a different scheme than the near-infrared HAWAII 2RG detectors that are used in other JWST instruments. In particular, frame time gets faster as the subarray gets closer to one edge of the detector. For instance, coronagraphic subarrays are located on the fast side of the array, as are the smallest imaging subarrays, SUB128 and SUB64. (The bold italic font indicates these are parameters in APT observing templates.)

Figure 3. Subarray locations for the MIRI imager



Subarray locations for the MIRI imager as viewed from the telescope looking down onto the detector. Imaging templates only provide access to the FULL, BRIGHTSKY, SUB256, SUB128, and SUB64 subarrays. The remaining subarrays are available for coronagraphic imaging (Ressler et al. 2015).

Table 2. MIRI subarrays

Subarray	Size (pixels)	Usable size (arcsec)	Frame time (s)
FULL	1024×1032	74×113	2.775
BRIGHTSKY	512×512	56.3×56.3	0.865
SUB256	256×256	28.2×28.2	0.300
SUB128	128×136	14.1×14.1	0.119
SUB64	64×72	7×7	0.085

Imager exposure specifications

Main article: [MIRI Detector Readout Overview](#)

See also: [JWST Detector MULTIACCUM Integration](#)

MIRI imaging supports two different detector [readout patterns](#):

1. **FAST**¹ mode (default)
2. **SLOW** mode (only in full array)

¹ Bold italics font style indicates parameters, parameter values, and special requirements that are set in the APT GUI.

References

[Bouchet, P. et al. 2015, PASP, 127, 612](#)

The Mid-Infrared Instrument for the James Webb Space Telescope, III: MIRIM, The MIRI Imager
[Updated version](#)

[Ressler, M.E. et al. 2015, PASP, 127, 675](#)

The Mid-Infrared Instrument for the James Webb Space Telescope, VIII: The MIRI Focal Plane System
[Updated version](#)

[Rieke, G. et al. 2015, PASP, 127, 584](#)

The Mid-Infrared Instrument for the James Webb Space Telescope, I: Introduction
[Updated version](#)

[JWST technical documents](#)

MIRI Coronagraphic Imaging

Coronagraphic imaging with JWST's [Mid-Infrared Instrument \(MIRI\)](#) provides high-contrast imaging in wavelength bands from 10 to 23 μm , using one Lyot-type coronagraph and three 4-quadrant phase-mask (4QPM) coronagraphs.

Introduction

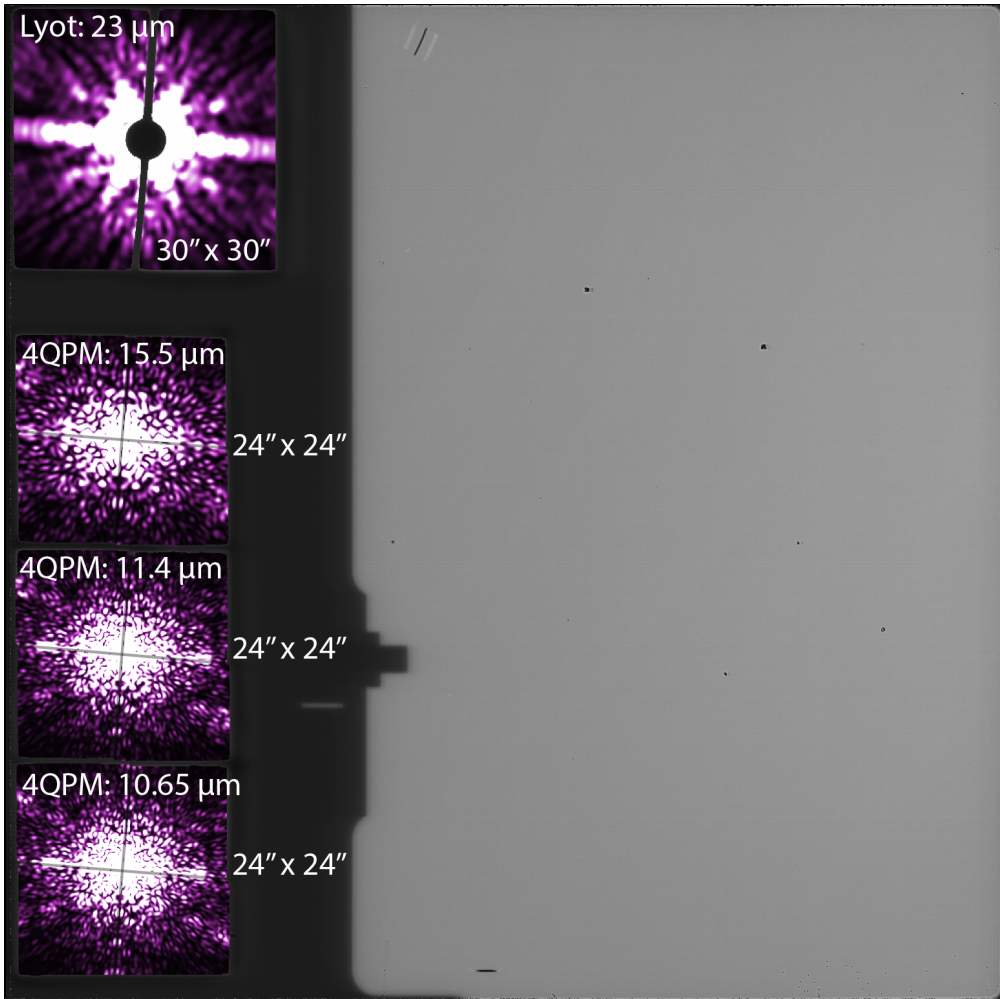
Parent page: [MIRI Observing Modes](#)

See also: [MIRI Coronagraphic Imaging Template APT Guide](#), [JWST High-Contrast Imaging](#), [JWST High-Contrast Imaging Optics](#)

The imaging channel on MIRI is equipped with 4 coronagraphs that provide high-contrast imaging (HCI), covering wavelength bands from 10 to 23 μm ([Boccaletti et al. 2015](#)).

In addition to the classical [Lyot coronagraph](#) (which provides an [inner working angle](#) (IWA) of $\sim 3\lambda/D$), MIRI also incorporates the [4-quadrant phase-mask coronagraph technology](#) (4QPM; [Rouan et al., 2000](#)) to provide the smallest possible IWA of $\sim 1 \lambda/D$ at 10 to 16 μm . These advantages might be used for studying exoplanets and other faint circumstellar sources.

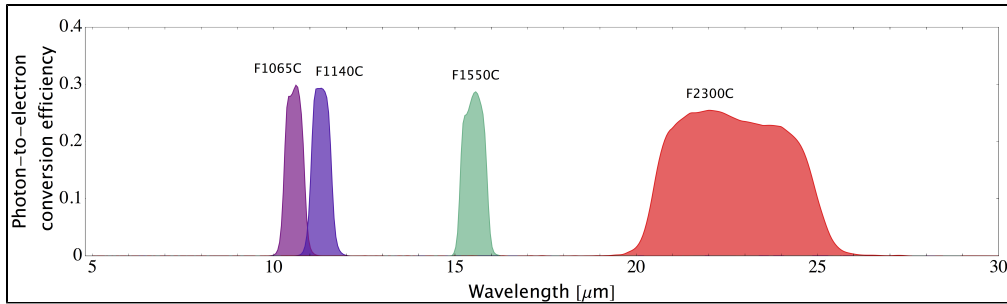
Each coronagraph is at a fixed position in MIRI's focal plane so that no mechanisms are used. The observer will have control over 2 primary variables for MIRI coronagraphy: (1) [fixed filter-coronagraph pairs](#), and (2) [exposure time](#) (via the number of frames and integrations).

Figure 1. The MIRI coronagraphic imaging FOV

In the imager [focal plane](#), the coronagraph sky views are positioned at the left side from top to bottom: the classical [Lyot coronograph](#) and the three [4-quadrant phase masks coronagraphs](#). This image includes simulated point spread functions (PSFs) for a point source behind each phase mask. The coronagraphs provide a [contrast](#) of ~ 0.01 . The image, however, does not indicate what the data will look like after the subtraction of a PSF reference star. After reference star subtraction, the coronagraphs are expected to yield a contrast of 10^{-5} – 10^{-6} .

Coronagraphic filters

4QPMs have narrow spectral bandpasses. Coronagraphic filters are associated directly with each coronagraph and are fixed for each of the 4 coronagraphs. Selecting the filter also selects the coronagraph—and vice versa

Figure 2. MIRI coronagraph filter bandpasses

Each MIRI coronagraph filter is associated with a specific coronagraph.

Table 1. Filter-coronagraph pair properties

Filter	Coronagraph	Pupil mask transmission (%) ¹	Central wavelength (μm)	Bandwidth ² (μm)	IWA ³ (arcsec)	Rejection ⁴ (on-axis)
F1065C	4QPM1	62	10.575	0.75	0.33	260
F1140C	4QPM2	62	11.40	0.8	0.36	285
F1550C	4QPM3	62	15.50	0.9	0.49	310
F2300C	Lyot spot ⁵	72	22.75	5.5	2.16	850

¹ Coronagraph filters are paired with pupil masks to reduce diffracted light from both the telescope pupil and the coronagraphic occulting spot, but at the expense of some loss of total intensity.

² Bandwidth is defined to extend down to wavelengths that correspond to 5%-10% of the transmission efficiency.

³ **Inner working angle** (IWA) is defined as the 50% transmission radius.

⁴ Rejection is the total flux attenuation of a star when centered onto the coronagraph. The term is unitless since it is a ratio of 2 intensities (out of mask / on the mask).

⁵ The spot refers to the occulting mask in the Lyot-type coronagraph.

Coronagraph exposure specification

See also: [MIRI Detector Readout Overview](#)

MIRI imaging supports only one detector [readout patterns](#):

1. **FAST**¹ mode (default)

¹ Bold italics font style indicates parameters, parameter values, and special requirements that are set in the APT GUI.

References

[Boccaletti, A. et al. 2015, PASP, 127, 633](#)

The Mid-Infrared Instrument for the James Webb Space Telescope, V: Predicted Performance of the MIRI Coronagraphs

[Updated version](#)

[Rouan, D. et al. 2000, PASP, 112, 1479](#)

The Four-Quadrant Phase-Mask Coronagraph. I. Principle

[Rouan et al. 2007, Proc. of SPIE, 6693, 16](#)

A new concept of achromatic phase shifter for nulling interferometry

[JWST technical documents](#)

MIRI Low-Resolution Spectroscopy

Low-resolution spectroscopy is an observing mode for JWST's [Mid-Infrared Instrument \(MIRI\)](#) that offers slit and slitless spectroscopy from 5 to 12 μm .

Introduction

Parent page: [MIRI Observing Modes](#)

MIRI's low-resolution spectrometer (LRS; [Kendrew et al. 2015](#)) offers both slit and slitless spectroscopy from 5 to 12 μm using a [double prism](#) mounted in the MIRI [filter wheel](#), designed to provide a spectral resolving power of $R = 40$ at 5 μm , and $R = 160$ at 10 μm for compact sources ($<2''$). The LRS forms part of the MIRI Imager, and spectra are imaged onto the imager detector array. The LRS can be operated with slit or in slitless mode; the latter is optimised for time series observations (TSOs). This page describes the differences between the two options.

Users should use the [Exposure Time Calculator](#) for all [sensitivity](#) calculations.

Observers will be asked to configure 5 aspects of their observations:

1. Subarray (which controls whether the observation will be slitless or with slit)
2. Target Acquisition
3. Dither or mapping pattern
4. Detector read mode and exposure settings
5. Mosaic settings

Slit vs. slitless spectroscopy

The LRS can be operated in slit or slitless mode. Incoming light travels the same path for both modes, and use the same [double prism](#) as disperser. The modes are very similar apart from the target placement in the field: for slit spectroscopy, the target is placed at the location of the slit, for slitless it is positioned at a specific pointing location in a dedicated detector region. Figure 1 shows the relevant detector locations in the imager focal plane layout.

The slit and slitless modes have some operational differences. Slitless LRS is a mode dedicated to time series observations (TSOs), and operation is optimised for high-precision spectrophotometry over long observations, e.g. of exoplanet transits. The LRS slit mode is suited to a broad range of spectroscopic observations and therefore supports a wider range of operational choices.

The single slit is 4.7" long (3.18 mm; 42.7 pixels) and 0.51" wide (0.33 mm; 4.6 pixels). The projected location

of the slit on the focal plane array lies between the imager field of view and the coronagraphy regions on the imager detector; its location is fixed. There is no subarray choice for LRS slit: for these observations the entire imager array is read out. The structure containing the slit blocks a large portion of the background from the detector, providing [better sensitivity](#) than the slitless mode.

Slitless LRS, in contrast, uses a dedicated [subarray region](#) on the detector (called SLITLESSPRISM), its location is shown in Figure 1. The use of a smaller subarray provides [faster read times](#) and thus a greater dynamical range. The [saturation limit](#) is several magnitudes brighter than for LRS slit. The absence of the slit however allows more background radiation to be dispersed over the science spectrum, reducing the [sensitivity](#) by around an order of magnitude. Whilst LRS slitless is ideal for high precision spectrophotometric observations of bright point source targets, the slit is expected to give better performance for faint targets.

As both modes use the same dispersing element, the dispersion profile is in principle the same for both. The nominal spectral range of 5–12 μm is dispersed over approximately \sim 370 pixels. The dispersion profile however folds over below 4.5 μm (where the prism throughput is very low), superimposing two parts of the spectrum on each other. A dedicated filter is mounted over the slit to block radiation shortward of 4.5 μm , to avoid this contamination. The effect is not mitigated for LRS in slitless mode.

The strengths and weaknesses of slit and slitless LRS modes are summarised in Table 1 below.

Figure 1. LRS slit and slitless spectra positions on MIRI imager focal plane

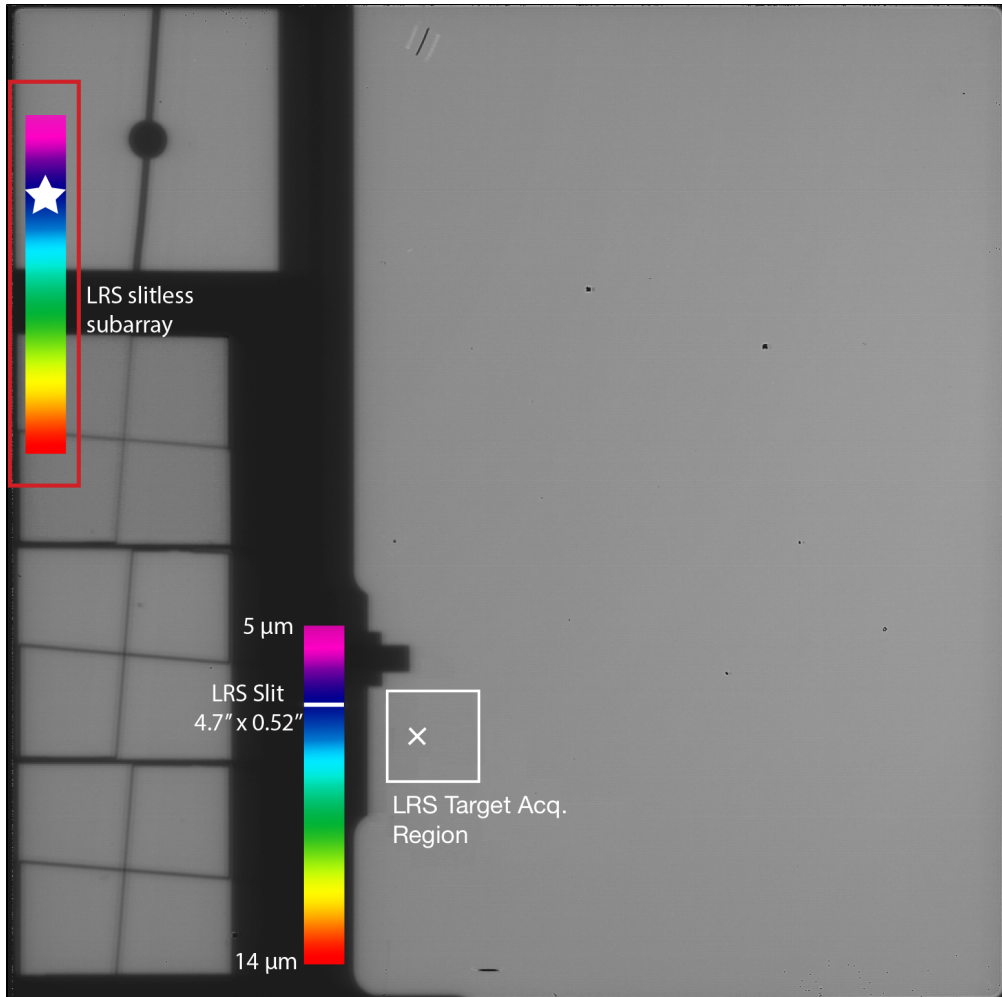


Table 1. Relative strengths and weaknesses of LRS slit and slitless modes

Mode	Strengths	Weaknesses
Slit	Sensitivity (10 times better than slitless) Allows dithering	Narrow slit (relative to the PSF) makes it more sensitive to pointing uncertainties and drifts Slit mask filter to mitigate spectral foldover at short wavelengths reduces throughput Saturation limit relatively faint
Slitless	Brighter saturation limits due to short read time Allows > 10,000 s exposures No slit losses	Sensitivity (10 times worse than slit) Spectral foldover around 4.5 μ m affects calibration

Sources in the imager field of view when performing LRS slit spectroscopy

There is no shutter or way to block light from entering the imager field of view (see Figure 1) when taking a low-resolution spectrum in slit mode. Point sources in the imaging field will therefore appear as slitless spectra on the imager FOV. The broad bandpass of the LRS prisms can easily cause the detector to saturate if bright and extended sources are present in the imager portion of the array. Such saturation can affect the detector behavior over the entire array, including calibration of the spectrum even if the spectrum itself is not saturated. Bright extended sources that are not saturated may cause a small amount of scattered light in the detector pixels below the LRS slit (<< 1%); this may be of concern for observations of very faint targets. Observers should take care to avoid bright targets in the imager portion of the field, to avoid saturation in the full array. This can be checked using the [Aladin visualization](#) option in APT. If a point source were to lie in the Lyot coronagraph field, however, the instrument has been designed so that this point source spectrum will not overlap with any source in the slit.

The spectra of sources coincidentally located in the imager field cannot be processed, nor calibrated.

¹ Bold italics font style indicates parameters, parameter values, and special requirements that are set in the APT GUI.

Target Acquisition

Main articles: [MIRI LRS Slit Target Acquisition](#), [MIRI LRS Slitless Target Acquisition](#)

Target Acquisition (TA) is available for both LRS slit and slitless observations, and in most cases recommended. The blind pointing accuracy of the telescope is not sufficient to place a point source target in the slit with the required accuracy for calibration. For slit spectroscopy, accurate knowledge of the source position in the slit is critical for calibration, in particular for correction of wavelength- and position-dependent slit losses, and for wavelength calibration. For slit spectroscopy of extended sources, the user should decide on the importance of TA given the telescope's pointing accuracy and the nature of the observations (e.g. a single pointing vs mosaic). TA can also be disabled for off-source background observations, which contain no science target.

For low-resolution slitless spectroscopy, which is optimised for time series observations, TA is required for placing the target at the nominal pointing position in the SLITLESSPRISM subarray with sub-pixel accuracy. This is particularly important if multiple observations from different epochs are to be combined to improve the signal to noise ratio.

Target acquisition uses dedicated "regions of interest" (ROIs) on the detector, measuring 64 x 64 pixels in size. The locations of these ROIs and the TA observations sequence is different for slit and slitless LRS. Further choices should be made when preparing the TA portion of an observing program, for the TA target, filter and exposure duration. We refer to the dedicated articles for further details on TA for both LRS modes.

The [Exposure Time Calculator](#) contains dedicated functionality for TA calculations. Users should use this capability for determining the appropriate TA settings.

Dithering

LRS Slit

Dithering is available and recommended for observations with the LRS in slit mode. Dithering can mitigate the effects of bad pixels, provide sub-pixel sampling, and provide observations of the background for background subtraction purposes. The majority of science observations will benefit from dithering.

Three dither options are offered in the [MIRI LRS Template](#) in APT:

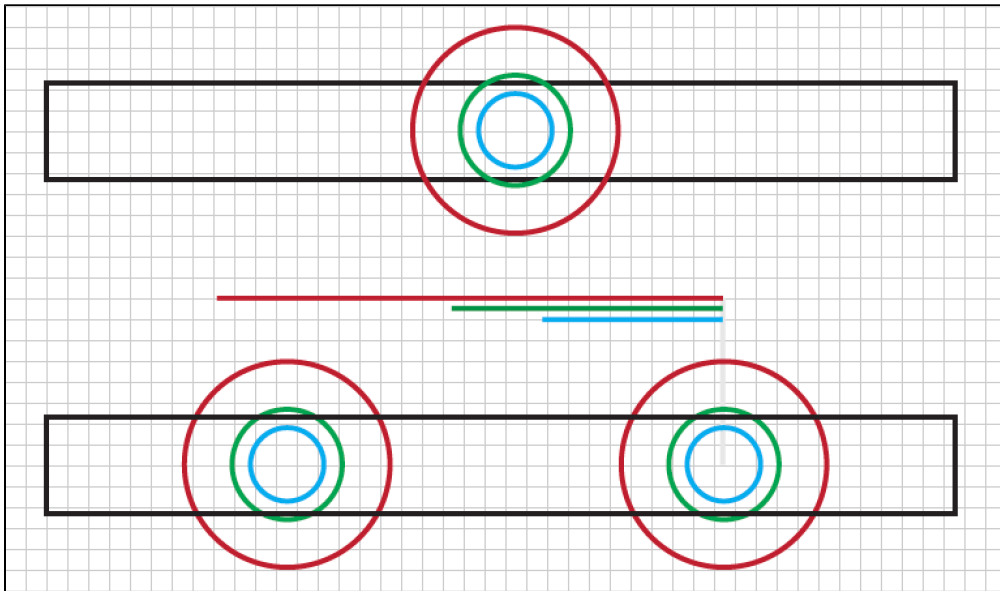
1. ALONG SLIT NOD
2. MAPPING
3. NONE (only for LRS slitless)

The 3rd option, dither = None, is only enabled for LRS slitless observations; it is not available for LRS slit mode.

The MAPPING option can be chosen to map a wider field. Selecting this option then asks the user to define the number of steps in the spatial and spectral directions, and the step size in each direction (in arcseconds).

Although the maximum dither size is set by avoiding the need to acquire new guide stars, a useful guideline is that [dithers larger than 20"](#) will be much slower than ones smaller than this limit.

Figure 2. MIRI LRS dither patterns



Top: For the MAPPING dither pattern type, the source is centered in the slit and the observer can specify a number of offsets in the spatial and/or spectral direction, and step size in each axis.

Bottom: For the ALONG SLIT NOD dither pattern type, the source is observed at two positions in the slit, at 1/3rd and 2/3rds of the slit length. The blue, green and red circles indicate the first dark Airy ring for 5, 7.7 and 14 μm , respectively. The blue green and red lines indicate the radius of the 4th dark Airy ring for 5, 7.7 and 14 μm , respectively.

LRS Slitless

In LRS slitless mode, dithering is disabled. This mode is optimised for high-precision spectrophotometry in time series observations; for such observations dithering is not scientifically useful and therefore not supported.

LRS exposure specifications

MIRI LRS slit spectroscopy supports two different detector [readout patterns](#):

1. [FAST](#) mode (default)
In slitless mode, only FAST mode is allowed.
2. [SLOW](#) mode

The maximum exposure duration for a single exposure with the LRS slit is 10,000 seconds. This limit applies to all JWST instruments and modes that are not time series observations. LRS slitless observations are always marked as time series observations; the 10,000 second limit is therefore waived to allow for lengthy observations of time-variable phenomena.

The user should refer to the [MIRI Generic Recommended Strategies](#) and [MIRI LRS Recommended Strategies pages](#) for dedicated advice for LRS exposure settings.

LRS Mosaics

The LRS can be used to produce mosaics of extended sources with slit spectroscopy, by either specifying a mapping pattern from the MAPPING option in the list of dither patterns or in the "Mosaic" tab. When using the latter, the user can specify the number of required rows and columns, and the percentage overlap between each pointing.

The user is always advised to check the layout of their mosaic using the [Aladin visualization capability](#) in APT.

References

[Kendrew, S. et al. 2015, PASP, 127, 623](#)

The Mid-Infrared Instrument for the James Webb Space Telescope, IV: The Low-Resolution Spectrometer
[Updated version](#)

[JWST technical documents](#)

MIRI Medium-Resolution Spectroscopy

Medium-resolution spectroscopy is an observing mode for JWST's [Mid-Infrared Instrument \(MIRI\)](#) for obtaining spatially resolved spectroscopic data between 4.9 and 28.8 μm over a FOV up to 7.2" \times 7.9".

Introduction

Parent page: [MIRI Observing Modes](#)

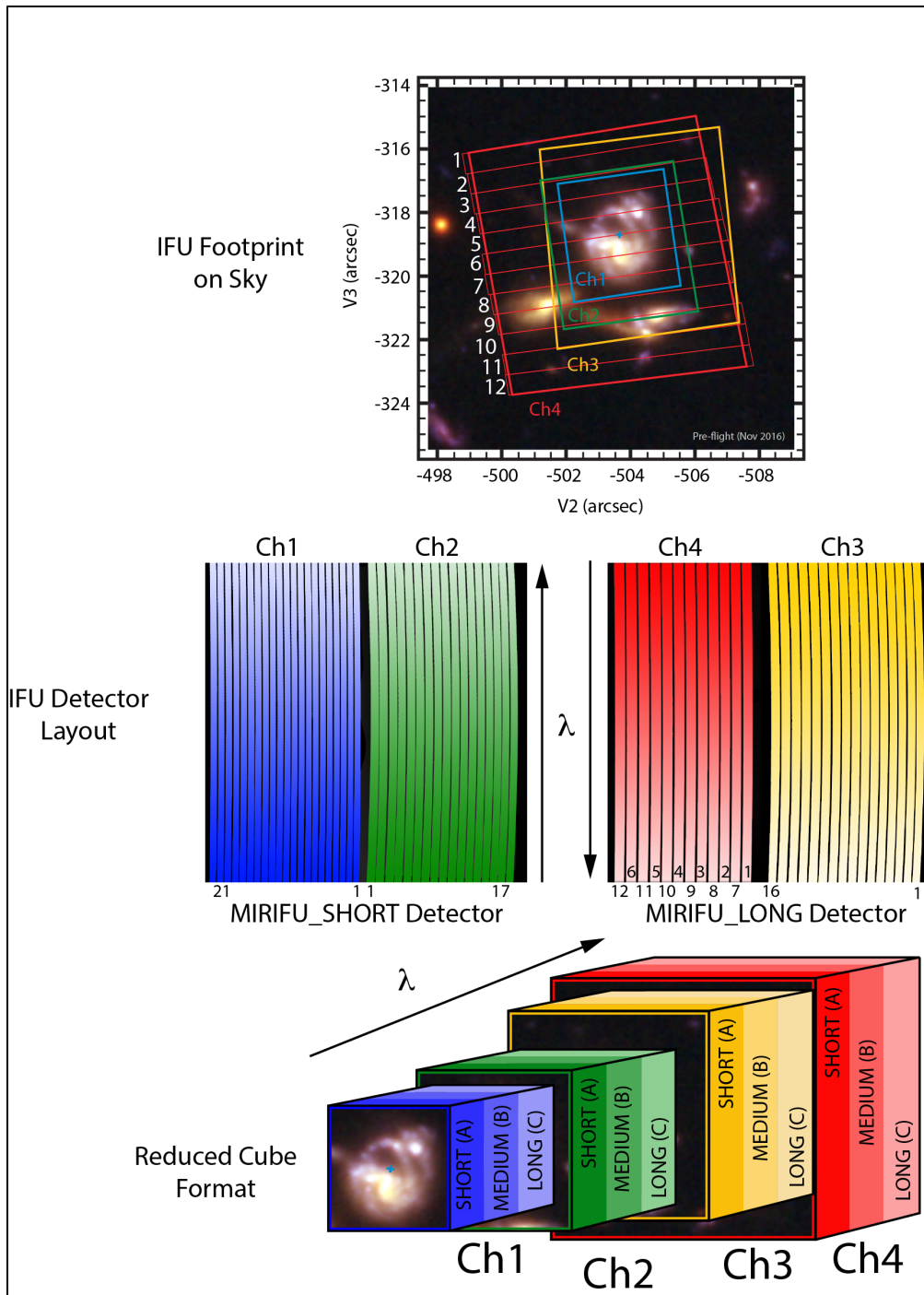
See also: [MIRI Medium Resolution Spectroscopy Template APT Guide](#)

The JWST MIRI medium-resolution spectrometer (MRS) ([Wells et al. 2015](#)) will observe simultaneous spatial and spectral information between 4.9 and 28.8 μm over a contiguous field of view up to 7.2" \times 7.9" in size. This is the only JWST configuration offering medium-resolution spectroscopy (with R from 1,500 to 3,500) longward of 5.2 μm .

MRS observations are carried out using a set of 4 [integral field units \(IFUs\)](#), each of which covers a different portion of the MIRI wavelength range. MRS IFUs split the field of view into spatial slices, each of which produces a separate dispersed "long-slit" spectrum. Post-processing produces a composite 3-dimensional (2 spatial and one spectral dimension) data cube combining the information from each of these spatial slices. This process is illustrated schematically in [Figure 1](#).

MRS operations have been designed to allow for efficient observations of point sources, compact sources, and fully extended sources. The observer will have control over 3 primary variables: (1) [wavelength coverage](#), (2) [dithering pattern](#), and (3) [detector read out mode](#) and [exposure time](#) (via the number of frames and integrations).

Figure 1. MRS overview diagram



Schematic overview of the MIRI MRS.

Top row: effective rectangular footprint of each of the 4 MRS channels on the sky in the spacecraft V2, V3 coordinate frame.

Channels 1, 2, 3, and 4 are shown in blue, green, yellow, and red respectively. Individual slice locations are shown for illustrative purposes for the 12 slices in channel 4.

Middle row: Format of the MRS spectra dispersed onto the two detectors for a single exposure. Each color-coded stripe represent the dispersed "long-slit" spectrum from a single slice. Slices that are adjacent on the sky are interleaved on the detector (as indicated for channel 4).

Bottom row: pipeline-rectified data cube combining information from all 4 channels and all 3 grating settings (SHORT ¹, MEDIUM, and LONG) into a regularly-sampled 3D format. Note the larger footprint of channel 4 compared to channel 1.

¹ Bold italics font style indicates parameters, parameter values, and special requirements that are set in the APT GUI.

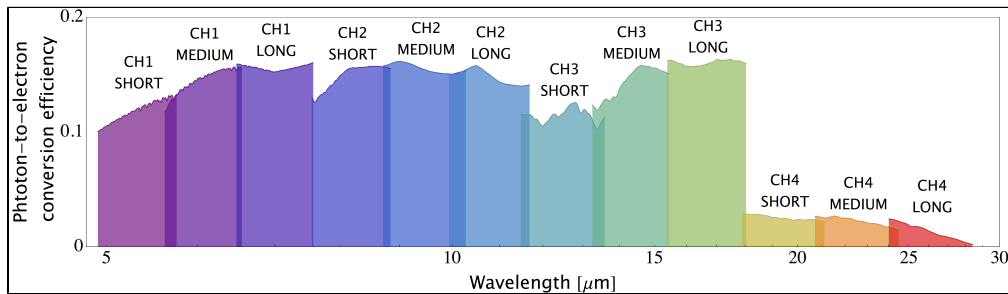
MRS wavelength coverage

The MRS has 4 separate IFUs (channels 1 through 4), each covering a separate wavelength range between 4.9 and 28.8 μm . All 4 channels are observed simultaneously, but each exposure can only cover one-third of the available wavelength range in a single configuration. For complete spectral coverage, 3 different spectral settings must be observed; SHORT (A), MEDIUM (B), and LONG (C). Therefore, there are 12 different wavelength bands, increasing in wavelength from 1A to 4C. These settings are summarized in [Table 1](#) and [Figure 2](#).

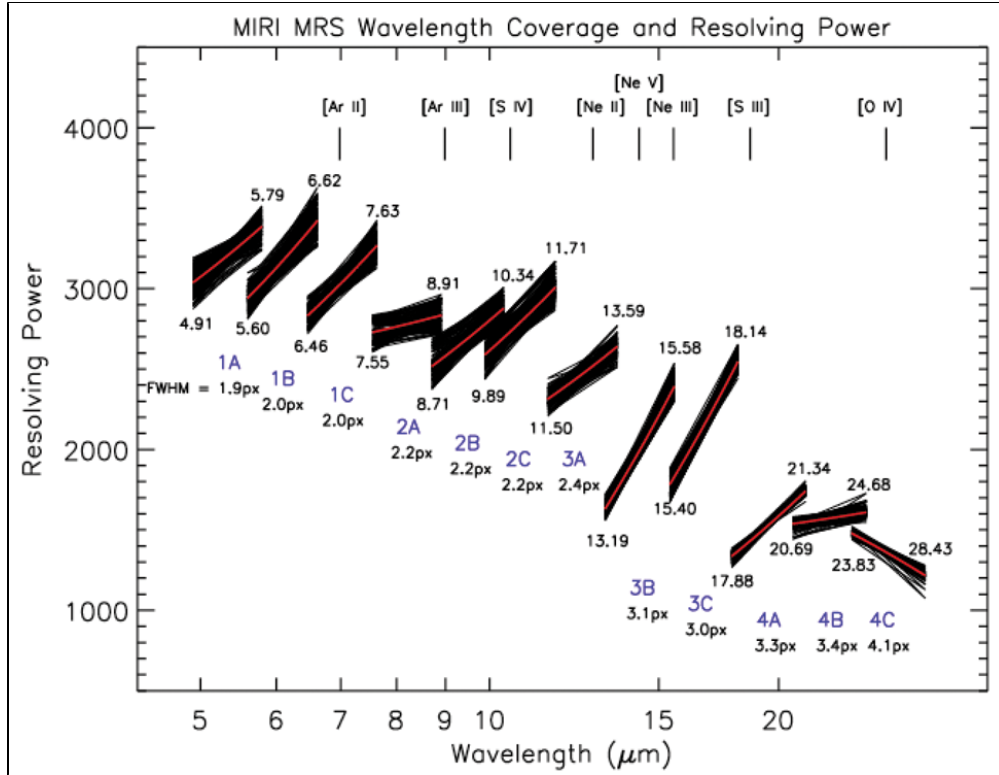
The spectral resolving power changes between each MRS band, and also varies spatially across the field of view as indicated by [Figure 3](#).

Table 1. Characteristics of the 4 IFU channels

FOV name λ -range (μm)	FOV (arcsec)	Number of slices	Slice width (arcsec)	Pixel size (arcsec)	Sub-band name	λ -range (μm)	Resolving power ($\lambda/\Delta\lambda$)
Channel 1 4.89–7.66	3.3×3.7	21	0.176	0.196	SHORT (A)	4.89–5.75	3320–3710
					MEDIUM (B)	5.65–6.64	3190–3750
					LONG (C)	6.52–7.66	3100–3610
Channel 2 7.49–11.71	4.2×4.8	17	0.277	0.196	SHORT (A)	7.49–8.78	2990–3110
					MEDIUM (B)	8.65–10.14	2750–3170
					LONG (C)	9.99–11.71	2860–3300
Channel 3 11.53–18.05	5.6×6.2	16	0.387	0.245	SHORT (A)	11.53–13.48	2530–2880
					MEDIUM (B)	13.37–15.63	1790–2640
					LONG (C)	15.44–18.05	1980–2790
Channel 4 17.66–28.45	7.2×7.9	12	0.645	0.273	SHORT (A)	17.66–20.92	1460–1930
					MEDIUM (B)	20.54–24.40	1680–1770
					LONG (C)	23.95–28.45	1630–1330

Figure 2. MRS filter bandpasses

Wavelength coverage of the MIRI MRS channels.

Figure 3. Resolving power as a function of wavelength for MIRI MRS

Resolving power of the MRS across the FOV for each sub-band. The red lines are spatially averaged values. The wavelength ranges of each sub-band are indicated, as well as some relevant mid-infrared lines. However, the resolving powers shown here may be underestimated by as much as 10%; therefore, the resolving powers in Table 1 may be a factor of 1.1 higher. Figure credit: Wells et al. 2015.

MRS spatial resolution and dithering

The 4 channels of the MRS each cover an overlapping but distinct region of the JWST focal plane (see [details on the MRS field of view, coordinate systems, and pointing origin](#)). The spatial point spread function (PSF) seen by the imager slicers is undersampled by design, as is the spectral line spread function (LSF) sampled by the detector pixels. Full sampling in both spatial and spectral dimensions therefore requires that objects be observed in at least 2 (and ideally 4) dither positions that include an offset in both the along-slice and across-slice directions. Assuming that such dithered observations are obtained, the MRS is nearly diffraction limited longward of 8 μm (see [MIRI MRS Dithering, Figure 1](#)).

A variety of different dither patterns are offered that optimize observations for a variety of different considerations:

1. Point source or extended source observations (prioritizing PSF separation between successive exposures, or large common field across all exposures)
2. Spatial sampling at specific wavelengths or at all wavelengths.
3. Number of dither locations (2 or 4)
4. Standard or inverted dither orientation

Details on the available patterns can be found at the [MIRI MRS Dithering](#) article. Information about mosaicing options can be found on the [MIRI MRS Mosaics](#) article.

MRS exposure time

MIRI MRS exposure times are not specified directly. Rather, the detectors are read using up-the-ramp sampling tied to specific timing readout patterns. Two detector [readout patterns](#) are supported for MRS spectroscopy:

1. [SLOW](#) mode (default)
2. [FAST](#) mode

The JWST exposure time calculator (ETC) should be used to determine which mode is best for a given set of observations, and how many frames and integrations are required in order to reach the target depth.

Additional considerations

A few additional considerations should be kept in mind:

1. Depending on the dither pattern selected, it may be necessary to include a [dedicated sky observation](#) in order to measure the astronomical foreground and background signal
2. A suitable target should be chosen that is adequate for [target acquisition](#)
3. The MIRI imager can be used at the same time as the MRS for [simultaneous imaging](#)
4. A variety of questions on usage are answered in the [MIRI MRS Recommended Strategies](#) article

All MRS articles

[JWST Integral Field Spectroscopy](#) provides an introduction to integral field spectroscopy with JWST

[MIRI Medium Resolution Spectroscopy](#) provides a main overview of the MIRI MRS (this page)

[MIRI MRS APT Guide](#): step-by-step instructions on how to fill out APT

[MIRI MRS Recommended Strategies](#): frequently asked questions on best practices for specifying observations

[MIRI MRS Dedicated Sky Observations](#): information on MRS dedicated background exposures

[MIRI MRS Dithering](#): detailed information on MRS dithering strategies

[MIRI MRS Field](#): overview of the MRS field of view, coordinate systems, and pointing origins

[MIRI MRS Hardware](#): overview of the MRS imager slicer hardware

[MIRI MRS Mosaics](#): information on MRS mosaicing strategies

[MIRI MRS Simultaneous Imaging](#): information on using the MIRI Imager during MRS observations

[MIRI MRS Target Acquisition](#): target acquisition procedures for the MRS

References

[Wells, M. et al. 2015, PASP, 127, 646](#)

"The Mid-Infrared Instrument for the James Webb Space Telescope, VI: The Medium Resolution Spectrometer"

[Updated version](#)

[JWST technical documents](#)

MIRI MRS Simultaneous Imaging

Simultaneous use of the JWST MIRI imager and the Medium Resolution Spectrometer (MRS) is offered for all observations where the MRS is the primary observing mode. Astrometry of stars in the imager field will result in more accurate data cube construction.

Introduction

Main article: [MIRI Medium-Resolution Spectroscopy](#)

See also: [MIRI Imaging](#)

The [MIRI imager](#) can be used for mid-infrared imaging simultaneously with the [MIRI medium resolution spectrometer](#). This is referred to as "simultaneous imaging" and is not a parallel imaging mode. This is the default operational mode for MRS observations, and it is highly recommended that simultaneous imaging be specified for all MRS observations as there are no data volume issues when using the imager and the MRS simultaneously. The only instance where simultaneous imaging should be turned off is if saturation of the imager would occur due to a long MRS observation or a bright target is in the imager field of view.

Purpose

Since the MIRI MRS has an extremely small field of view, its absolute astrometric solution cannot always be tied to an external reference frame using MRS data alone. If data are taken without a prior target acquisition observation (for instance, when mapping an extended diffuse source) the absolute astrometry of a given visit may be in error by 0.5" or more. This poses a challenge to combining exposures across multiple different visits, and also for comparing source locations against extant multi-wavelength data. The simultaneous imaging mode helps to alleviate this problem by obtaining data across the much larger MIRI imaging field of view that can be used offline (in combination with the well-known relation between the imaging and MRS fields) to improve the astrometric solution of individual MRS exposures by cross-matching multiple sources in the imaging field against known catalog positions.

Science applications

Simultaneous imaging can also be used to obtain additional science observations of an extended object. For example, MRS observations of a small portion of a nebula can be complemented by simultaneous imaging of adjacent regions of the nebula (depending on the roll of the observatory, which is significantly constrained for JWST). Figure 1 shows the spacing and orientation of the imager and MRS FOVs. Specific examples of simultaneous imaging science applications can be found in the descriptions of the GTO programs ([JWST GTO Observation Specifications](#)).

Figure 1. Spacing and orientation of the imager and MRS FOVs

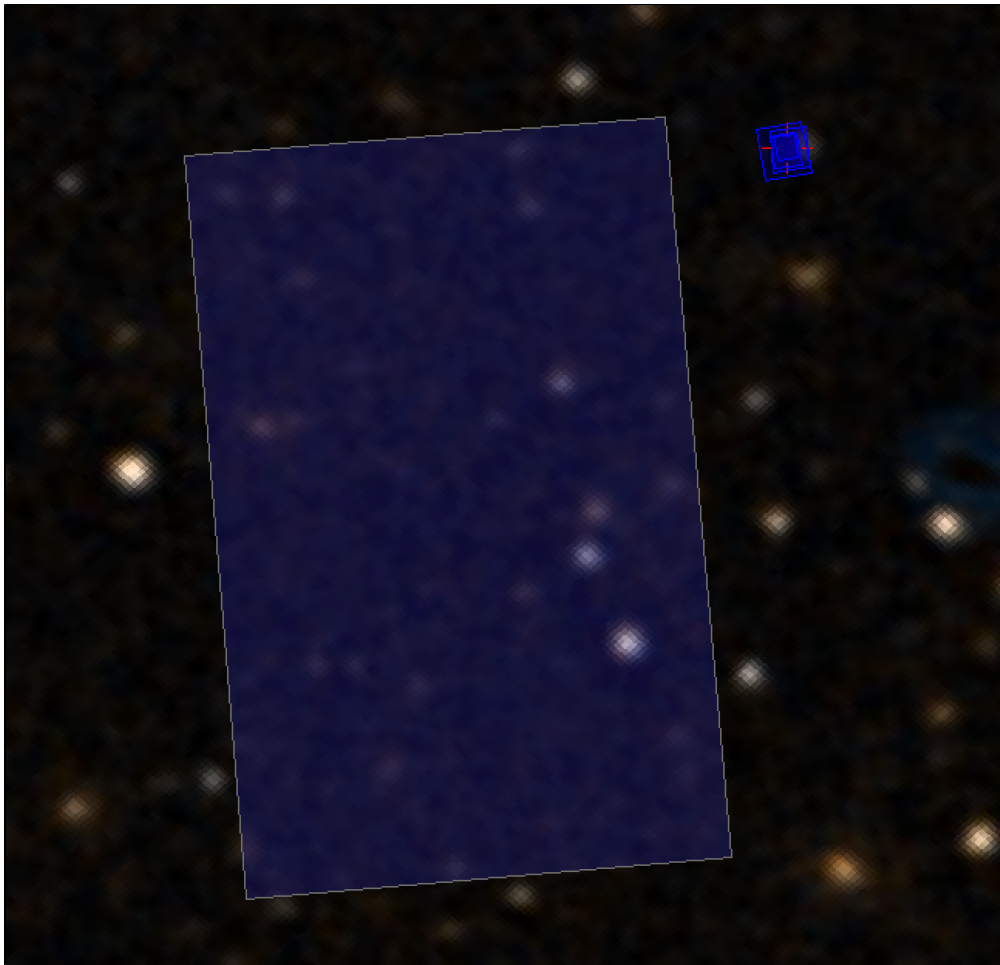
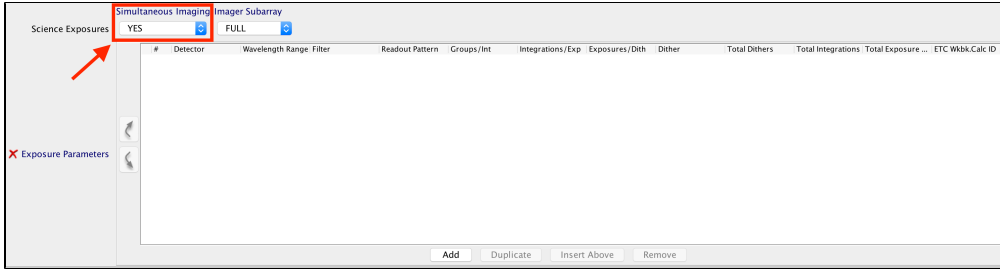


Image from the Aladdin viewer in APT of the MIRI imager FOV (large rectangle) and the MRS FOVs for each channel (off the top right corner of the MIRI imager FOV).

Selecting simultaneous imaging in APT

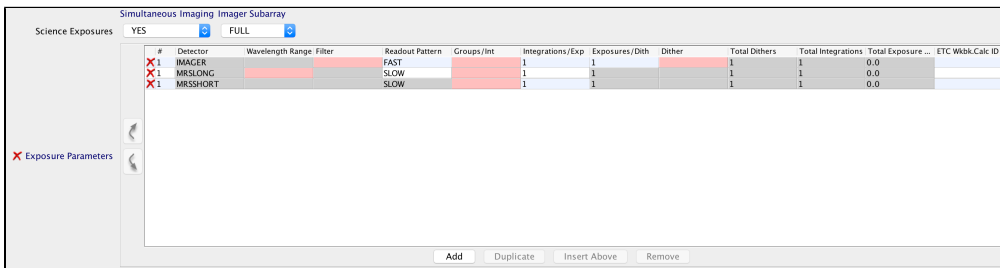
The following figures walk through how to select simultaneous imaging when MIRI Medium Resolution Spectroscopy¹ is selected as the observing template. Note: MRS parameters cannot be specified when MIRI Imaging is selected as the observing template.

Figure 2. Selecting simultaneous imaging in the MIRI Medium Resolution Spectroscopy APT template



In the **MIRI Medium Resolution Spectroscopy APT** observation template's **MRS Parameters panel**, select YES or NO under the **Simultaneous Imaging** drop-down menu. The default, and recommended selection, is YES. All **MIRI imaging subarray options** are available under the **Imager Subarray** drop-down menu.

Figue 3. MIRI MRS and imager observations



View of imager and MRS observations list after clicking the Add button at the bottom of the box. Any of the **MIRI imaging filters** may be selected for simultaneous imaging, though some will give warnings (see next section below). The Total Exposure Time for the IMAGER must be less than or equal to the Total Exposure Time of the MRSLONG and MRSSHORT detectors.

Selecting multiple simultaneous imaging filters

A different imaging filter can be selected for each exposure in a given observations. For instance, if an observation contained 3 exposures (one each for the MRS wavelength ranges SHORT, MEDIUM, and LONG, thereby covering the entire MRS wavelength range), then simultaneous imaging could correspondingly be obtained in 3 different filters.

Long wavelength filter warning

Selecting the F1280W, F1500W, F1800W, F2100W, or F2550W filters for simultaneous imaging will result in the following warning message: "Warning (Form): Imager Filter overlap." This is due to the large size of the **PSF FWHM** in those filters compared to the smallest of the **MRS dither patterns**; executing a small dither for the MRS will result in the PSFs of point sources in the imager overlapping between subsequent exposures, which can be problematic when performing image subtraction.

Simultaneous imaging and target acquisition

MRS target acquisition (TA) uses the FULL subarray of the MIRI imager. If TA is selected, the FULL imager subarray must also be selected for simultaneous imaging, otherwise APT will generate a warning that the imager data quality may be adversely affected. If no MRS TA is selected (option available starting in APT 25.4.2), there is no restriction on the subarray mode available for simultaneous imaging.

Simultaneous imaging overheads

If simultaneous imaging is selected, there will be an additional small overhead for each dither position. For example, if a 4-point dither is selected, and observations are set up with all 3 Wavelength Ranges, this results in 12 dithers and each of those dithers incurs its own small overhead.

¹ Bold italics font style indicates parameters, parameter values, and special requirements that are set in the APT GUI.

References

MIRI Instrumentation

The JWST [Mid-Infrared Instrument \(MIRI\)](#) contains optical, spectral, occulting and detector hardware components to support its [4 observing modes](#).

The JWST [Mid-Infrared Instrument \(MIRI\)](#) provides [4 observing modes](#) from 5 to 28.5 μm . The major pieces of instrumentation hardware necessary to support these modes include the components listed below:

- [Optics and focal plane](#): The [imager \(MIRIM\)](#) and [medium resolution spectrometer \(MRS\)](#) are fed from a single pick-off mirror (POM).
- [Filters](#): There are 10 filters for [imaging](#), 4 filter-diaphragm combinations for [coronagraphy](#), one neutral density filter, one ZnS-Ge double prism for the [LRS mode](#), one opaque position for darks, and one for a lens used during ground tests.
- [Coronagraph masks](#): One occulter is based on the classic [Lyot design](#) and there are 3 occulters that incorporate [4-quadrant phase masks \(4QPMs\)](#).
- [Spectroscopic elements](#): A double prism is used for the [low-resolution spectrometer](#) and there are 2 dichroic filter combination [wheels](#) for the [medium-resolution spectrometer](#).
- [Detectors](#) are 3 impurity band conduction (Si:As IBC) devices.
- [Integral field units \(IFUs\)](#): There are 4 IFUs for the [medium resolution spectrometer](#).

MIRI Optics and Focal Plane

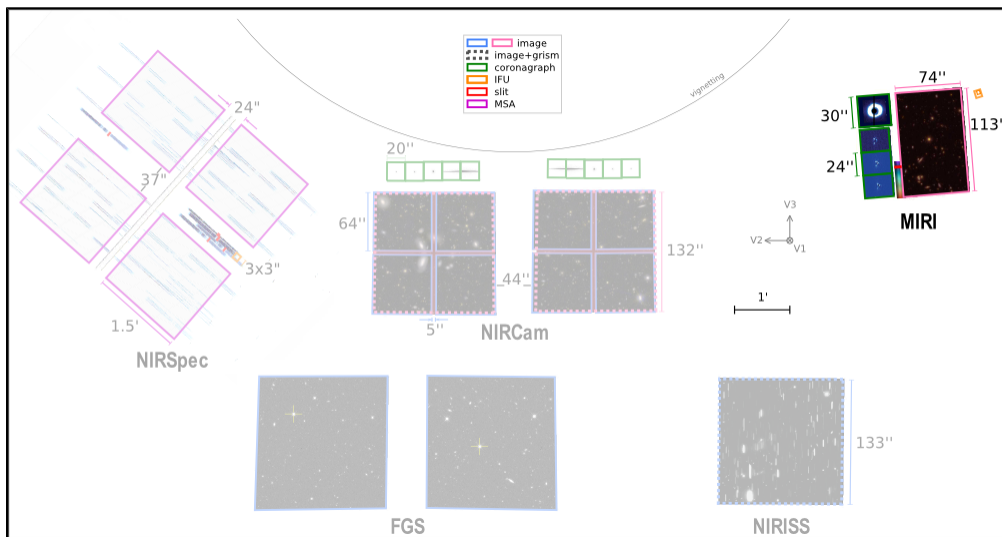
The JWST [Mid-Infrared Instrument \(MIRI\)](#) optical light path divides into 2 channels: a spectrometer and an imager. The spectrometer is also optically configured for integral field unit (IFU) spectroscopy.

Introduction

Parent page: [MIRI Instrumentation](#)

Figure 1 shows the [Mid-Infrared Instrument \(MIRI\)](#) field of view in relation to fields of view of other instruments.

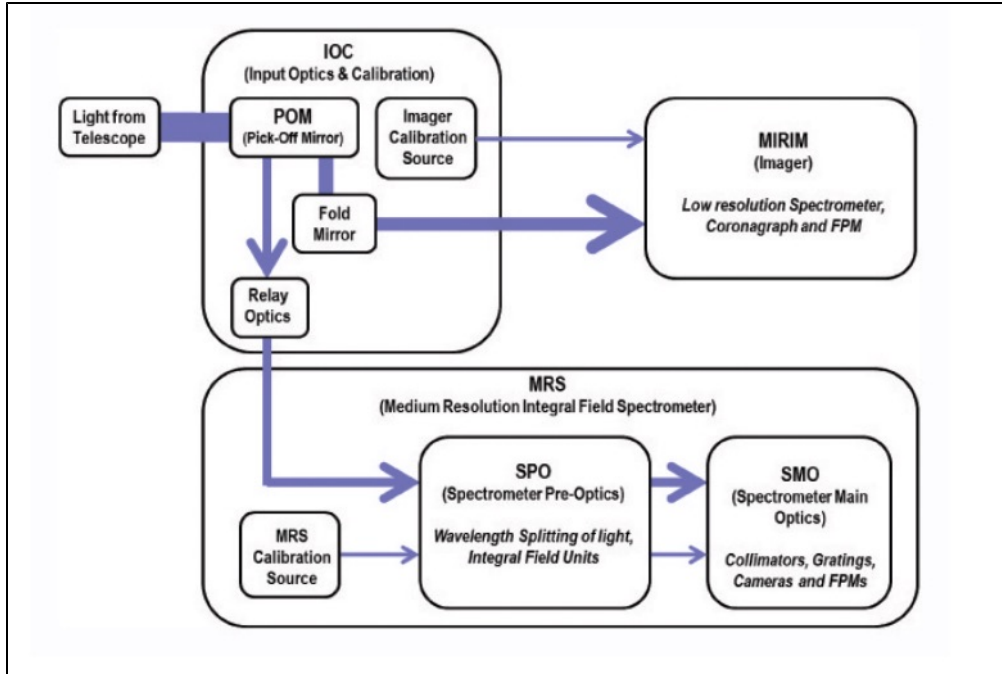
Figure 1. Science instruments fields of view as projected onto the sky



The science instruments fields of view as projected onto the sky using the JWST Science and Operations Center convention. For an observatory orientation angle of 0°, the V3 axis is aligned with celestial north and is up in this diagram. The MIRI field of view, in the upper right, is highlighted.

Optically, the instrument is divided into two channels: (1) an imager channel ([MIRIM](#)), with one detector array, and (2) a spectrometer channel ([MRS](#)) where light is further subdivided into long- and short-wavelength modules that each have a detector array.

MIRI's pick-off mirror, in front of the JWST optical telescope assembly focal plane, directs the MIRI field of view towards the imager. A small fold mirror adjacent to the imager light path picks off the small (up to 8'' × 8'') field of view of the spectrometer. A second fold in the spectrometer optical path is used to select either the light from the telescope or from the MIRI calibration system.

Figure 2. MIRI optical architecture

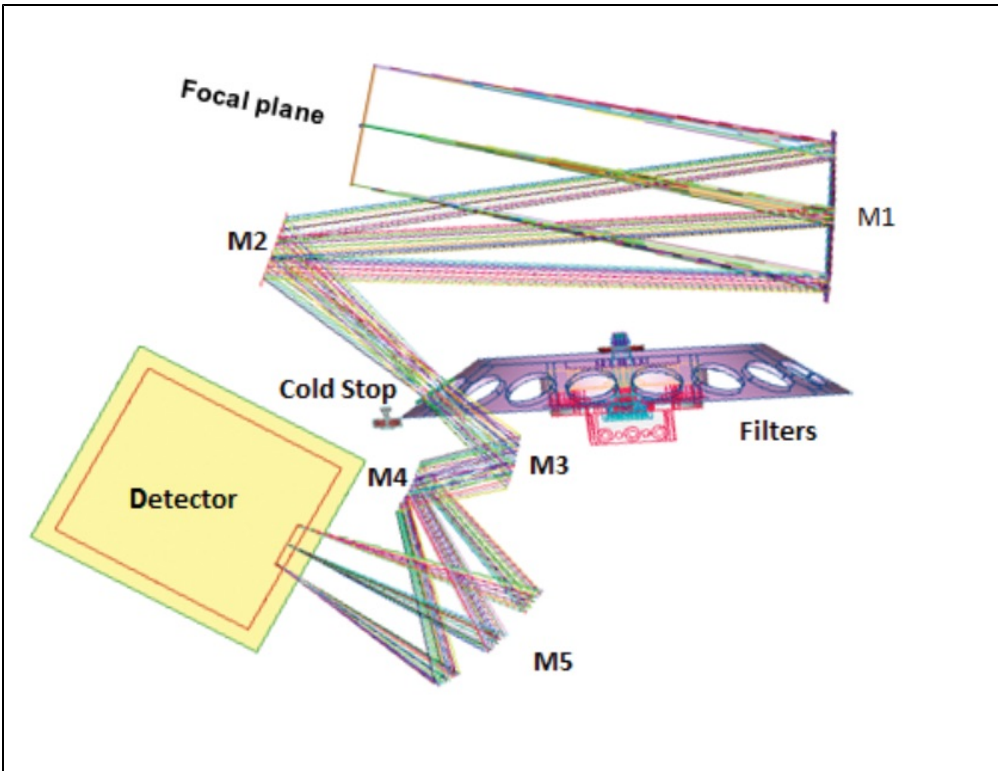
Overview of the MIRI optical architecture, showing the primary components (detailed components for MIRIM and MRS are given below). The science light path through the MIRI modules are shown in blue. Figure credit: Wright et al. 2015, Figure 2.

Imager (MIRIM)

The optics are configured to place the entrance focal plane just outside the MIRIM housing; this allows the focal plane module (which houses the [coronagraph masks](#) and [low-resolution spectrometer slit](#)) to be bolted directly to the housing in a very simple interface.

Inside MIRIM, the [field of view \(FOV\)](#) is partitioned into 3 functional areas on the instrument focal plane: [imager](#), [coronograph](#), and [low-resolution spectrometer](#). First, the light is collimated. At the pupil image formed by the collimator, a filter wheel holds the following: [filters](#) for both the imager and coronagraphs, a prism assembly for the low-resolution spectrometer, a blank for dark current measurements, and a pupil imaging lens. This entrance focal plane is imaged onto the detector using a 3-mirror anastigmat camera with separate areas of the detector being dedicated to the imaging, coronagraphy and spectroscopy functions. The region of the focal plane for each function is selected by a fold mirror close to the telescope focal plane.

Figure 3. MIRIM optical layout



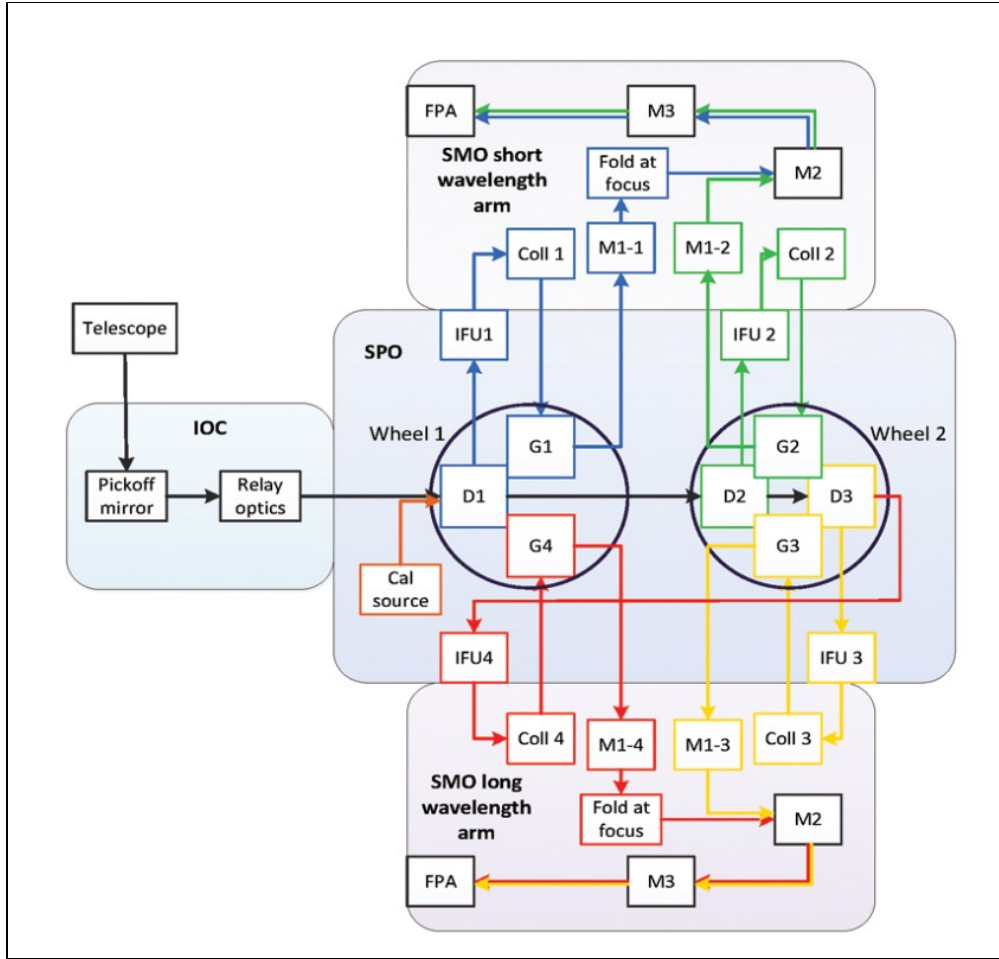
M1 forms the pupil where the filters and cold stops are placed, M2 folds the beam, and M3–M5 form an anastigmat that re-images the telescope focal plane onto the detector array. ([Bouchet et al. 2015, Figure 2](#))

Medium-resolution spectrometer (MRS)

The [MRS](#) provides diffraction-limited integral field spectroscopy (IFU) over the whole wavelength range from 5 to 28.5 μm . This mode consists of two modules: the spectrometer pre-optics (SPO) and spectrometer main optics (SMO).

The SPO spectrally splits the light into the 4 spectrometer channels and spatially reforms the rectangular fields of view into slits at the entrance of the SMO.

Figure 4. Block diagram of the MRS showing main optical functions



The 3 dichroics needed to divide the spectral band among the 4 spectrometer channels for one of the three sub-bands are indicated as D1, D2, and D3. (Wells et al. 2015, Figure 1)

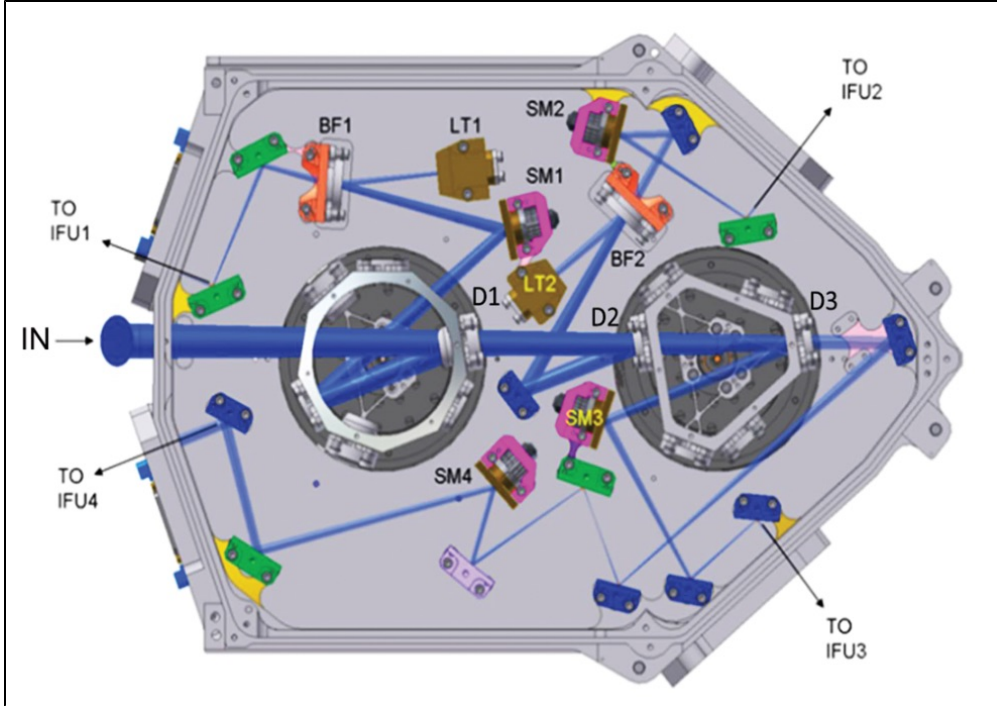
Spectrometer pre-optics (SPO)

Inside the SPO, the light is divided into 4 different wavelength channels using 3 dichroics.

Each channel has its own dedicated integral field unit (IFU), and the spectra from each of the 4 channels occupy half of one of the two MRS detectors.

Each channel is split, by an additional dichroic chain, into 3 sub-bands that are observed sequentially by rotation of just two mechanisms that carry both the wavelength sorting dichroics and the dispersion gratings in a very compact and efficient configuration.

Figure 5. Layout of the dichroic and fold mirrors for all channels in the spectrometer pre-optics (SPO)



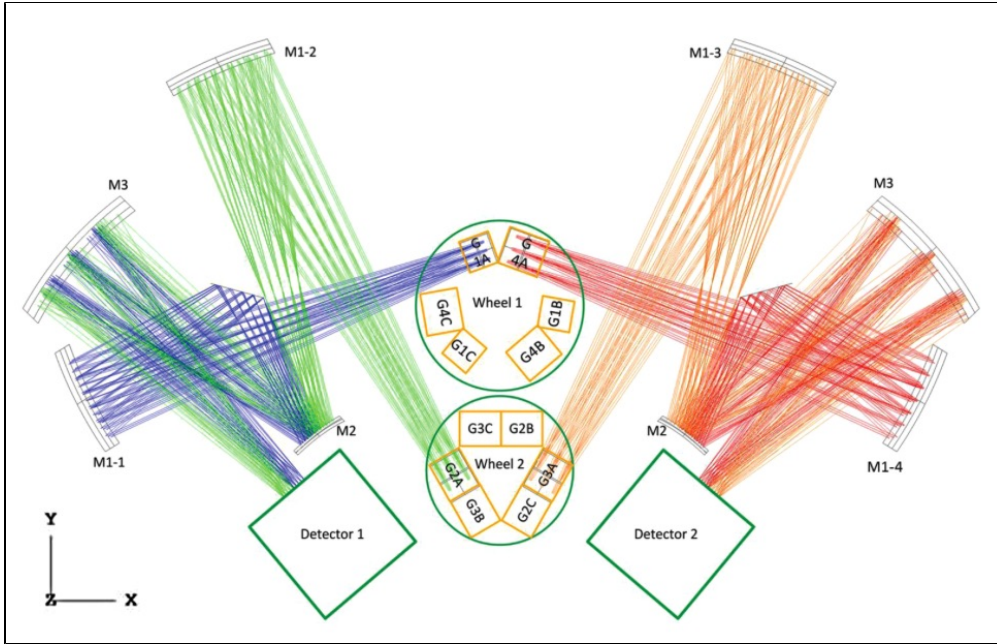
The position of the input pupil and fold mirror are labelled "IN." The locations of blocking filters (BF), light traps (LT), powered mirrors (SM) and dichroics (D) are shown. After the light has been divided into the appropriate spectral ranges, it is output to the integral field units (IFU) for the 4 spectrometer channels. ([Wells et al. 2015, Figure 3](#))

Spectrometer main optics (SMO)

The SMO consists of two arms which perform the following 3 functions: (1) collimation of the output beams of one of the 4 IFUs, (2) dispersion of the collimated beam with [diffraction gratings](#), and (3) imaging of the resulting spectrum onto one-half of one of the 2 focal plane arrays.

One of the two spectrometer arms includes the 2 short wavelength channels (1 and 2), and the other the long wavelength channels (3 and 4). Each spectrometer arm uses 6 gratings (to allow for any combination of two wavelength channels and three sub-band exposures). The dispersed beams are imaged by 3-mirror-anastigmat (TMA) camera systems (M1-M2-M3). Folding flats reflect the channel 1 and channel 4 beams such that the combined (channel 1 + 2) and (channel 3 + 4) beam pairs are imaged onto opposite halves of the detectors.

Figure 6. Cross-section of the camera symmetry plane in the spatial direction



Light arrives at the gratings (GIA, G2A, G3A, G4A) from the IFU output collimating mirrors. ([Wells et al. 2015, Figure 8](#))

Integral field units (IFUs)

The optical path through the IFUs begins with the 4 toroidal mirrors, which comprise the anamorphic preoptics (APO) module. The APO reimages the input focal plane ($8'' \times 8''$) onto the image slicer mirror. Light exits the IFU through individual pupil masks for each beam, then through individual slitlets. Reimaging mirrors behind the slitlets relay the beam to the input of the appropriate spectrometer.

Figure 7. Optical trace of the MIRI IFU

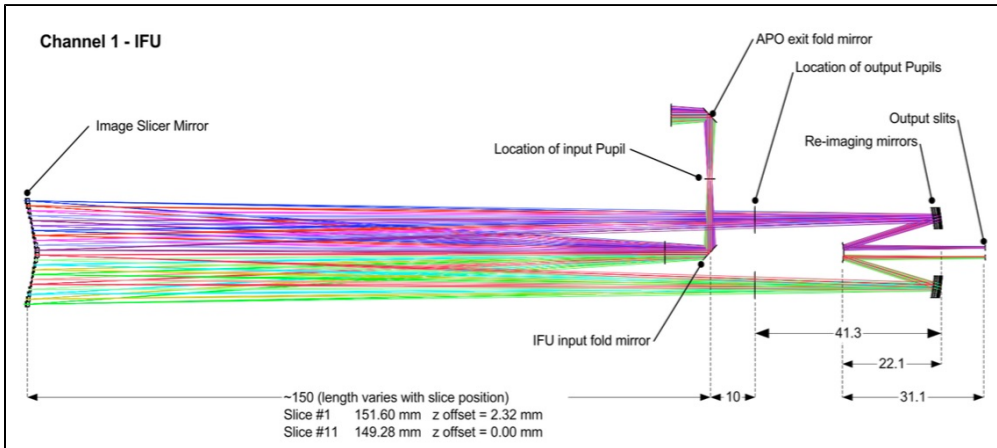
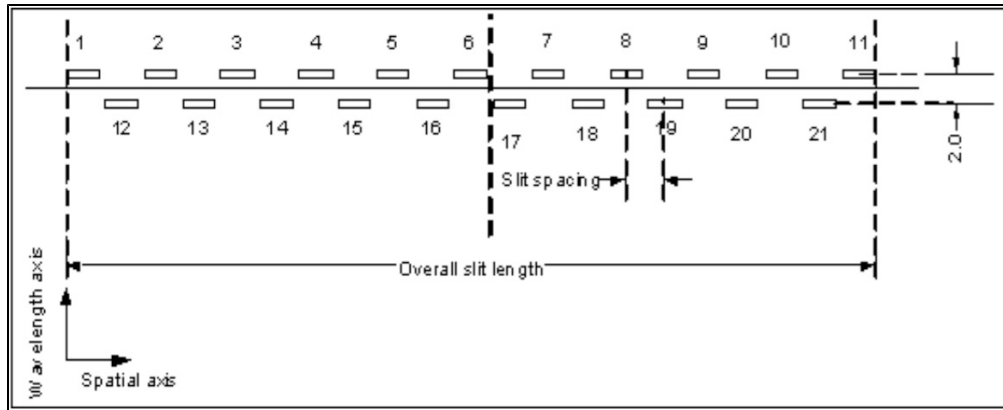


Figure 8. MIRI IFU output slits



References

Boccaletti, A. et al. 2015, PASP, 127, 633

The Mid-Infrared Instrument for the James Webb Space Telescope, V: Predicted Performance of the MIRI Coronagraphs

Bouchet, P. et al. 2015, PASP, 127, 612

The Mid-Infrared Instrument for the James Webb Space Telescope, III: MIRIM, The MIRI Imager

Wright, G. et al. 2015, PASP, 127, 595

The Mid-Infrared Instrument for the James Webb Space Telescope, II: Design and Build

[JWST technical documents](#)

MIRI MRS Field

JWST MIRI's medium resolution spectrometer has 4 separate integral field units, resulting in a non-unique and discontinuous mapping of the telescope focal plane to the 2 MRS detectors.

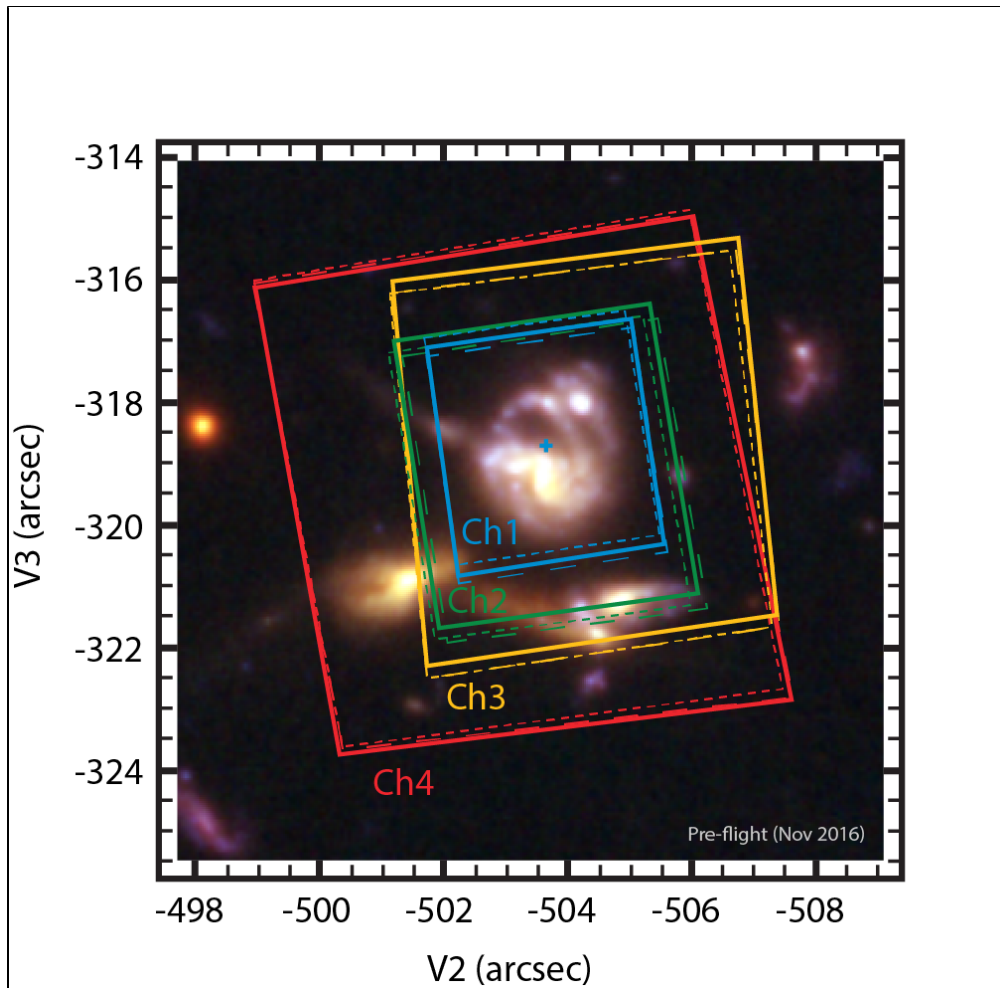
Introduction

Parent page: [MIRI Instrumentation](#)

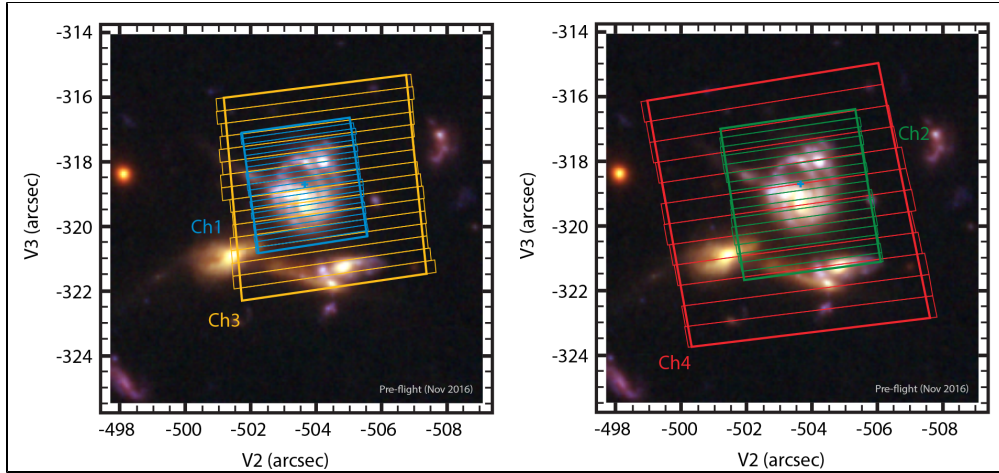
Main article: [MIRI Medium-Resolution Spectroscopy](#)

The MRS footprint on the sky is often depicted as nearly square for each channel, with slight differences for each sub-band (see [Figure 1](#)). However, this is only an approximation; the footprint at each wavelength is actually the combined collection of rectangular footprints from each individual optical slicer element of the integral field unit (IFU). These slices are not perfectly aligned with each other, and produce a staggered effective footprint on the sky (see [Figure 2](#)). The simplified fields of view shown in [Figure 1](#) (and displayed by APT) are calculated by inscribing a nominal rectangular field within the individual slice boundaries. Individual slices thus extend slightly beyond the simplified field boundary for a given MRS band, ensuring complete coverage within the nominal field. [Table 1 in MIRI Medium-Resolution Spectroscopy](#) gives the nominal field sizes calculated by averaging over the 3 sub-bands within each MRS channel.

Figure 1. MRS spatial footprint



MIRI MRS fields of view in the JWST coordinate frame (V2, V3): the field borders are drawn as solid lines (sub-band A), dashes (sub-band B), and dots (sub-band C) for channels 1 (blue), 2 (green), 3 (yellow), and 4 (red).

Figure 2. MRS individual-slice footprints

Similar to [Figure 1](#), but in this case the individual slices (of sub-band A) that make up the field of view are illustrated for channels 1 (blue), 2 (green), 3 (yellow), and 4 (red).

MRS coordinate frames

The MRS uses a variety of coordinate reference frames:

- The (V2,V3) coordinate frame is a spherical coordinate system tied to JWST that can be mapped to astronomical right ascension and declination by a series of Euler angle rotations. (V2,V3) is measured in units of arcseconds relative to the telescope boresight.
- The (α , β) coordinate frame is defined locally to each of the 12 MRS bands in which α and β correspond to the along-slice and across-slice directions respectively. (α, β) is measured in units of arcsec relative to the center of the IFU field of view.
- The [ideal](#) coordinate frame is used to define the dither offsets applied by APT, and for the MRS is defined such that +X_{ideal} lies along -V2, and +Y_{ideal} along +V3.

As illustrated in [Figure 1](#) above, due to the differing optical paths each of the 12 MRS bands is rotated by a slightly different amount with respect to the JWST V2,V3 coordinate system, and further distorted such that the along-slice (α) direction at the top and bottom of the IFU are not quite parallel to each other. On average, however, the along-slice direction of MRS is rotated by 8.4°, 8.1°, 7.7°, and 8.3° with respect to the V2,V3 coordinate system for channels 1, 2, 3, and 4 respectively. Since the MIRI imager is itself rotated by about 4.5° with respect to V2,V3, the MIRI imager and the MRS are therefore rotated with respect to each other by about 3.6°.

This angle between the different MRS fields of view and the ideal coordinate frame must be taken into account if specifying a particular position angle for observations. For instance, a position angle of -8.4° would orient the IFU such that the channel 1 across-slice direction is north-south on the sky, while a position angle of 90° - 7.7° = 82.3° would align the channel 3 across-slice direction east-west on the sky.

MRS pointing origins

Since each of the MRS channels has a slightly different field of view, they each have a different pointing origin with respect to which dither offsets are defined. These are defined for the 4 channels as the $(\alpha, \beta) = (0,0)$ locations in the Ch1A, Ch2A, Ch3A, and Ch4A coordinate frames respectively, and given in [Table 1 in MIRI Medium-Resolution Spectroscopy](#) with their corresponding (V2,V3) locations. This defines the location at which an astronomical target would be placed in the field of view when observing with a given primary channel set in APT if no dither offset were applied.

Since all 4 channels are observed simultaneously, for purposes of the JWST pipeline and world coordinate system specifications, the channel 1 pointing origin is defined to be the reference point (V2_REF, V3_REF) for all MRS observations.

Table 1. MRS pre-flight pointing origins

Channel	V2_PO (arcsec)	V3_PO (arcsec)
1/ALL	-503.65447	-318.74246
2	-503.63609	-319.09146
3	-504.37241	-318.79844
4	-503.12848	-319.48786

MIRI Filters and Dispersers

The JWST MIRI filter wheel has 10 filters for imaging, 4 filter-diaphragm sets for coronagraphy, and one double prism assembly for [low-resolution spectroscopy](#). The [medium-resolution spectrometer](#) has 2 wheels for controlling gratings and dichroics positions.

Introduction

Parent page: [MIRI Instrumentation](#)

For the [Mid-Infrared Instrument \(MIRI\)](#), both the [imager \(MIRIM\)](#) and [medium-resolution spectrometer \(MRS\)](#) channels are fed from a single pick-off mirror (POM).

The imager has a single [filter wheel](#) that holds all the elements necessary for MIRI's 3 functional areas: [imager](#), [coronagraph](#), and [low-resolution spectrometer](#) (LRS). For low-resolution spectroscopy, a double prism is used to disperse the light; it is mounted in the imager filter wheel, with its position designated P750L.

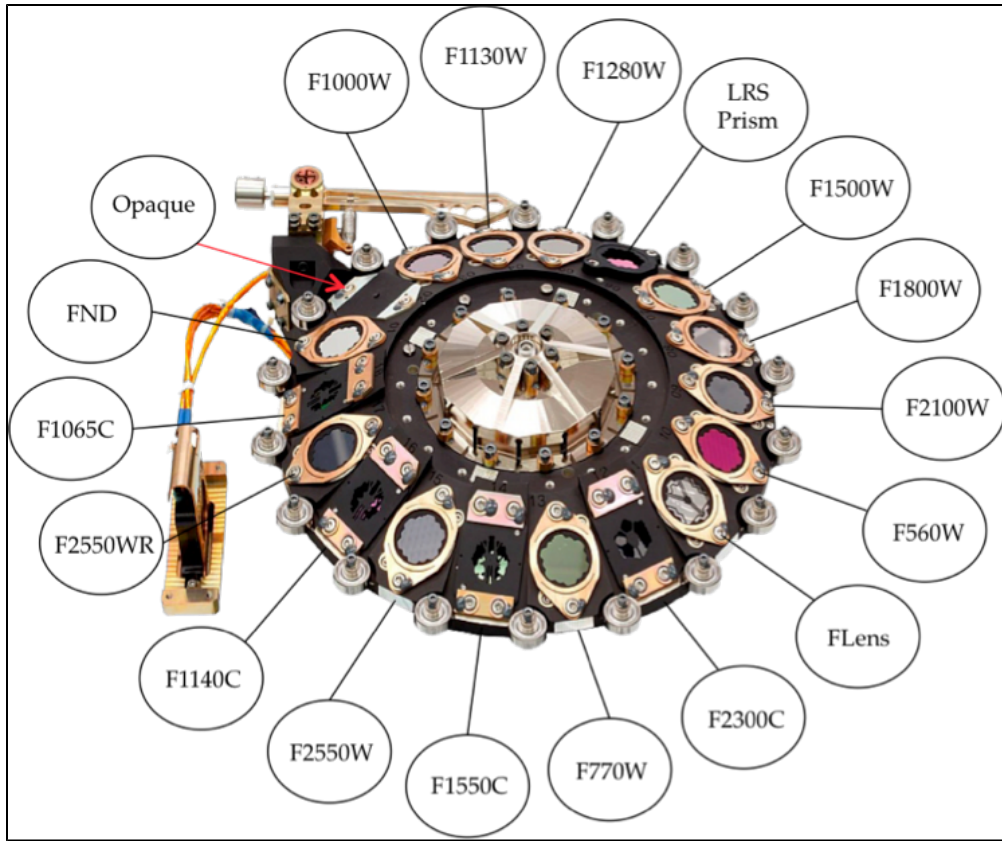
The [MRS](#) has its own [dichroic filter/grating wheels](#) that move gratings and dichroics simultaneously to allow for a specific wavelength coverage.

Imager

The MIRI imager filter wheel includes:

- 10 filters for imaging (F2550WR is redundant)
- 4 filter-diaphragm combinations for coronagraphy
- one neutral density filter
- one ZnS-Ge double prism for the LRS mode
- one opaque position for darks
- one lens for ground testing purposes

Figure 1. MIRI imager filter wheel



Locations of filters in the filter imager wheel. (Figure adapted from Wright et al. 2015)

Imaging filters

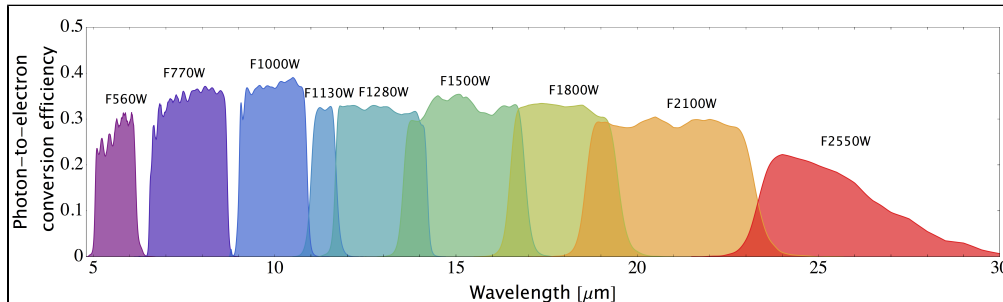
The MIRI imaging mode allows users to select amongst 10 filters for observations.

Table 1. Imaging filter properties

Filter name	λ_0 (μm)	$\Delta\lambda$ (μm)	FWHM ¹ (arcsec)	Comments
F560W	5.6	1.2	0.22	Broadband Imaging
F770W	7.7	2.2	0.25	PAH, broadband imaging
F1000W	10.0	2.0	0.32	Silicate, broadband imaging
F1130W	11.3	0.7	0.36	PAH, broadband imaging
F1280W	12.8	2.4	0.41	Broadband imaging
F1500W	15.0	3.0	0.48	Broadband imaging
F1800W	18.0	3.0	0.58	Silicate, broadband imaging
F2100W	21.0	5.0	0.67	Broadband imaging
F2550W	25.5	4.0	0.82	Broadband imaging
F2550WR	25.5	4.0	0.82	Redundant filter, risk reduction
FND	~13	10	--	For bright target acquisition
Opaque	blackened blank	N/A	N/A	Darks

¹ FWHM refers to the PSF

Figure 2. MIRI imaging filter throughputs



Coronagraphic imaging filters

These filters are associated directly with each coronagraph and are not interchangeable. Selecting the filter selects the coronagraph.

Table 2. Coronagraph filter-mask combinations

Filter	Coronagraph	Pupil mask transmission (%) ¹	Central wavelength (μm)	Bandwidth ² (μm)	IWA ³ (arcsec)	Rejection ⁴ (on-axis)
F1065C	4QPM1	62	10.575	0.75	0.33	260
F1140C	4QPM2	62	11.40	0.8	0.36	285
F1550C	4QPM3	62	15.50	0.9	0.49	310
F2300C	Lyot spot ⁵	72	22.75	5.5	2.16	850

¹ Coronagraph filters are paired with pupil masks to reduce diffracted light from both the telescope pupil and the coronagraphic occulting spot, but at the expense of some loss of total intensity.

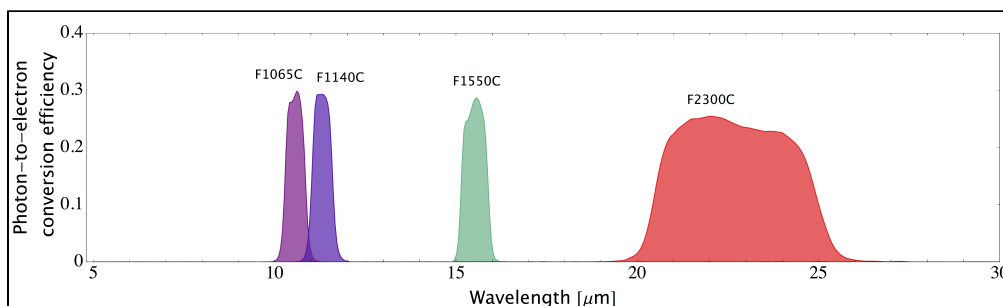
² Bandwidth is defined to extend down to wavelengths that correspond to 5%-10% of the transmission efficiency.

³ [Inner working angle](#) (IWA) is defined as the 50% transmission radius.

⁴ Rejection is the total flux attenuation of a star when centered onto the coronagraph. The term is unitless since it is a ratio of 2 intensities (out of mask / on the mask).

⁵ The spot refers to the occulting mask in the Lyot-type coronagraph.

Figure 3. MIRI coronagraphic imaging filter throughputs



Medium-resolution spectrometer (MRS)

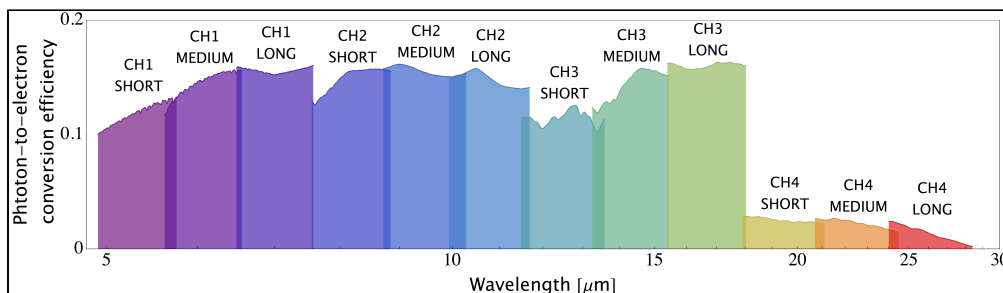
The MRS has 4 separate IFUs (called channels 1-4), each covering a separate wavelength range between 5-28.5 μm . All 4 channels are observed simultaneously, but each exposure can only cover one-third of the available wavelength range in a single configuration.

For complete spectral coverage, 3 different spectral settings must be observed, called SHORT (A), MEDIUM (B), and LONG (C). The dichroic filter wheel comprises of 3 working positions to move gratings and dichroics simultaneously. Each is located on separate wheel discs. The two wheels feed light into the 4 spectrometer channels inside MIRI. Filters (and associated resolving power) are summarized in both Figure 4 and Table 3.

Table 3. MRS wavelength coverage

FOV name λ -range (μm)	FOV (arcsec)	Sub-band name	λ -range (μm)	Resolving power ($\lambda/\Delta\lambda$)
Channel 1 4.89-7.66	3.3×3.7	A	4.89-5.75	3320-3710
		B	5.65-6.64	3190-3750
		C	6.52-7.66	3100-3610
Channel 2 7.49-11.71	4.2×4.8	A	7.49-8.78	2990-3110
		B	8.65-10.14	2750-3170
		C	9.99-11.71	2860-3300
Channel 3 11.53-18.05	5.6×6.2	A	11.53-13.48	2530-2880
		B	13.37-15.63	1790-2640
		C	15.44-18.05	1980-2790
Channel 4 17.66-28.45	7.2×7.9	A	17.66-20.92	1460-1930
		B	20.54-24.40	1680-1770
		C	23.95-28.45	1630-1330

Figure 4. MIRI MRS IFU channels filter throughputs



References

[Wright, G. et al. 2015, PASP, 127, 595](#)

The Mid-Infrared Instrument for the James Webb Space Telescope, II: Design and Build

[MIRI Filter Throughput Curves](#) (University of Arizona MIRI webpage)

[JWST technical documents](#)

MIRI Coronagraph Masks

JWST's MIRI has 4 coronagraph occulters for [coronagraphic imaging](#). One is based on the classic [Lyot design](#), while the other 3 incorporate [four-quadrant phase masks \(4QPMs\)](#).

Introduction

Parent page: [MIRI Instrumentation](#)

MIRI offers [coronagraphic imaging](#) with 4 individual coronagraph occulters, located with the [LRS slit](#) on a mounting bracket placed at the [focal plane](#). One of the coronagraphs is based on the classic [Lyot design](#), while the other 3 incorporate [4-quadrant phase masks \(4QPMs\)](#). (Please refer to the [JWST High-Contrast Imaging](#) page for additional information about high-contrast imaging (HCI) optics.)

The classical Lyot coronagraph places an occulting spot in the focal plane to block light from a bright point source from reaching the detector. For a typical Lyot coronagraph, this spot is of order 3–6 λ/D in radius so that it blocks the majority of the light from the Airy core, including a few bright rings. Although classical Lyot coronagraphs can provide excellent contrast outside the area blocked by the occulting spot, they are limited with regard to their inner-working angle (IWA) to the projected radius of this spot.

Phase mask coronagraphs are designed to decrease the IWA to near 1 λ/D by replacing the occulting spot with a transparent mask that imparts phase differences across the focal plane so that when the reimaged pupil is formed, the light interferes more destructively than with a Lyot mask, hence rejecting the starlight outside the geometrical pupil. The theory of 4QPMs was developed as described in [Rouan et al. \(2000\)](#) and [Rouan et al. \(2007\)](#).

In addition to the focal plane masks, Lyot stops sandwiched with the passband filters are located at a re-imaged pupil to attenuate the residual light from the diffraction pattern associated with the telescope aperture and a particular coronagraph design, and from phase and amplitude aberrations of the wavefront in the optical train.

Lyot coronagraph

The [Lyot coronagraph](#) is a traditional design that incorporates a Lyot spot mask of radius of 2.16", which is 3 λ/D in radius at 23 μm . The spot is suspended in the focal plane by 2 supporting struts in the mounting bracket, which themselves block light in the FOV. MIRI's Lyot coronagraph is offered at 23 μm for two reasons: (1) a lack of suitable transmissive optical materials to fabricate more advanced 4QPM masks at these wavelengths, and (2) to provide a broad spectral band to maximize the sensitivity on planetary debris disks (4QPMs only operate over a narrow passband). The Lyot mask is useful for investigating objects, structures and diffuse emission near bright sources such as the outer regions of protoplanetary and debris disks, extended structures around post-AGB stars, and the host galaxies and scattering/ionization "cones" of AGN.

Figure 1. Image of the Lyot coronagraph pupil masks



The Lyot coronagraph pupil masks were manufactured at LESIA (the Laboratory for Space Studies and Astrophysics Instrumentation, at the Paris Observatory). Figure Credit: [Boccaletti et al. 2015](#).

Figure 2. Optical path for the Lyot coronagraph

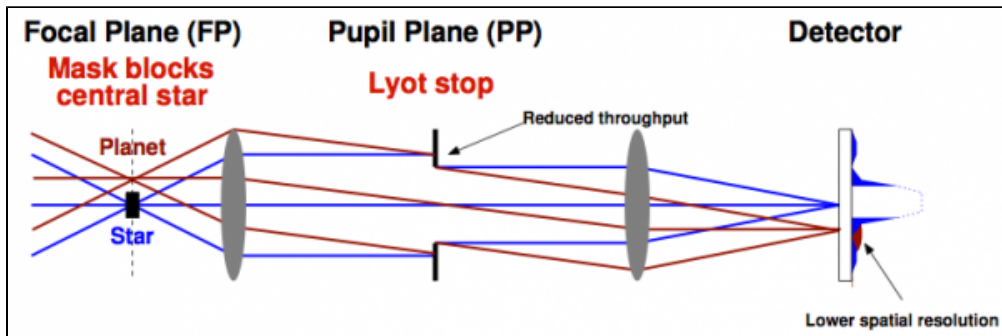


Figure Credit: [Kenworthy 2017](#).

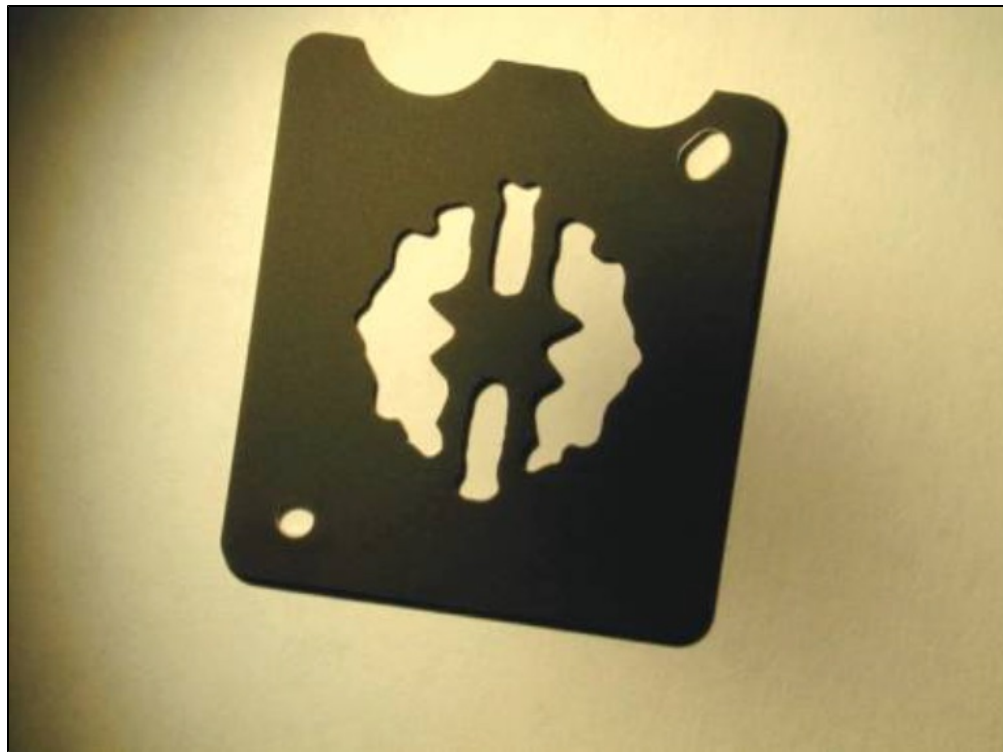
4-quadrant phase mask (4QPMs) coronagraphs

Lyot coronagraphs provide excellent contrast outside the occulter, but their IWA is limited to the projected radius of this occulter ($\geq 3\lambda/D$). Phase mask coronagraphs reduce the IWA to near $1 \lambda/D$ by replacing the occulting spot with a transparent mask that imparts phase differences throughout the focal plane so that the light interferes destructively for a point source placed at the apex of the 4 quadrants. The 4QPMs are useful

for investigating objects, structures and diffuse emission very close to bright point sources, such as the inner regions of debris disks and exoplanets orbiting close to a star, very tight binary star systems, and the near-nuclear environments of AGN.

While there are several implementations of phase mask coronagraphs, 4QPMs have been chosen for MIRI ([Rouan et al. 2000, 2007](#)). 4QPMs work by introducing a 180° phase shift of the light transmitted through 2 of the quadrants on the diagonal. This cancels the signal from the central point source via destructive interference of light that lands equally in the 4 quadrants. The disadvantage of a 4QPM is that it operates only over a narrow wavelength range. Therefore, maximum cancellation takes effect only when the appropriate filter (and Lyot stop) is in position. Furthermore, the linear boundaries between adjacent quadrants will attenuate light. Therefore, the [4QPM](#) has reduced sensitivity (as low as 10%) in the field along the 4 edges of the mask.

Figure 3. Image of the 4QPM coronagraph pupil masks



The 4QPM coronagraph pupil masks is also manufactured at LESIA. Figure Credit: [Boccaletti et al. 2015](#)

Figure 4. Optical path for the 4QPM coronagraph

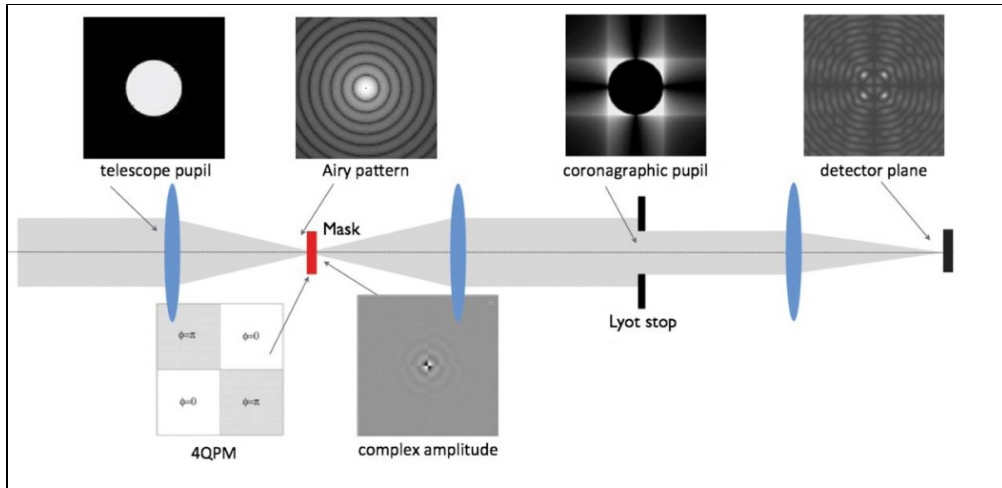


Figure Credit: [Boccaletti et al. 2015](#).

References

[Boccaletti, A. et al. 2015, PASP, 127, 633](#)

The Mid-Infrared Instrument for the James Webb Space Telescope, V: Predicted Performance of the MIRI Coronagraphs

Kenworthy, Matthew, 2017, "[Apodizing Phase Plate Coronagraph](#)," Leiden Observatory website [Updated 2017/09/13]

(Leiden Observatory webpage on [coronagraphy optics](#))

[Apodizing Phase Plate Coronagraph](#)

[Rouan, D. et al. 2000, PASP, 112, 1479](#)

The Four-Quadrant Phase-Mask Coronagraph. I. Principle

[Rouan, D. et al. 2007, Proc. of SPIE, 6693, 16](#)

A new concept of achromatic phase shifter for nulling interferometry

[JWST technical documents](#)

MIRI Spectroscopic Elements

JWST MIRI's [low-resolution spectroscopy](#) mode is enabled by a double prism, while MIRI [medium-resolution spectroscopy](#) is enabled by two dichroic filter-grating combination wheels and 4 integral field units (IFUs).

Introduction

Parent page: [MIRI Instrumentation](#)

MIRI offers observing modes for both [low-resolution spectroscopy](#) and [medium-resolution spectroscopy](#). Each mode utilizes different spectroscopic elements to produce spectra.

The low-resolution spectrograph (LRS) uses:

- [double prism](#)

The medium-resolution spectrograph (MRS) uses:

- [integral field units \(IFUs\)](#)
- [dichroic filter/grating combination wheels](#)

Low-resolution spectrograph (LRS)

Double prism

The LRS slit is located at the telescope [focal plane](#) (along with the [coronagraph masks](#)).

Figure 1. The mounting bracket focal plane module for the 4 coronagraph image-plane masks and LRS slit

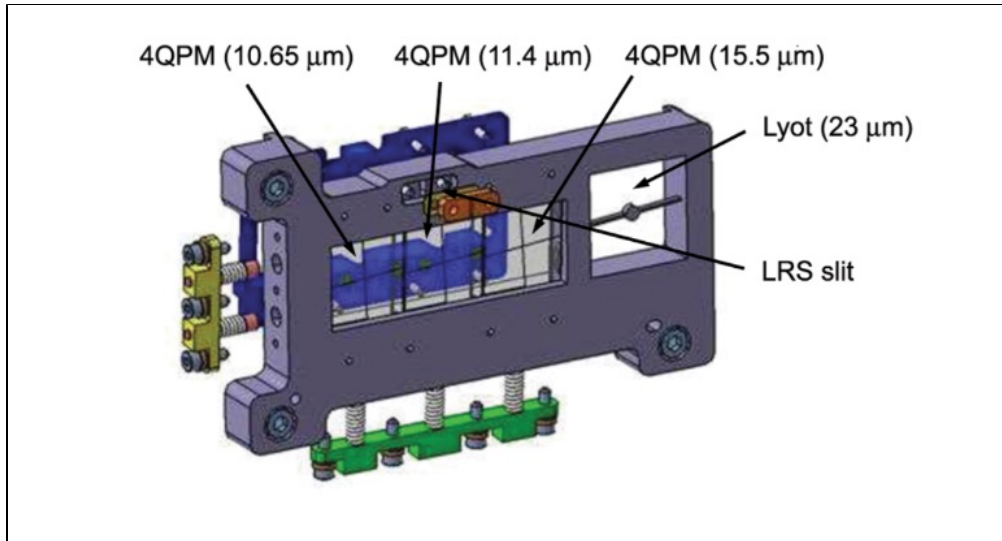
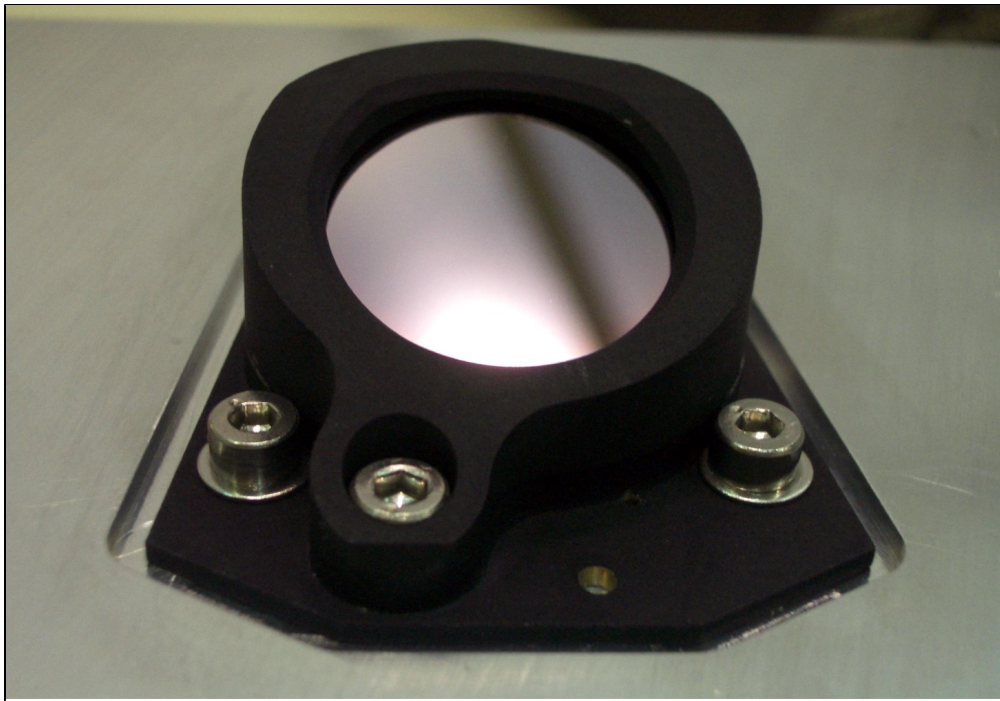


Figure Credit: [Boccaletti et al. 2015](#)

The LRS shares all of its [optics](#) with the [imager](#), except the dispersing element. Its mode (i.e., slit or slitless) is determined solely by the placement location of the target source in the focal plane. Light passing through the focal plane is collimated, forming a pupil image at the filter wheel location that holds a Ge/ZnS double prism ([Fischer et al. 2008](#)).

Expected efficiency for the set of prisms is near 80% from 5 to 10 μm (at cold temperatures) but drops below 25% for wavelengths longer than 12 μm if slit losses are included. To mitigate the effect of the fold-over in the dispersion profile, a mask is mounted on the slit to block light at wavelengths short of 4.5 μm .

Figure 2. Flight model of the LRS double prism assembly



The flight model of the LRS double prism assembly (DPA), showing the ZnS side. Figure Credit: Fischer et al. 2008

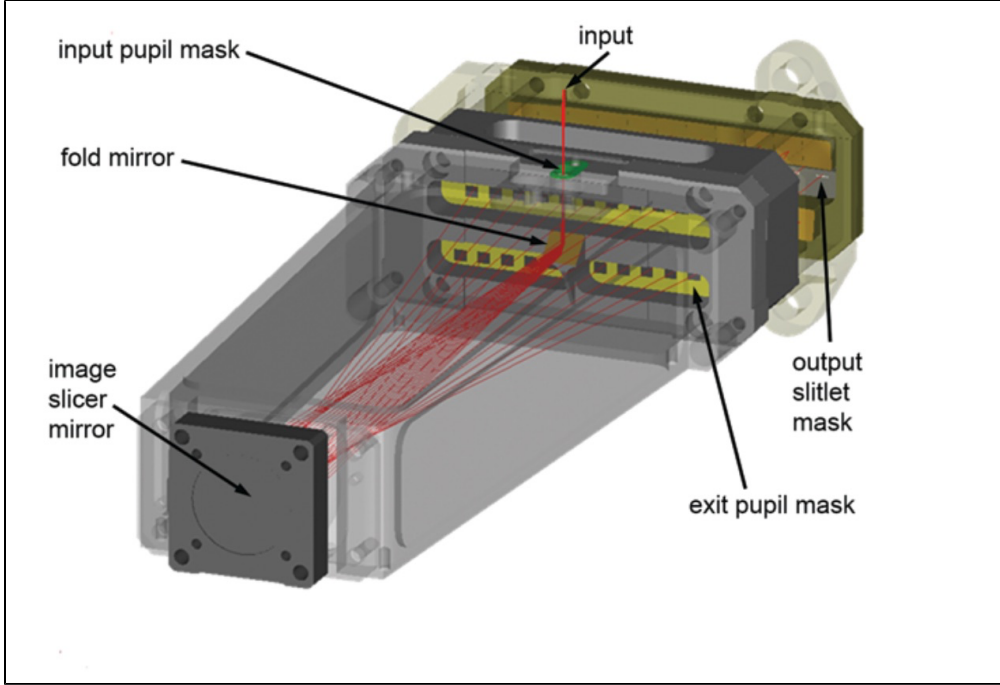
Medium-resolution spectrograph (MRS)

Integral field units (IFUs)

The MIRI [MRS](#) has 4 separate integral field units (IFUs) called channels 1, 2, 3 and 4. Each IFU covers a separate wavelength range between 5 and 28.5 μm . An IFU serves primarily to divide a field of view into multiple spectra. Its design has several advantages: (1) easier acquisition of point sources, (2) no slit losses due to vignetting, and (3) allowance for spatial variations as a function of wavelength for which a slit cannot account.

The MIRI IFU design consists of several components, including an entrance pupil, an input fold mirror, an image slicer mirror, a mask carrying exit pupils for the individual sliced images, a mask carrying slitlets for the individual images, and an array of reimaging mirrors behind the slitlets.

Figure 3. Three dimensional view of the channel 3 IFU



Three-dimensional view of the channel 3 IFU with labels identifying the major components, including an entrance pupil, an input fold mirror, an image slicer mirror, a mask carrying exit pupils for the individual sliced images, a mask carrying slitlets for the individual images, and an array of reimaging mirrors behind the slitlets. Figure Credit: Wells et al. 2015

The IFU itself can be implemented with several different types of technology. The MRS IFU utilizes an [image slicer](#), as illustrated in Figure 4. The slicer has rows that reflect light from different parts of the field of view into different directions. The image slices are then directed through a regular spectrograph slit and diffracted by a grating, thereby resulting in a spectrum for each row. Spatially, the image is sampled in the dispersion direction by the IFU slicing mirrors and in the slice direction by the detector pixels. Spectrally, the width of the slices defines the spectrometer entrance slit and the width of the image (in pixels) of the slice at the detector defines the width of the spectral sample. In the across slice (dispersion) direction, one slice width is matched to the full-width half-maximum (FWHM) of the JWST point spread function (PSF) at the shortest IFU wavelength.

Figure 4. Visual representation of how an IFU image slicer works

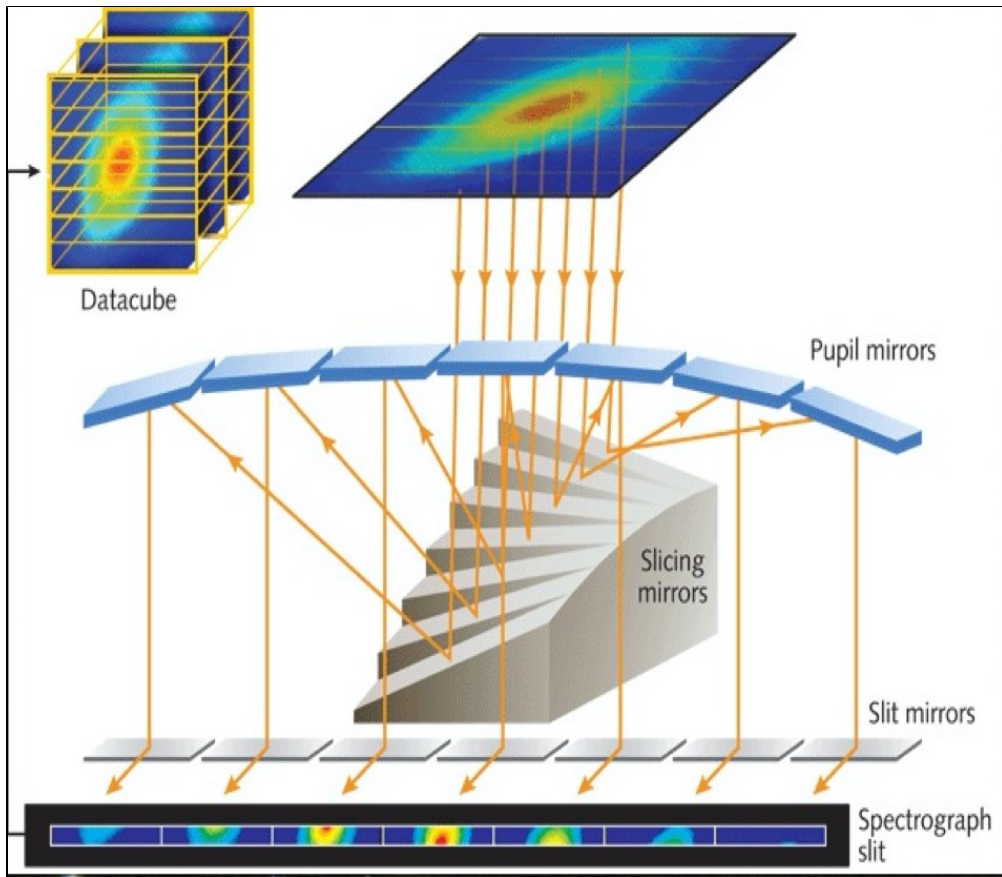
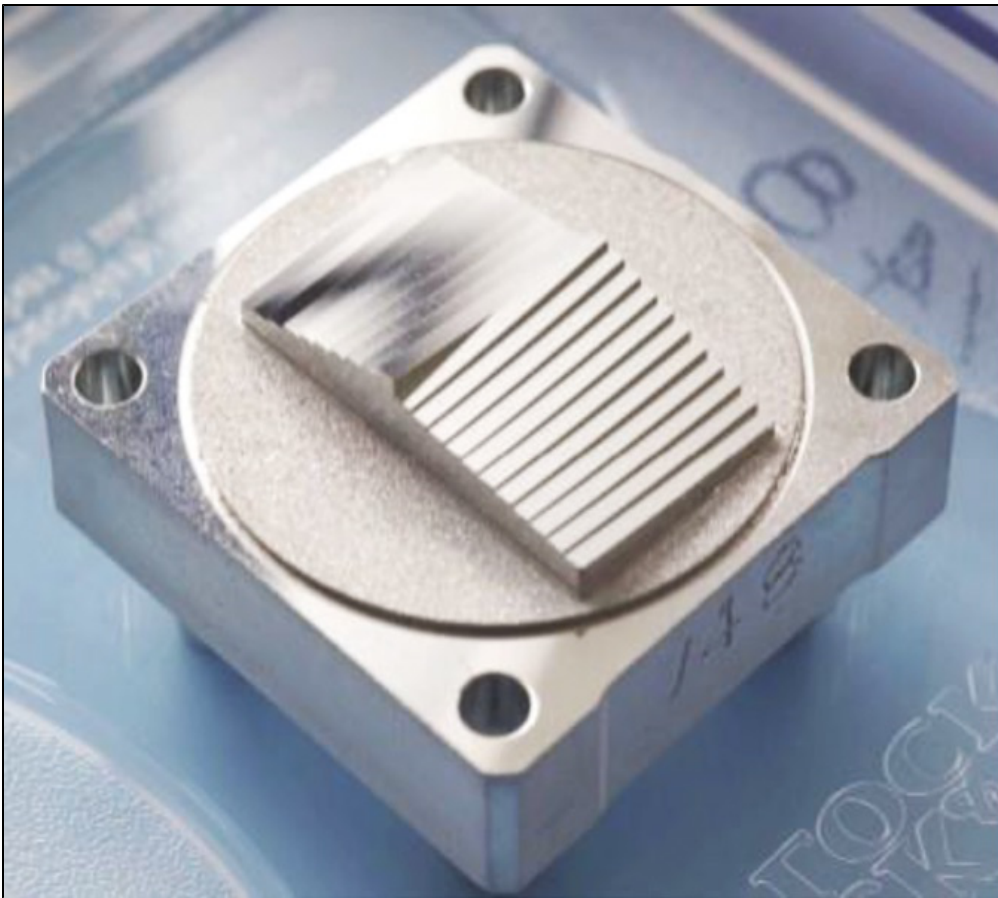


Figure 5. Channel 1 image slicer hardware



The slices are 1mm wide and 12 mm long. Figure Credit: [Wells et al. 2015](#)

Dichroic filter/grating combination wheels

All 4 [MRS](#) channels are observed simultaneously, but each exposure can only cover one-third of the available wavelength range in a single configuration. For complete [spectral coverage](#), 3 different spectral settings must be observed, termed SHORT (A), MEDIUM (B), and LONG (C). Two [dichroic filter/grating wheels](#) have 3 working positions to move gratings and dichroics simultaneously.

Figure 6. MRS dichroic and grating wheels

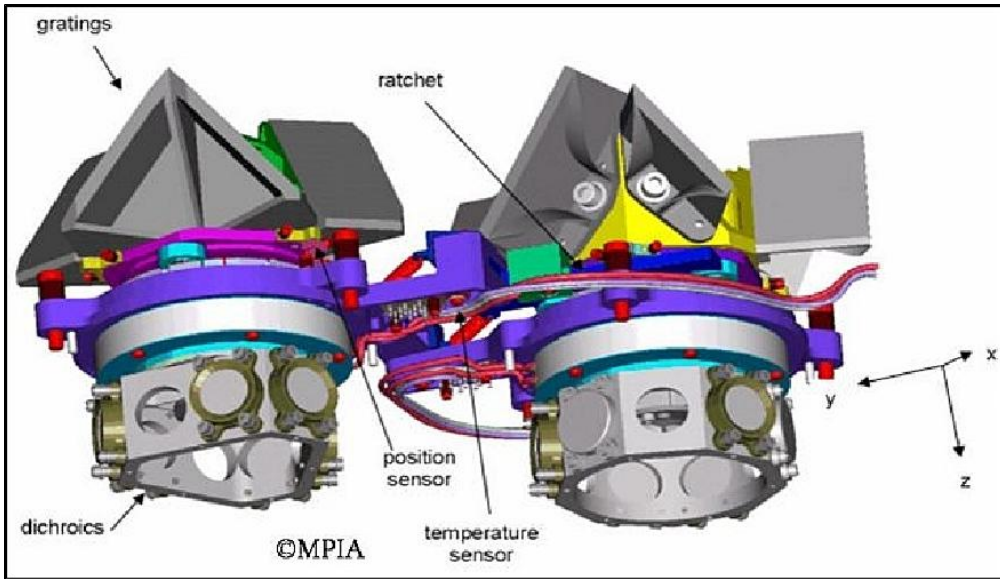


Image credit: [ESA 2000-](#)

References

[Boccaletti, A. et al. 2015, PASP, 127, 633](#)

The Mid-Infrared Instrument for the James Webb Space Telescope, V: Predicted Performance of the MIRI Coronagraphs

[Fischer, S. et al. 2008, Proc. of SPIE, 7010, 103](#)

The JWST MIRI double-prism: design and science drivers

European Space Agency (ESA), 2000- "[JWST \(James Webb Space Telescope\)](#)," Earth Observation Portal [Updated November 2017]

[Wells, M. et al. 2015, PASP, 127, 646](#)

The Mid-Infrared Instrument for the James Webb Space Telescope, VI: The Medium Resolution Spectrometer Updated version

[JWST technical documents](#)

MIRI Detector Overview

JWST [MIRI](#) uses 3 arsenic-doped silicon impurity band conduction (Si:As IBC) detectors, one in the [imaging](#) module, and two in the [medium-resolution spectrometer \(MRS\)](#).

Introduction

Parent page: [MIRI Instrumentation](#)

MIRI has 3 nearly identical [detectors](#). One is used in the [imager](#). The other 2 are in the [medium-resolution spectrometer \(MRS\)](#), one for the short-wave channel and the other for the long-wave channel.

The MIRI photodetectors are composed of semiconductor material that creates free charge carriers (i.e., electrons) when photons are absorbed. These arsenic-doped silicon impurity band conduction (Si:As IBC) devices are sensitive to electromagnetic radiation from 5 to 28.5 μm ([Rieke et al. 2015](#)).

For science observations, observers must consider:

- [detector performance](#), which includes basic detector characteristics such as gain, read noise, quantum efficiency, and dark current;
- [readout patterns](#) that determine the total integration time; and
- [subarrays](#) that allow for smaller regions of interest (ROI) to be read out at faster speeds to allow for brighter targets and specific observing modes.

Figure 1. Three MIRI Si:As IBC detectors

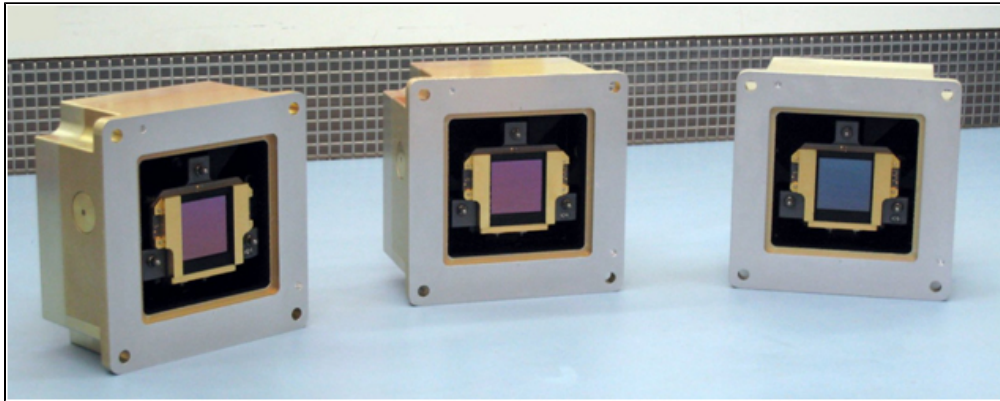


Table 1. MIRI Si:As IBC detector properties

Property	Value
Components	Si:As IBC devices manufactured by Raytheon Vision Systems (RVS)
Wavelength Range	5 to 28 μm
Pixel format	1024 \times 1024
Pixel Size	25 μm
Plate Scale	0.11 " /pixel
Nominal Operating Temperature	\leq 6.7 K
Dark Current	<0.2 e ⁻ /s/pix (median)
Readnoise	\sim 14 e ⁻ (CDS)
Full Well	\sim 250,000 e ⁻
Conversion Gain	5.5 e ⁻ /DN

Impurity band conduction (IBC) devices

The MIRI Si:As IBC differ from the shorter wavelength HgCdTe near-IR photodiodes, which would have too high a dark current if tuned for longer wavelengths. ([Rieke et al. 2007](#))

The IBC detectors have a long heritage, as similar devices were used in all 3 Spitzer instruments ([IRAC \[Hora et al. 2008\]](#); [IRS \[Van Cleve et al. 1995\]](#), [[Houck et al. 2004](#)]; [MIPS \[Gordon et al. 2004\]](#)), in [WISE \(Mainzer et al. 2008\)](#), in [MSX \(Mill et al. 1994\)](#), and in [Akari \(Onaka et al. 2007\)](#). These detectors benefit from high quantum efficiencies (QE), low dark current, and resistance to the effects of cosmic radiation. A schematic of the IBC detector technology is shown in Figure 2. The design is referred to as either a blocked impurity band (BIB) or impurity band conductor (IBC device), depending on the vendor.

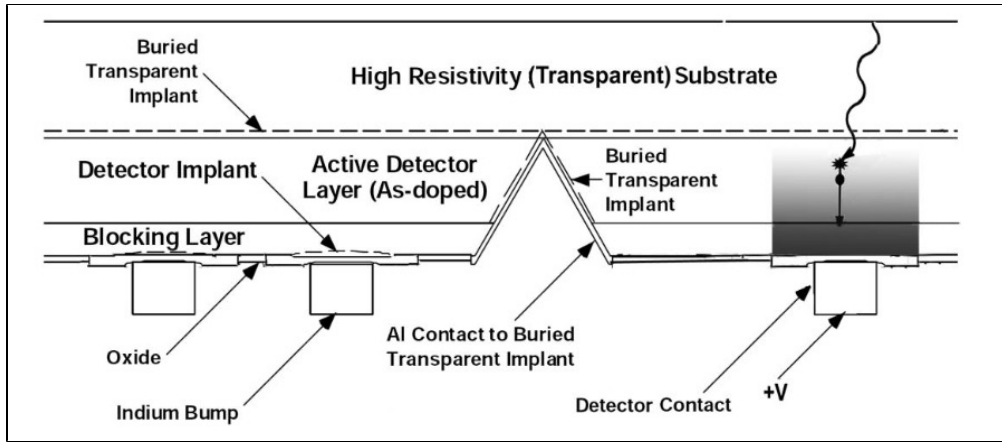
Figure 2. Side view illustration of the Si:As IBC devices

Figure credit: Love et al. 2005, Rieke et al. 2015

The MIRI Si:As IBC detectors are manufactured on a transparent substrate (top layer) that is lightly doped (high resistivity). Doping is a process that intentionally introduces impurities into a semiconductor to obtain the desired electrical properties. The next layer is 25–35 μm thick, arsenic doped, and absorbs the photons. An electric field (shaded grey) is set up across this layer using both the detector contact and the buried transparent implant. The purpose of the electric field is to draw the freed charge carriers towards the readout electronics. The next layer (bottom layer) is set up to both block thermal generated free charge carriers in the arsenic impurity level and allow photoelectrons to pass towards the readout electronics. This array is ultimately hybridized to a readout wafer by making contact to an output amplifier through the individual bump bonds of indium metal for each pixel.

References

[Glasse, A. et al. 2015, PASP, 127, 686](#)

The Mid-Infrared Instrument for the James Webb Space Telescope, IX: Predicted Sensitivity

[Hora, J. L. et al. 2008, PASP, 120, 1233](#)

Photometry using the Infrared Array Camera on the Spitzer Space Telescope

[Houck, J. R. et al. 2004, Proc. of SPIE, 5487, 62](#)

The infrared spectrograph on the Spitzer Space Telescope

[Mainzer, A. et al. 2008, Proc. of SPIE, 7021, 70210X-1](#)

Characterization of flight detector arrays for the wide-field infrared survey explorer

[Mill, J. D. et al. 1994, JSpRo, 31, 900](#)

Midcourse space experiment: Introduction to the spacecraft, instruments, and scientific objectives

[Onaka, T. et al. 2007, PASJ, 59, 401](#)

The Infrared Camera (IRC) for AKARI -- Design and Imaging Performance

[Ressler, M. E. et al. 2015, PASP, 127, 675](#)

The Mid-Infrared Instrument for the James Webb Space Telescope, VIII: The MIRI Focal Plane System

[Rieke, G. H. et al. 2004, ApJS, 154, 25](#)

The Multiband Imaging Photometer for Spitzer (MIPS)

[Rieke, G.H. 2007, ARA&A, 45, 77](#)

Infrared Detector Arrays for Astronomy

[Rieke, G. H. et al. 2015, PASP, 127, 665](#)

The Mid-Infrared Instrument for the James Webb Space Telescope, VII: The MIRI Detectors

[Van Cleve, J. E. et al. 1995, Proc. of SPIE, 2553, 502](#)

Evaluation of Si:As and Si:Sb blocked-impurity-band detectors for SIRTF and WIRE

[JWST technical documents](#)

External websites

[University of Arizona MIRI page](#)

MIRI Detector Readout Overview

JWST [MIRI detectors](#) can be read out using several different modes, each with their own advantages. They're associated with specific parameters used to define an observation.

Introduction

Parent page: [MIRI Instrumentation](#) → [MIRI Detector Overview](#)

The MIRI readout patterns fall within the framework of the general [MULTIACCUM](#) readout patterns adopted by the JWST mission so that all instruments will have similar exposure interfaces. MIRI offers 2 readout modes:

1. [SLOW](#)¹ (**NSAMPLE** = 9, t_1 = 23.890 s)
2. [FAST](#) (**NSAMPLE** = 1, t_1 = 2.775 s)

where **NSAMPLE** is the number of samples per pixel per frame and t_1 is the resulting frame time.

¹ Bold italics font style indicates parameters, parameter values, and special requirements that are set in the APT GUI.

Timing

In MULTIACCUM mode, an exposure consists of one or more identical integrations that are grouped together. The number of integrations, n_{int} , determines the exposure time as follows:

$$t_{\text{exp}} = n_{\text{int}} \times t_{\text{int}}$$

For instance, if exposing for 5 integrations with a $t_{\text{int}} = 27.75$ s, then $t_{\text{exp}} = 138.75$ s and during this exposure time there were 5 resets of the array.

Each integration is a ramp composed of a number of groups. Unlike the other instruments, each MIRI group is limited to only one frame. The value of **NSAMPLE** determines the time, t_1 , between each group (i.e., frame) up the ramp. The value of **NGROUP** determines the integration time, t_{int} , as follows:

$$t_{\text{int}} = n_{\text{group}} \times t_1$$

For example, 10 frames of FAST mode yield a $t_{\text{int}} = 10 \times 2.775 = 27.75$ s.

The optimal combination of groups and integrations depends on the specific science case. The [MIRI Best Practices](#) article explains how to optimize the number of samples, groups, integrations, and exposures.

Readout Scheme

The MIRI readout scheme for the sensor chip assembly (SCA) includes a “fast” direction (horizontal across the rows) and a “slow” direction (vertical along the columns). The detector has a total of 1024×1024 active pixels. There are 4 additional reference pixels at both the beginning and end of each row. All pixels are read out through 4 interleaved data outputs (i.e., 258×1024 pixels per output). The outputs are read simultaneously, resulting in a full-frame readout in just under 3 seconds given the sampling rate of $10 \mu\text{s}$ per pixel.

In general, every exposure begins with a read-reset. The pixels are reset by row pairs (i.e., 2 rows, 2064 pixels, at a time). For example, row 1 will be read, then row 2 will be read, then they will be reset together, then row 3 will be read, etc. This approach enables a final read immediately before resetting the SCA, and thus captures the longest possible integration time.

References

[Ressler, M. E. et al. 2015, PASP, 127, 675](#)

[The Mid-Infrared Instrument for the James Webb Space Telescope, VIII: The MIRI Focal Plane System](#)

[JWST technical documents](#)

MIRI Detector Readout Slow

JWST MIRI's "slow mode" readout pattern offers fewer detector artifacts and slightly lower detector noise than the "[fast mode](#)", making it a good choice for faint source medium-resolution spectroscopy where the sky backgrounds are very low.

Introduction

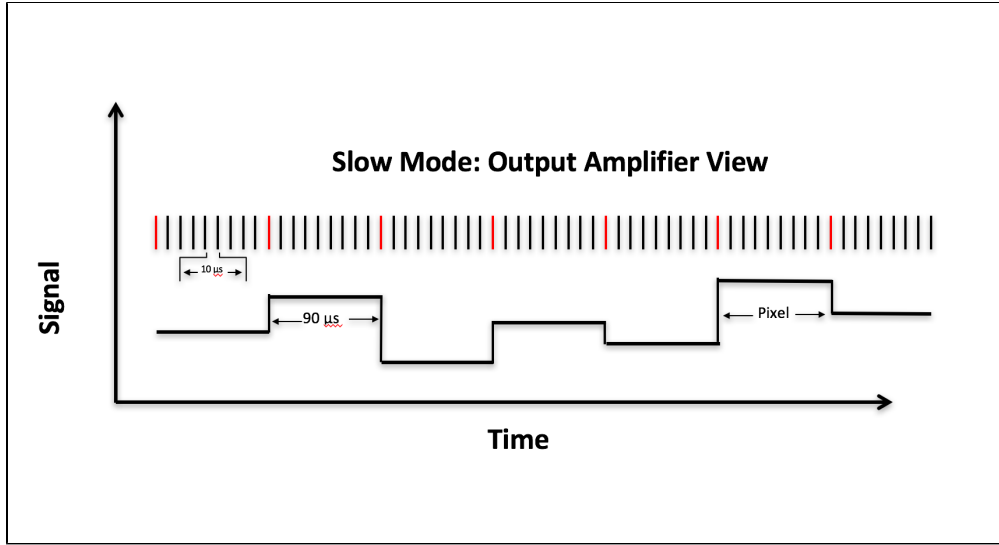
Long MULTIACCUM exposures can maximize signal-to-noise in detector noise-dominated regimes. "SLOWMode" is therefore the default readout mode for [medium-resolution spectroscopy](#) (although "FASTMode" will be available in the case of bright targets.) Just like FASTMode, $n_{\text{groups}} > 4$ is required (and $n_{\text{groups}} > 10$ is suggested) to optimize the calibration procedure, particularly cosmic-ray removal.

Following [MIRI readout terminology](#), SLOWMode obtains 9 samples of a pixel ($n_{\text{sample}} = 9$; $t_1 = 23.88992$ s). The first sample is ignored and the remaining 8 samples are averaged to output a single result before being returned to the ICDH (ISIM¹ Command and Data Handling). $n_{\text{sample}} = 9$ is a fixed parameter in SLOWMode and cannot be altered by the observer. The user can alter the number of groups (n_{groups}) and integrations (n_{int}). All groups will be stored and downloaded.

Pixel perspective

From a pixel's point of view, SLOWMode patterns starts with a read-reset frame, followed by $n_{\text{groups}} - 1$ read-only frames while integrating. The focal plane electronics (FPE) dwells at each pixel for $n_{\text{sample}} = 9$ (90 μs in total). However, the FPE will only record the final 8 measurements to allow for ample pixel settling time. Those 8 samples will be averaged in the FPE signal chain and reduced to 16 bits before being sent to the ICDH. The time between sampling each pixel is $t_1 = 23.88992$ s because the entire sensor chip assembly (SCA) is read before returning to a particular pixel. The integration ends with a read-reset after the specified number of n_{groups} ; this integration timing pattern may be repeated n_{int} times for an exposure.

Figure 2. SLOWMode sampling pattern from the output amplifier point of view



The horizontal axis is time and the vertical axis is pixel signal strength. Each signal level corresponds to a different pixel. The pixel signal levels chosen here are just for illustrative purposes, but the horizontal line highlights that the values are assumed to be relatively constant over the $80 \mu\text{s}$ of the sampling. Pixel sampling is represented by vertical black lines. Note that the FPE will only record the final 8 measurements to allow for ample settling time. The time between samples is $10 \mu\text{s}$, with the first and last sample ignored in each group.

MIRI Detector Readout Fast

JWST's MIRI "fast mode" detector readout pattern is the default readout mode for [imaging](#), [low-resolution spectroscopy](#), and [coronagraphy](#). Fast mode is only available for [subarray](#) imaging and target acquisition.

Introduction

"FASTMode" provides short MULTIACCUM exposures to maximize dynamic range and minimize noise in a background-dominated regime. "FASTMode" is the default readout mode for [imaging](#), [low-resolution spectroscopy](#), and [coronagraphy](#), and is the only mode available for [subarray](#) imaging.

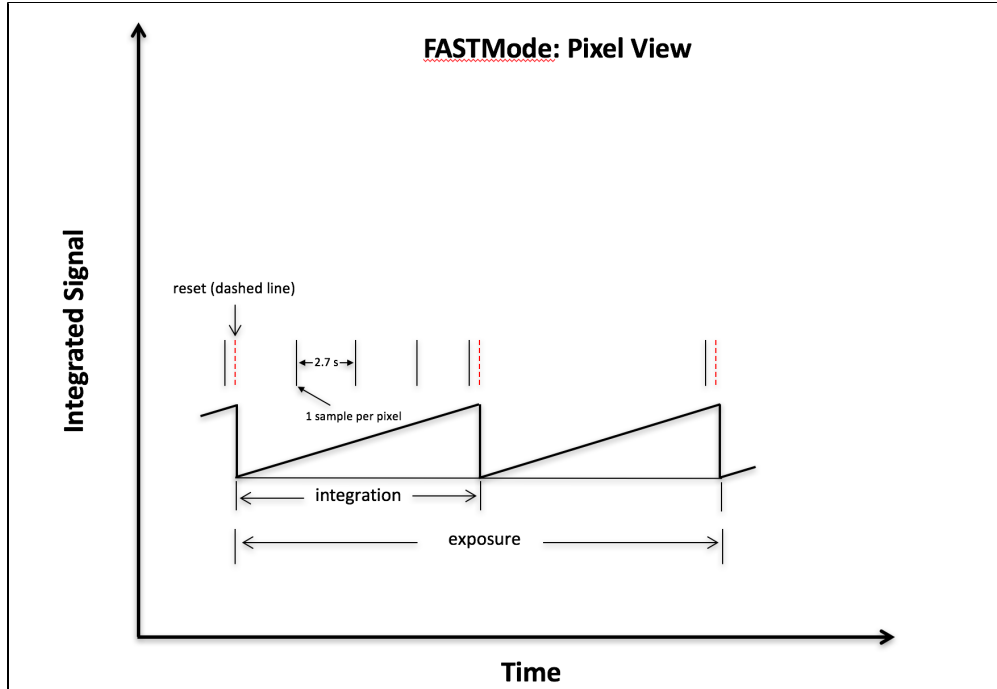
Following [MIRI readout terminology](#), "FASTMode" obtains one sample of a pixel ($n_{\text{sample}} = 1$; $t_1 = 1 \times 2.775 = 2.775$ s) and returns it to the ICDH (ISIM Command and Data Handling [ICDH]; ISIM is Integrated Science Instrument Module).

$n_{\text{sample}} = 1$ is a fixed parameter in FASTMode and cannot be altered by the observer. FASTMode currently requires a minimum of 4 groups ($n_{\text{groups}} = 4$) per integration to optimize the slope-fitting algorithm. The user can alter the number of groups (n_{groups}) and integrations (n_{int}). All groups will be stored and downloaded.

Pixel perspective

From a pixel's point of view, FASTMode patterns will start with a read-reset frame, followed by $n_{\text{groups}} - 1$ non-destructive frames while integrating. The focal plane electronics (FPE) dwells at each pixel for $n_{\text{sample}} = 1$ (10 μ s total). The time between sampling the pixel is $t_1 = 2.775$ s because the entire sensor chip assembly (SCA) is read before returning to the pixel. The integration ends with a read-reset after the specified number of n_{groups} and this integration timing pattern may be repeated n_{int} times for an exposure.

Figure 1. Sampling up the ramp FASTMode read out scheme seen from a single pixel's point of view



The sampling up-the-ramp FASTMode readout scheme, as seen from a single pixel's point of view for $n_{sample} = 1$, $ngroups = 4$, and $nint = 2$. The x-axis is time and the y-axis is voltage or signal strength. Each black vertical tick mark notes a read of the pixel and each red vertical tick mark notes a reset of the pixel. In this scheme, each reading of a pixel will have only one sample at each pixel. The time to read an entire frame is ~ 3 s and there is only one frame per integration.

MIRI Detector Performance

JWST MIRI's detector performance characteristics, such as read noise, dark current, saturation level, and persistence, were measured during ground testing.

Introduction

The [MIRI detectors](#) offer relatively low dark current, read noise, and persistence. These types of detectors were used very successfully on all 3 of the Spitzer instruments. However, compared with detectors used in the optical and near-infrared, the MIRI detectors have a number of additional calibration challenges ([Ressler et al. 2015](#), [Rieke et al. 2015](#)). Unless otherwise specified, the following values were measured during ground testing in a flight-like configuration. Because the instrument's operating temperature will not be known until on-orbit commissioning, some of these values are subject to change.

Table 1 provides a summary of measurements obtained in "CV3" cryogenic vacuum ground testing followed by more detailed descriptions of the various parameters and measurement methods.

The values in Table 1 can provide some guidance, but users should ultimately use the [Exposure Time Calculator](#) for all sensitivity calculations.

Table 1. Average MIRI detector properties measured in ground testing

Parameter	Value
Read noise (e ⁻ rms)	~14
Dark current (e ⁻ /s)	~0.2
Latent images (%)	~0.5
Full well (e ⁻)	~250,000

Pixel gain

Conversion gain, g_c (e⁻/ADU), is a fundamental parameter in detector characterization that is used to measure many detector properties, including quantum efficiency (QE), dark current, and read noise. Measuring these parameters to a higher precision is becoming more important as the demand for low signal observations increases and the scientific requirements evolve in complexity. The MIRI detectors have a gain of ~5.5 e⁻/ADU.

Dark current

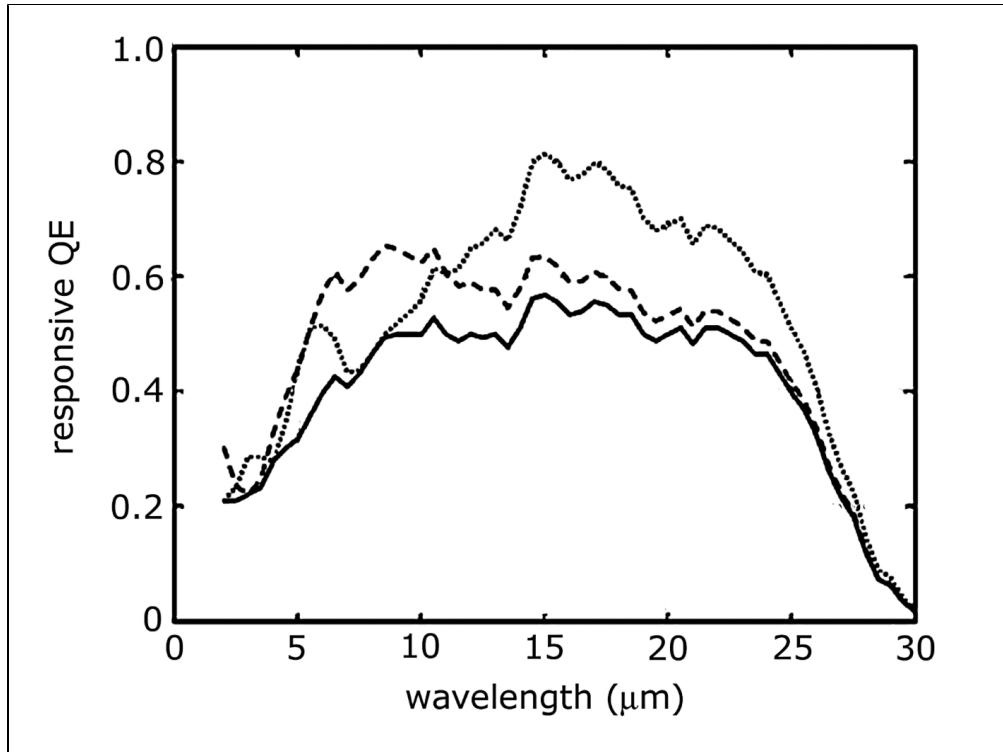
MIRI darks were obtained with the contamination control cover closed to make the instrument interior as dark as possible (although, as always, one can measure only upper limits to the true dark current, given the possibility of photon leaks). In processing the data, the first and last frames of an integration ramp were rejected, to circumvent the effects of the reset anomaly and last-frame effect. Dark currents were then determined by the slopes of the integration ramps over a 100×100 pixel region selected to avoid bad pixels. The slope calculations included all exposures in a test run; the effects of settling of the detector output artificially elevate the apparent dark current, again making the results upper limits.

Read noise

The read noise was measured by setting the detector bias voltage to 0 V; in this way, any dark or photocurrent was eliminated and only the voltage noise of the readout output amplifiers were measured. Experiments leaving the detector bias at 2 V were also performed to look at noise in the dark frames. The results were identical until the temperature climbed to ~ 7.5 K. At this point, shot noise from the dark current began to dominate the noise, and the total noise began to exceed the requirement.

Quantum efficiency (QE)

Spectral quantum efficiency in [impurity band conduction \(IBC\)](#) IR devices is often referred to as "quantum yield" since it's only possible to measure the quantum efficiency times the internal gain. The QE of the detectors cannot be measured trivially in detector array form, so it's necessary to rely on measurements of test structures included on each wafer from which the flight detectors are selected.

Figure 1. NIRCam detector quantum efficiencies

Measured responsive quantum efficiency of bare detector material (solid line). The dashed line is a computed result assuming the array has an antireflection coating applied optimized for 6 m, and the dotted line is for an AR coating optimized for 16 m. Figure credit: Rieke et al. 2015.

Persistence

Bright sources leave latents on the MIRI arrays, typically at a level of about 1% immediately after the source has been removed. The decay of these images shows multiple time constants, suggesting that there are a number of mechanisms that contribute to the effect. Further characterization of this complex behavior is needed to determine ways to correct it in the MIRI pipeline.

Imaging properties

The response of the arrays is uniform, with pixel-to-pixel variations of no more than 3% rms. The best arrays have a small proportion of inoperative pixels (either hot or dead), of order 0.1%. All measurements indicate a level close to 3% for the cross talk to the 4 adjacent pixels around one receiving signal. A plausible cause of this behavior is interpixel capacitance, although there may be secondary contributions from electron diffusion and optical effects (Rieke & Morrison 2012). In addition, at 5.6 μm there is an additional cross-like imaging artifact.

References

[Ressler, M. E. et al. 2015, PASP, 127, 675](#)

The Mid-Infrared Instrument for the James Webb Space Telescope, VIII: The MIRI Focal Plane System

[Rieke, G. H. et al. 2015, PASP, 127, 665](#)

The Mid-Infrared Instrument for the James Webb Space Telescope, VII: The MIRI Detectors

Rieke, G. H., & Morrison, J. 2012, MIRI Internal Report

Pixel Correlations in the MIRI Arrays

[JWST technical documents](#)

MIRI Detector Subarrays

JWST MIRI imaging, coronagraphic imaging, and low-resolution spectroscopy utilize a pre-defined set of 9 subarrays for different observing strategies. Each subarray configuration has its advantages and recommended uses.

Introduction

MIRI's [detector arrays](#) have the ability to read out partial frames through the manipulation of clocking patterns. Subarray readouts reduce the frame time to less than the nominal ~2.7 s per full frame. The portion of the full array that forms the subarray is read out and stored while the remaining parts of the array are reset.

Nine different subarrays are available for [imaging](#), [coronagraphic imaging](#), and [low-resolution spectroscopy](#) ([Figure 1](#)): 4 separate coronagraphs, one for high background, 3 for bright objects, and one slitless LRS spectrum. No subarrays are available for the [medium-resolution spectrometer](#).

Figure 1. Subarray locations for the MIRI imager as viewed from the telescope looking down onto the detector

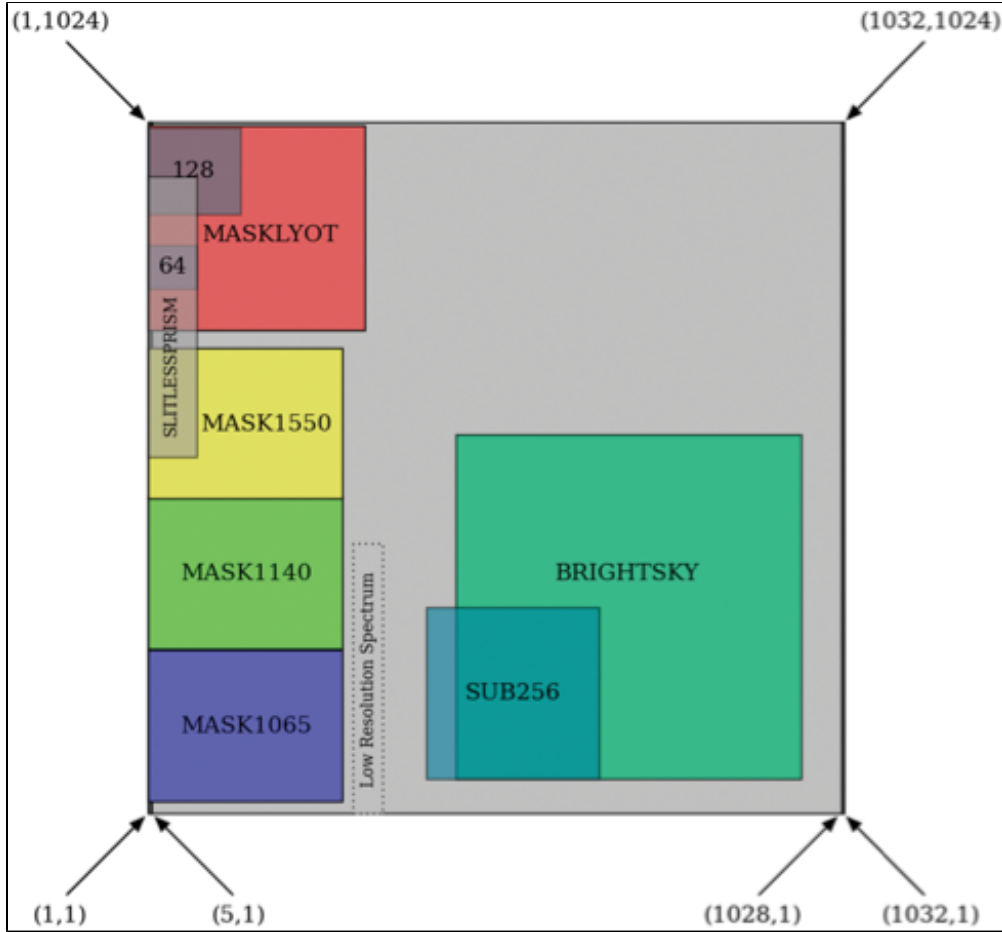


Figure credit: Ressler et al. 2015

Subarray Readout

Subarray coordinates cannot be randomly accessed so the row and column shift registers must step from the origin (1,1) to the starting subarray corner before proceeding. In other words, at the beginning of each frame read, the first two rows of the full array are accessed briefly and reset, then the 2nd pair, etc., until the subarray is reached. In the first row of the subarray, pixels on the left that are not part of the subarray are clocked through (and not digitized), then the pixels that are part of the subarray are read. Pixels to the right of the subarray are ignored by resetting the column shift register to 0 immediately after the last subarray pixel. This pattern is repeated through all the rows contained within the subarray. The rows after the subarray are stepped through quickly and reset as were the rows before the subarray. It follows that subarrays are slower the farther they are from the left hand edge of the array.

This readout scheme drove the orientation of the imager array, since it is advantageous to have the fastest subarrays located within the coronagraph. It also means that it takes exactly the same amount of time to read a 256×256 subarray starting at (257,257) as it does to read a 512×256 subarray starting at (1,257); the

only difference is the amount of data passed to the solid state recorders and the ground. Other issues that determined the subarray location included: the ability to utilize reference pixels, minimizing dead time from the clocking to access the first pixel, bad pixels on the array, and the best imaging location for the optics.

For more efficient subarray operation, a “burst mode” clocks through the left-hand columns at 5 times the normal speed. In the first row of the region of interest (ROI), pixels on the left that are not part of the ROI are clocked through (and not digitized), after which the pixels that are part of the ROI are read. Pixels to the right of the ROI are ignored by resetting the column shift register to zero (recall the special shift register definition) immediately after the last ROI pixel. This pattern is repeated through all the rows contained within the ROI. The rows after the ROI are stepped through quickly and reset as are the rows before the ROI.

Imaging

Imaging subarrays are generally used to image bright sources or bright backgrounds without saturating the detector. The size for the high background subarray is determined by the readout time governing the dynamic range needed to image faint sources in the background glow of the Orion Nebula region. Sizes for bright object subarrays are determined by the saturation limits needed to observe known radial velocity planet host stars.

Table 1. MIRI imaging subarray characteristics

Subarray	Size in pixels (rows × columns)	First row corner	First column corner	Usable size	Frame time*
FULL ¹	1024 × 1032	1	1	74" × 113"	2.775 s
BRIGHTSKY	512 × 512	51	457	56.3" × 56.3"	0.865 s
SUB256	256 × 256	51	413	28.2" × 28.2"	0.300 s
SUB128	128 × 136	889	1	14.1" × 14.1"	0.119 s
SUB64	64 × 72	779	1	7" × 7"	0.085 s

* Frame times are calculated for **FAST** mode only. **SLOW** mode readout will only be available for the FULL array.

¹ Bold italics font style indicates parameters, parameter values, and special requirements that are set in the APT GUI.

Coronagraphic imaging

In coronagraphic imaging, each subarray is tied to a specific filter. The subarray choice is therefore hidden from the user in the JWST [Astronomer's Proposal Tool \(APT\)](#).

Table 2. MIRI coronagraphic imaging subarray characteristics

Subarray	Filter	Size in pixels (rows × columns)	First row corner	First column corner	Size	Frame time*
MASK1065	F1065C	224 × 288	19	1	24" × 24"	0.240 s
MASK1140	F1140C	224 × 288	245	1	24" × 24"	0.240 s
MASK1550	F1550C	224 × 288	467	1	24" × 24"	0.240 s
MASKLYOT	F2300C	304 × 320	717	1	30" × 30"	0.324 s

* Frame times are calculated for [FAST](#) mode only. [SLOW](#) mode readout will only be available for the FULL array.

Low-resolution spectroscopy

The size of the slitless prism subarray is determined by the number of pixels needed to cover the 5–14 μm low-resolution spectrometer spectrum in the dispersion direction and provide adequate sky observations for background subtraction in the spatial direction.

Table 3. MIRI low-resolution spectroscopy imaging subarray characteristics

Subarray	Size in pixels (rows × columns)	First row corner	First column corner	Frame time*	Notes
FULL	1024 × 1032	1	1	2.775 s	Slit spectrum
SLITLESSPRISM	416 × 72	529	1	0.159 s	Slitless spectrum

* Frame times are calculated for **FAST** mode only. **SLOW** mode readout will only be available for the FULL array.

MIRI Operations

The operational facts and features of JWST's [MIRI](#) define how its observatory-level capabilities can be applied for science.

The operational capabilities include:

- [MIRI Target Acquisition Overview](#)
- [MIRI Dithering Overview](#)
- [MIRI Mosaics Overview](#)
- [MIRI Parallel Observations](#)

MIRI Target Acquisition Overview

The JWST [Mid-Infrared Instrument \(MIRI\)](#) provides target acquisition (TA) capabilities for the [low-resolution spectroscopy](#), [medium-resolution spectroscopy](#), and [coronagraphic imaging](#) modes.

Target acquisition (TA) is a procedure that centroids a source and places it accurately within an aperture, region of interest (ROI), or [subarray](#). The filters available for MIRI TA are F560W, F1000W, F1500W and FND. TA procedures are discussed in the context of the observatory in memos and reports by [Gordon & Meixner \(2008\)](#), [Meixner et al. \(2006\)](#), [Nelan et al. \(2005\)](#), and [Meixner et al. \(2004\)](#).

TA procedures within the [Astronomer's Proposal Tool \(APT\)](#) are available for:

- [Low-resolution spectroscopy](#)
- [Medium-resolution spectroscopy](#)
- [Coronagraphic imaging](#)
- [Imaging](#)

References

[Gordon, K. & Meixner, M., 2008, JWST-STScI-001407 \(PDF\)](#)

Mid-Infrared Instrument (MIRI) Target Acquisition Strategies and Use Cases

[Gordon, K., 2008, JWST-STScI-001347 \(PDF\)](#)

Mid-Infrared Instrument (MIRI) Low Resolution Target Acquisition for Faint Sources

Meixner, M. et al., 2004, STScI-JWST-TM-2004-0018A

Mid-Infrared Instrument (MIRI) Target Acquisition Requirements and Strategies

Nelan, E. et al., 2005, STScI-JWST-R-2005-0001

JWST Science Instrument Target Acquisition Concepts

[JWST technical documents](#)

MIRI Imaging Target Acquisition

In general, target acquisition (TA) is not required for imaging observations with MIRI. For the special case of high precision photometry of [bright sources](#), such as time-series observations (TSOs), TA may be desired. The MIRI imager can be used to obtain high precision photometry of bright sources that may be useful for time-series observations (TSOs). Given the high stability and photometric precision required for such observations, target acquisition (TA) is usually recommended to ensure that the target is very accurately placed in the nominal pointing position for the required subarray. This is particularly important for repeated observations, where different exposures will be combined.

TA for MIRI Imaging is not currently supported, but is expected to be available in the future.

Related links

[JWST User Documentation Home](#)
[MIRI Bright Source Limit](#)
[MIRI Filters](#)
[MIRI Subarrays](#)
[MIRI Time Series Observations \(TSOs\)](#)

References

[JWST technical documents](#)

MIRI Coronagraphic Imaging Target Acquisition

The JWST MIRI [coronagraphic imaging](#) mode requires target acquisition procedures.

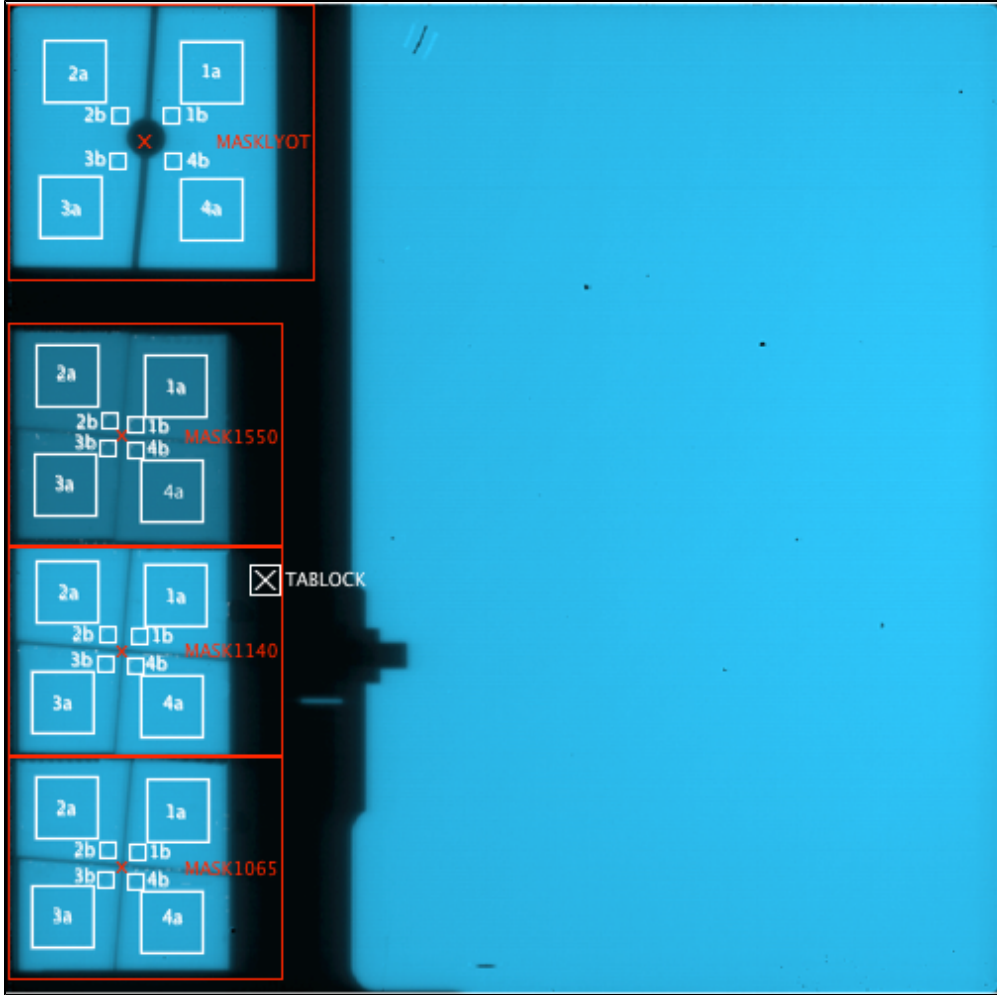
Introduction

MIRI [coronagraphic imaging](#) observations require precise and accurate positioning of a bright source at the location of maximum attenuation by the [Lyot spot mask or 4QPMs](#): for the 4QPM, this is the apex between the 4 quadrants; for the Lyot, it is at the center of the occulting spot.

For the 4QPM, the required absolute accuracy of placing a star at the apex is 10 mas (1- σ per axis), but the ultimate positioning of the object on the mask requires a repeatable precision of 5 mas (1- σ per axis).

For the Lyot coronagraph, the pointing accuracy and precision are less stringent due to the $3 \lambda/D$ spot size. This relaxes the requirements to 22.5 mas. The neutral density filter requirements for the target acquisition have ensured that Vega can be observed in the coronagraph's subarray mode.

Figure 1. Footprints of the coronagraph masks on the MIRI imager focal plane



The 32×32 pixel region labeled TABLOCK is the location for placing the coronagraphic target when the telescope is initially slewed to the target. The larger 4 white boxes in each coronagraphic subarray indicate the initial coronagraphic target acquisition (TA) regions of interest (ROIs; 64×64 pixels) in each quadrant (e.g., 1a, 1b). The smaller 4 white boxes, closer to the center of each coronagraphic subarray, indicate the second coronagraphic TA ROIs in each quadrant (e.g., 1b, 2b). Reference points are indicated by a cross. The background image is an FM flood-illuminated image taken in F1065C.

Two effects make the TA process complex:

1. For the 4QPM coronagraphs, the phase mask can distort the image of a star close to its center and undermine the accuracy of the centroid determination; and
2. The detector arrays have latent images that could mimic planets or other exciting astronomical phenomena if, during the centroiding process, the target star is placed close to those latent images.

These effects would make adequate TA very difficult at the nominal JWST offsetting accuracy specifications described above. Fortunately, it is projected that small angle offsets up to $20''$ are expected to be accurate to 5 mas (1σ per axis). Simulations of the centering accuracy on the coronagraph using the projected performance and a fiducial distance of $2''$ from the coronagraph center indicate a scatter of ~ 7 mas (rms) and average centering errors of 2–4 mas. The details depend on the particular strategy, i.e., whether one utilizes a

single position for target acquisition, or uses more than one to acquire additional information about the pointing. None of the strategies quite reaches the desired centering performance for the 4QPM coronagraphs (the Lyot is much more relaxed in this area), so further optimization is expected during commissioning.

The observer will choose one of the 4 quadrants on the subarray for the initial TA. Due to the fact that spacecraft roll orientations are very restricted, the observer is allowed to select which of the 4 locations within the coronagraphic subarray to perform the target acquisition (TA). He or she will also have the option to repeat the entire observation, but with the TA performed within a region of the subarray that is diagonally opposed to the original TA. This ability ensures that the observer can mitigate confusion in the science images from persistent images from the TA process.

Software processing requirements for the target acquisition image include a flat field of the 64×64 pixel ROI surrounding the coronagraph sweet spots of which there will be 16 in the baseline strategy. A centroiding algorithm for the targets in the sweet spots is outlined in [Lajoie et al. \(2014a\)](#). These exposures will be normally short; therefore, cosmic rays should not be an issue.

Lyot coronagraph target acquisition

For Lyot coronagraphy, the point source will be placed in one of the 4 target acquisition ROIs in the Lyot coronagraphic field of view (MASKLYOT, 304×320 pixels). The readout times for each subarray in **FAST**¹ mode is 0.324 s. Given the brightness of the sources, it is possible that target acquisition will leave latent images in the target acquisition regions.

To mitigate confusing the latent image with a nearby faint source, it will be optimal to take two coronagraphic observations: one with target acquisition using the 1st ROI and one with target acquisition using a second 2nd ROI that is diagonally opposed to the first one. Any persistence images will be different between the two coronagraphic observations allowing for discrimination of faint sources and these persistence images.

Discrimination is possible since the observations taken with the 1st target acquisition region will not have persistence images in the 2nd target acquisition region, and the persistence images are variable in time such that the persistence images in the 1st ROI will have decayed by the time the 2nd ROI target acquisition observations are done. The goal is to have the ROIs located as close to the center of the Lyot spot (radius = 2.4"; Renouf 2006) as possible without being affected by any edge effects. The accuracy of spacecraft small angle maneuvers from 2"-20" is expected to be <~4-6 mas ([Lajoie et al. 2014a](#)).

¹ Bold italics font style indicates parameters, parameter values, and special requirements that are set in the APT GUI.

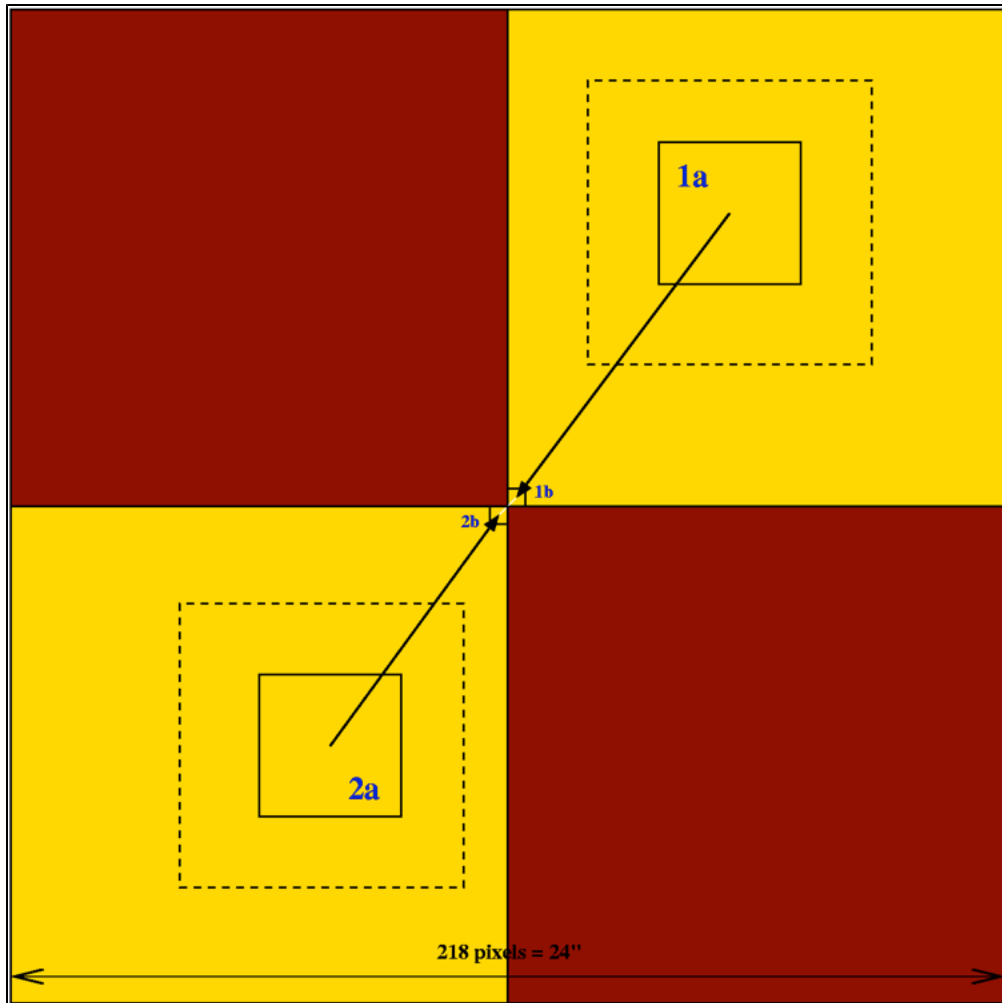
4QPM target acquisition

There are several possible approaches to 4QPM TA, which are discussed in detail by [Lajoie et al. \(2012, 2013, 2014a, 2014b\)](#). The baseline approach to 4QPM TA, described below, assumes that offset slew accuracy is consistent with NASA's pre-launch estimates. First, a TA ROI, approximately in the center of one of the 4 quadrants, is used to locate the target. A spacecraft move is then used to place the source in a second TA ROI

closer (~1"-5") to the center of the coronagraphic field of view. The target is located again and then moved into the center of the coronagraphic field of view (i.e., at the apex of the 4QPM) using the most precise small spacecraft move. For 4QPM coronagraphy, there are specific readout subarrays defined for each mask (MASK1550, MASK1140 & MASK1065; each 216 × 216 pixels).

Due to persistence images, this procedure can be done twice where the center is approached from two directions, 180° apart. The persistence images will be different between the 2 coronagraphic observations allowing for discrimination of faint sources and persistence images. Such discrimination is possible because the observations taken with the 1st target acquisition ROIs (1a & 1b in Figure 2) will not have latents in the 2nd target acquisition ROIs (2a & 2b in Figure 2), and the latents are variable in time such that the latents in the 1st ROIs will have decayed by the time the 2nd ROIs target acquisition observations are completed. The “a” ROIs are 64 × 64 pixels and the “b” ROIs are 16 × 16 pixels. The uncertainty in the position of the source in the “b” ROIs is approximately 20 mas (8" spacecraft move from “a” to “b” ROIs). Thus, the sizes of the “b” subarrays (0.77" × 0.77") are large enough so the source will always be in the “b” ROIs after the “a” target acquisition.

Figure 2. Target acquisition with the 4QPM



The large dashed boxes are where the regions of interest (ROIs) for the “a” coronagraphy 4QPM target acquisition should be located and the small solid boxes are the approximate proposed locations. The required spacecraft offsets are shown using arrows.

References

- Lajoie, C.-P., Soummer, R., Hines, D., 2012, JWST-STScI-003065,
Simulations of Target Acquisition with MIRI Four-Quadrant Phase Mask Coronagraph (II).
- Lajoie, C.-P., Hines, D., Soummer, R., and The Coronagraphs Working Group, 2013, JWST-STScI-003546,
Simulations of MIRI Four-Quadrant Phase Mask Coronagraph (III): Target Acquisition and CCC Mechanism Usage

Lajoie, C.-P., Soummer, R., Hines, D., and The Coronagraphs Working Group, 2014a, JWST-STScI-003712:, Simulations of Target Acquisition with MIRI Four-Quadrant Phase Mask Coronagraph (IV): Predicted Performances Based on Slew Accuracy Estimates

Lajoie, C.-P., Soummer, R., Hines, D.C., & Rieke, G.H. 2014b,
Simulations of JWST MIRI 4QPM Coronagraphs Operations and Performances, SPIE, 9143, 91433R

[Rieke, et al. 2006 \(JWST-STScI-001012\)](#).

Soummer, R., Hines, D.C. & Perrin, M. 2012, JWST-STScI-003063,
Simulations of Target Acquisition with MIRI Four-Quadrant Phase Mask Coronagraph (I).

Soummer, R. et al. 2014, JWST-STScI-004141,
Coronagraphic Operations Concepts and Super-Template Definition for the Astronomer's Proposal Tool.

[JWST technical documents](#)

MIRI LRS Slit Target Acquisition

The JWST [MIRI low resolution spectrometer \(LRS\)](#) slit requires target acquisition (TA) for point sources.

Introduction

Calibration of MIRI LRS data requires accurate knowledge of the location of the target on the detector. To this end, users are advised to perform a target acquisition (TA) as part of their observation; this ensures that the target is placed with sub-pixel accuracy at the nominal slit or slitless position.

LRS slit and slitless modes each have their own custom TA procedure. For slit spectroscopy, TA is particularly important to avoid slit losses and wavelength calibration issues that can arise from off-center source placement. For slitless mode, TA ensures that different observations of the same target always fall onto the same detector pixels. Note that for LRS slitless observations, TA is mandatory. When using the slit, it is highly recommended but optional. Mapping observations of extended targets may not need TA.

Pointing performance of the telescope is described in [these articles](#).

TA target

Typically the science target is used for TA. However, the procedure can also be carried out with a nearby bright star, which should be within 60" from the science target. Use of an offset target may be desirable if the science target is not a point source, or if the TA exposure would add an unacceptably long overhead to the observation (see "TA exposures" below).

TA filters

As for the other MIRI modes, LRS has [4 filters](#) available for TA:

- F560W
- F1000W
- F1500W
- FND (a neutral density filter)

Users should always use the JWST [Exposure Time Calculator \(ETC\)](#) to help choose the best TA filter for their science.

TA exposures

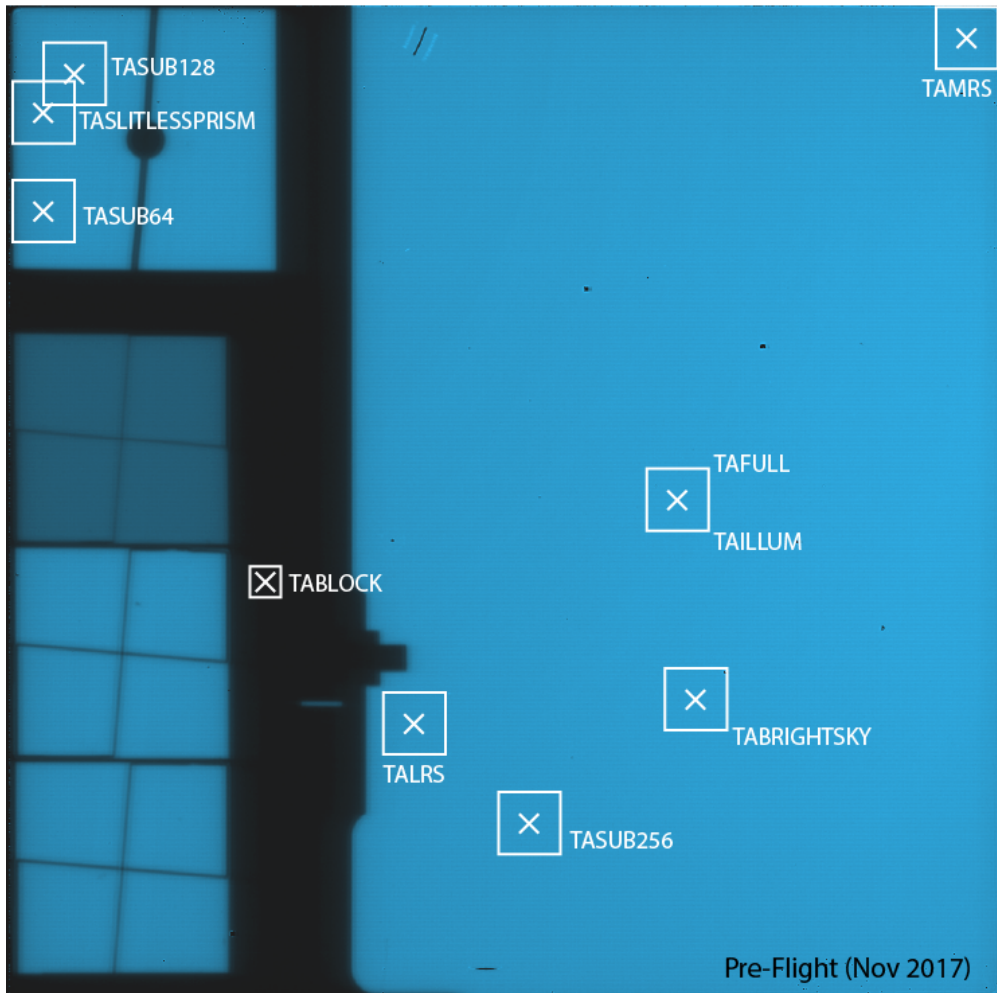
TA exposure settings should be calculated using the ETC. The exposure should be carried out in a single integration, with a limit of approximately 1,000 s to avoid too many cosmic ray hits. The TA integration can contain a maximum of 99 groups. If sufficient SNR cannot be reached on the science target in this time (SNR > 20 is recommended), use of an offset target should be considered. The minimum number of groups in an integration for TA is 3.

TA can be carried out in FAST or FASTGRPAVG mode. In the latter, each group represents the average of 4 reads; this mode can be used to increase the exposure time of the TA exposure without exceeding the 99 groups limit.

LRS region of interest

The LRS slit target acquisition requires a region of interest (ROI) located as close to the LRS slit as possible. A 64 x 64 pixel ($\sim 7 \times 7''$) ROI is located in the imager portion of the field of view, near the slit location. Note that the ROI is not a detector subarray; TA exposures are performed with FULL¹ array read mode.

Figure 1. MIRI field of view showing LRS slit target acquisition region of interest



The box labeled "TALRS" in the imager region is where the LRS slit target acquisition 64 x 64 pixel region of interest (ROI) is located. The reference point is taken to be the midpoint of this ROI.

¹ Bold italicics font style indicates parameters, parameter values, and special requirements that are set in the APT GUI.

LRS slit TA sequence

The target acquisition procedure begins with placing the TA target, i.e., the science target itself or a suitable offset star, in the ROI in the imager field of view. An exposure is taken according to the setup specified by the user in APT. This exposure must be limited to a single integration. A dedicated algorithm will perform centroiding on the resulting image to identify the location of the target centroid at sub-pixel accuracy. The images taken in TA will be available to the user.

After the centroiding algorithm has completed, the filter wheel will move from the TA filter position to the P750L location, which is the double prism. Following the filter wheel move, the telescope will perform a small angle maneuver (SAM) to place the target into the slit at the required position (at the slit centre, or the first nod position). The first science exposure can begin.

References

[Gordon, K., 2008, JWST-STScI-001347 \(PDF\)](#)

Mid-Infrared Instrument (MIRI) Low Resolution Target Acquisition for Faint Sources

[JWST technical documents](#)

MIRI MRS Target Acquisition

The [MIRI medium-resolution spectrometer \(MRS\)](#) requires target acquisition (TA) procedures for point sources, and may be used with or without target acquisition for extended sources.

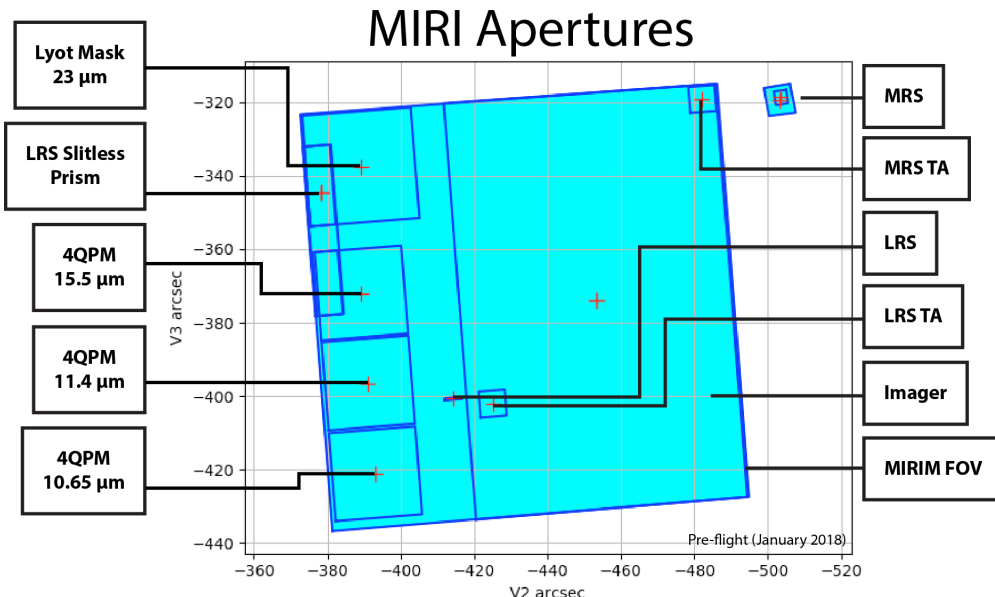
Observations with the [MIRI medium-resolution spectrometer \(MRS\) integral field unit \(IFU\)](#) may wish to use a target acquisition (TA) procedure in order to refine the blind [JWST pointing accuracy](#) prior to science observations, especially at the shortest wavelengths. This TA improves the pointing precision of the MIRI MRS to 90 mas (1σ radial), which is approximately the half width of a slice at the shortest wavelength. TA may be performed with the [FND](#), [F560W](#), [F1000W](#) and [F1500W](#) filters. Note that the TA centroiding procedure loses accuracy if the pixels are saturated so a brightness limit (Table 1) must also be considered for the target.

Table 1. Saturation limits for MRS target acquisition for sources of a given blackbody temperature

Filter	300 K hard saturation (Jy)	1,000 K hard saturation (Jy)
FND	4.7	5.5

The MRS target acquisition sequence uses a region of interest (ROI) on the MIRI imager located as close to the MRS as possible to minimize offset distances after target acquisition. As illustrated in the figure below, a 64×64 pixel ROI is defined at the upper right corner of the MIRI imager.

Figure 1. Target acquisition box in MIRI MRS FOV



The MIRI field of view is shown with the MRS TA box identified. The V2 and V3 axes represent a spherical coordinate system measured in arcsec that maps to the sky, where the coordinates are Euler angles. See [MRS coordinate frames](#) for further detail.

Science targets that are spatially extended should not be used for target acquisition. Instead, bright point sources can be used for target acquisition if they are within 16" of the science target (the TA source position must not require a greater than 40" spacecraft move to put the science target in the IFU; see [Target Acquisition Considerations](#)). This requires accurate coordinates for both the science target and the TA source.

Additionally, some observations with the MRS either do not require or cannot perform target acquisition. Examples of such observations are spectral mapping of extended objects, measurements of faint diffuse targets, or [dedicated background observations](#). APT 25.4.2 now supports this no-TA mode.

MIRI Bright Source Imaging Target Acquisition

High precision imaging photometry of [bright sources](#) with the JWST [Mid-Infrared Instrument \(MIRI\)](#), such as time-series observations (TSOs), require target acquisition to ensure repeatable measurements. The MIRI imager can be used to obtain high precision photometry of bright sources that may be useful for time-series observations (TSOs). Given the high stability and photometric precision required for such observations, target acquisition (TA) is usually recommended to ensure that the target is very accurately placed in the nominal pointing position for the required subarray. This is particularly important for repeated observations, where different exposures will be combined.

TA for MIRI imaging is not currently supported, but will be available in the future.

MIRI LRS Slitless Target Acquisition

The JWST MIRI low resolution spectrometer mode requires target acquisition when operated in slitless mode for time series spectroscopy. A dedicated procedure has been defined for the mode.

Introduction

The MIRI LRS is used in slitless mode exclusively for time series observations (TSOs). Such high precision spectrophotometric observations place specific demands on the instruments to achieve the highest precision; precise placement of the target to its nominal pointing position and precise repeatability of this placement are critical to account for any inter- or intra-pixel response variations. As for LRS in slit mode, the wavelength calibration also requires accurate knowledge of the source position.

We describe in this section the target acquisition (TA) procedure for slitless LRS observations. TA is mandatory for such observations.

The [Exposure Time Calculator](#) should always be used to determine the optimal filter choice and exposure settings for Target Acquisition. [Dedicated documentation pages](#) are available describing how to perform TA calculations in the ETC for MIRI.

TA target

Typically the science target is used for TA. However, the procedure can also be carried out with a nearby bright star, which should be within 60" from the science target. Use of an offset target may be desirable if the science target is not a point source, or if the TA exposure would add an unacceptably long overhead to the observation.

TA filters

As for the other MIRI modes, LRS slitless has [4 filters](#) available for TA:

- F560W
- F1000W
- F1500W
- FND (a neutral density filter)

TA exposures

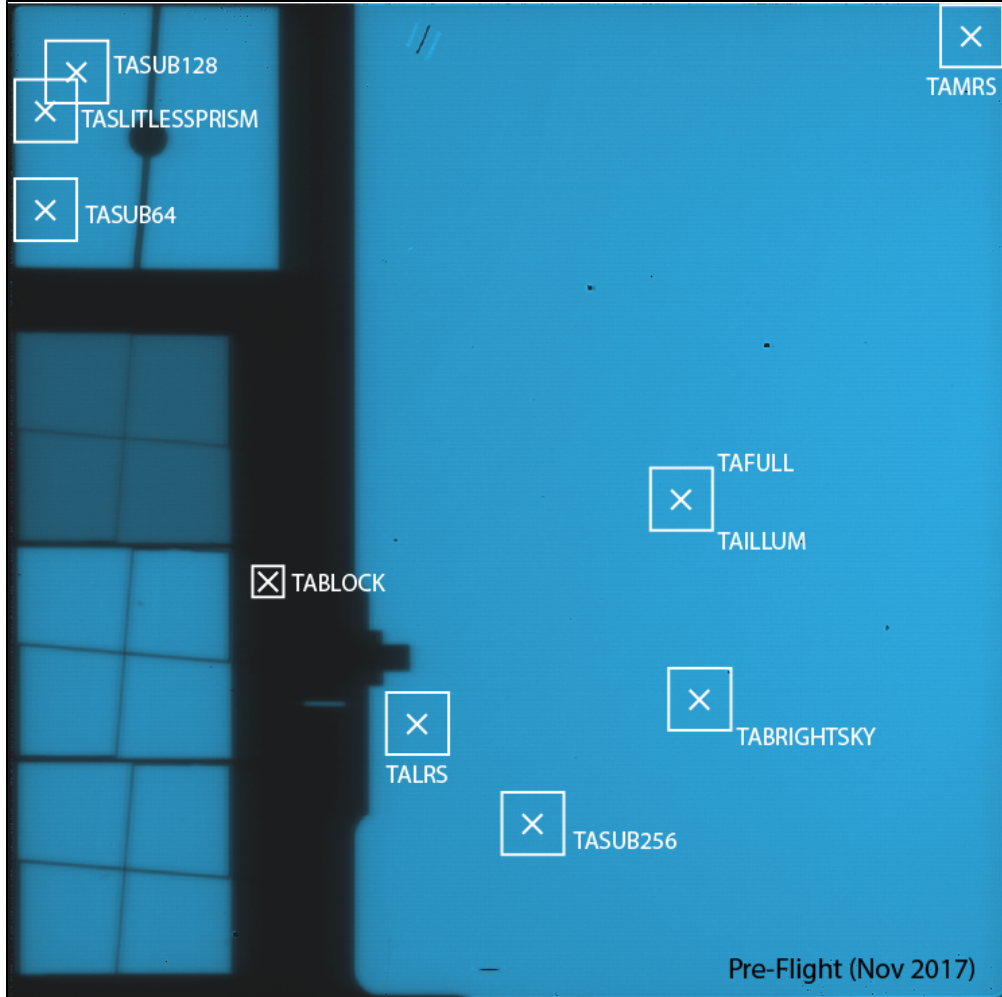
TA exposure settings should be calculated using the ETC. The exposure should be carried out in a single integration, with a limit of approximately 1000 seconds to avoid too many cosmic ray hits. The maximum number of groups in a TA integration is 99. If sufficient SNR cannot be reached on the science target in this time (SNR > 20 is recommended), use of an offset target should be considered. The minimum number of groups in an integration for TA is 3.

TA will typically be performed with the FAST readout mode. However, the FASTGRPAVG mode is also available to achieve longer integration times within the 99 group limit. In FASTGRPAVG, each group represents the average of 4 reads.

LRS slitless subarray and region of interest

The MIRI LRS uses the SLITLESSPRISM subarray for its slitless time series observations, to increase the dynamic range of the mode and allow observations of brighter targets. The [frame read time](#) in FAST mode is 0.16 seconds, compared with 2.77 seconds for a FULL frame read. To avoid switching between FULL and SLITLESSPRISM array configurations on short timescales, which can cause undesirable detector artefacts, the TA region of interest (ROI) defined for LRS slitless TA is part of the SLITLESSPRISM subarray itself, occupying 64×64 pixels of the subarray ($\sim 7 \times 7''$) and positioned such that overlap with the science spectrum is minimal. The location of the TA ROI is shown in Figure 1.

Figure 1. MIRI field of view showing LRS slitless target acquisition region of interest



The box labeled "TASLITLESSPRISM" in the imager region is where the LRS slitless target acquisition 64×64 pixel region of interest (ROI) is located. The reference point is taken to be the midpoint of this ROI.

TA sequence

Before the TA sequence is begun, the target is placed behind the focal plane metering structure, to avoid saturation. The filter wheel then moves to the TA filter, specified by the user in the proposal template. Once the filter has been acquired, the target is moved into the SLITLESSPRISM subarray, and placed in the ROI defined for target acquisition. An exposure is taken with the user-specified exposure setup, the centroiding algorithm calculates the precise location of the target, and the offset to the pointing location for the science exposure is computed.

The telescope then performs a small angle maneuver (SAM) to place the target at the nominal pointing position, ready for science. Before performing the filter wheel move to acquire the double prism disperser, a second exposure is taken with the same setup parameters as the TA exposure, to allow the user to verify the

target positioning during data analysis. Following this exposure, the filter wheel will be moved to the double prism location, and the science exposure will begin.

Both the TA image and the verification image will be available to the observer.

Related links

[JWST User Documentation Home](#)

[JWST Time-Series Observations](#)

[MIRI-Specific Time-Series Observations](#)

[MIRI LRS Recommended Strategies](#)

[MIRI Target Acquisition Overview](#)

[JWST Pointing Performance](#)

References

[JWST technical documents](#)

MIRI Dithering Overview

The JWST [Mid-Infrared Instrument \(MIRI\)](#) provides dithering capabilities for the [imaging](#), [low-resolution spectroscopy](#), [medium-resolution spectroscopy](#), and [coronagraphic imaging](#) modes for optimal sampling, bad pixel mitigation, and background subtraction.

Related links

[JWST User Documentation Home](#)

[JWST Astronomers Proposal Tool Overview](#)

[MIRI Coronagraph Imaging Dithering](#)

[MIRI Imaging Dithering](#)

[MIRI LRS Dithering](#)

[MIRI MRS Dithering](#)

[JWST Dithering Overview](#)

References

[Arendt, R. G., et al., 2000, ApJ, 536, 500](#)

Dithering Strategies for Efficient Self-Calibration of Imaging Arrays

[JWST technical documents](#)

MIRI Imaging Dithering

The JWST MIRI [imaging](#) mode provides dither templates for both point and extended sources.

Introduction

See also: [MIRI Imaging Recommended Strategies: Dithering](#)

This article goes into detail on all the available dither patterns for MIRI Imaging. Recommendations on which pattern to choose for your observation can be found in [MIRI Imaging Recommended Observing Strategies](#).

The JWST MIRI [imaging](#) pixel scale, 0.1" per pixel, provides Nyquist sampling at 7 μm . At longer wavelengths, the point spread function (PSF) is oversampled; at shorter wavelengths, it is undersampled.

Dithering patterns for shorter wavelengths will both oversample the PSF and remove bad pixels.

At wavelengths longer than 15 μm , thermal self-emission, mostly from the primary mirror and sun shield, dominate the total [background](#). Since the telescope thermal emission is not expected to be constant, self-calibration may be needed for observations at these wavelengths in order to self-consistently solve for the background and flat field (Meixner, 2006). Therefore, some dither patterns for longer wavelengths will both optimize self-calibration and remove bad pixels.

Types of dither patterns

[JWST dithering](#) allows for moves specific to MIRI imaging. Dither patterns for observation can be implemented in the [Astronomer's Proposal Tool \(APT\)](#) with the JWST APT MIRI imaging template.

The following types of dither patterns will be offered in APT for MIRI Imaging¹:

1. [CYCLING](#)¹
2. [4-Point-Sets](#)
3. [REULEAUX](#)
4. [2-Point](#)

Additionally, there are two limited access options:

1. [Sparse](#)
2. [No dithering](#)

A list of all dither options and details about them is available in [Table 2](#) at the end of this article.

Lists of all MIRI imaging dither pattern points are compiled in this .csv format file: [MIRI_Imaging_Dithers.csv](#). Each list contains a set of offset positions from a fiducial point that satisfy various sampling requirements. These fiducials are typically the center of the array or subarray as specified in the Science Instrument Aperture File (SIAF).

For subarrays and filters, different dither patterns may be necessary depending on the selected

[subarray](#) and [filter](#).

¹ Bold italics font style indicates parameters, parameter values, and special requirements that are set in the APT GUI.

CYCLING

The CYCLING pattern consists of 311 points. The CYCLING pattern is a random Gaussian pattern designed to be flexible. Observers will be able to choose (1) the starting position in the dither table and (2) the number of dither positions to maximize observational flexibility. For observers who request more than 311 dither positions, the CYCLING pattern will wrap so that the 312th dither position is the same as the 1st position. Each set of 4 consecutive dithers provides complete ½ pixel sampling.

4-Point-Sets

Centering of the 4-point dither patterns on the BRIGHTSKY and FULL arrays.

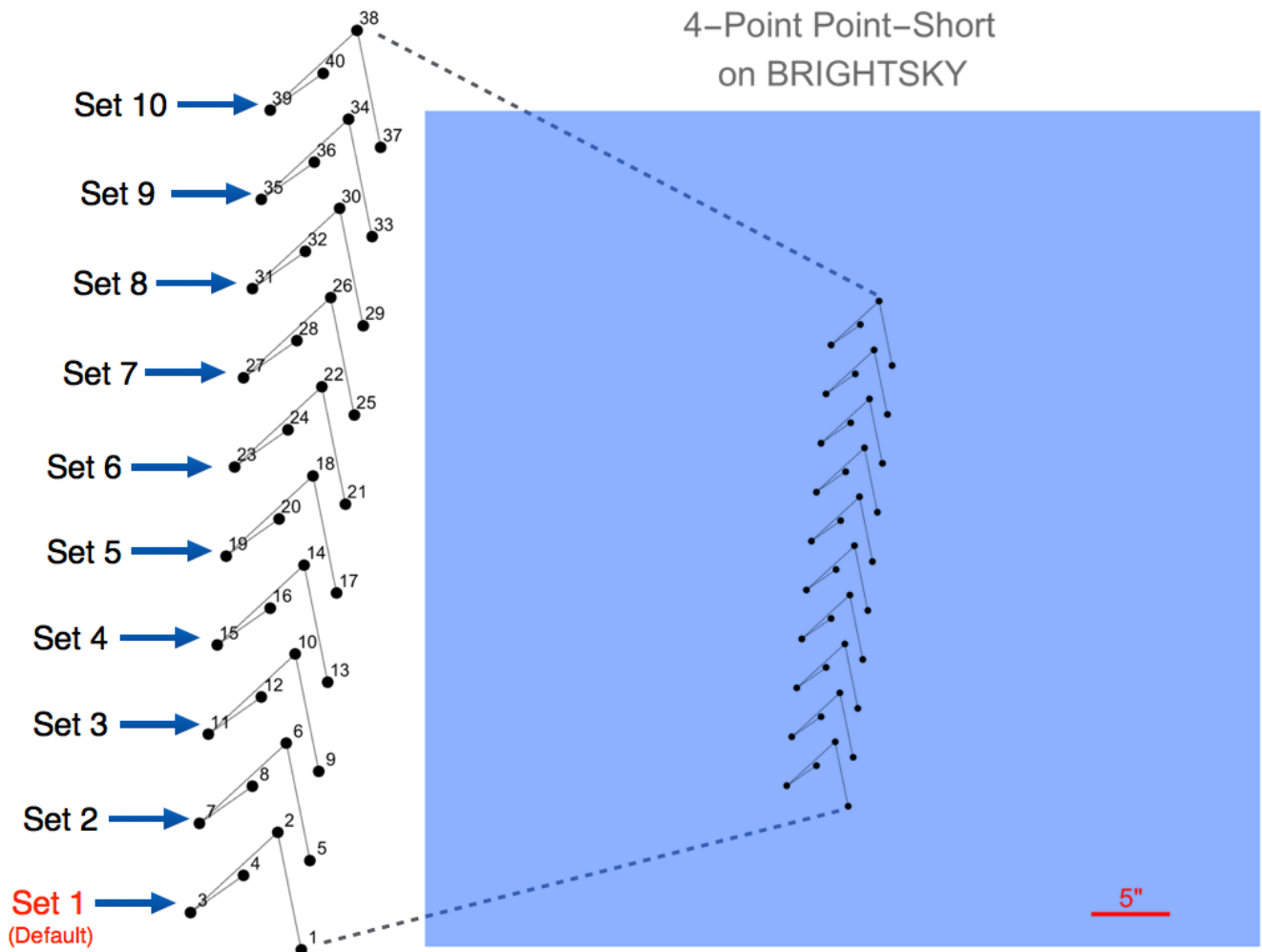
The user must select a Starting Set and Number of Sets in APT for the FULL and BRIGHTSKY arrays. It is important to note that for these dither patterns, the single set of 4-point dithers that is centered on the subarray of choice is going to be Starting Set = 5 or Starting Set = 6. A Starting Set = 1 will start the 4-point pattern towards the bottom of the subarray

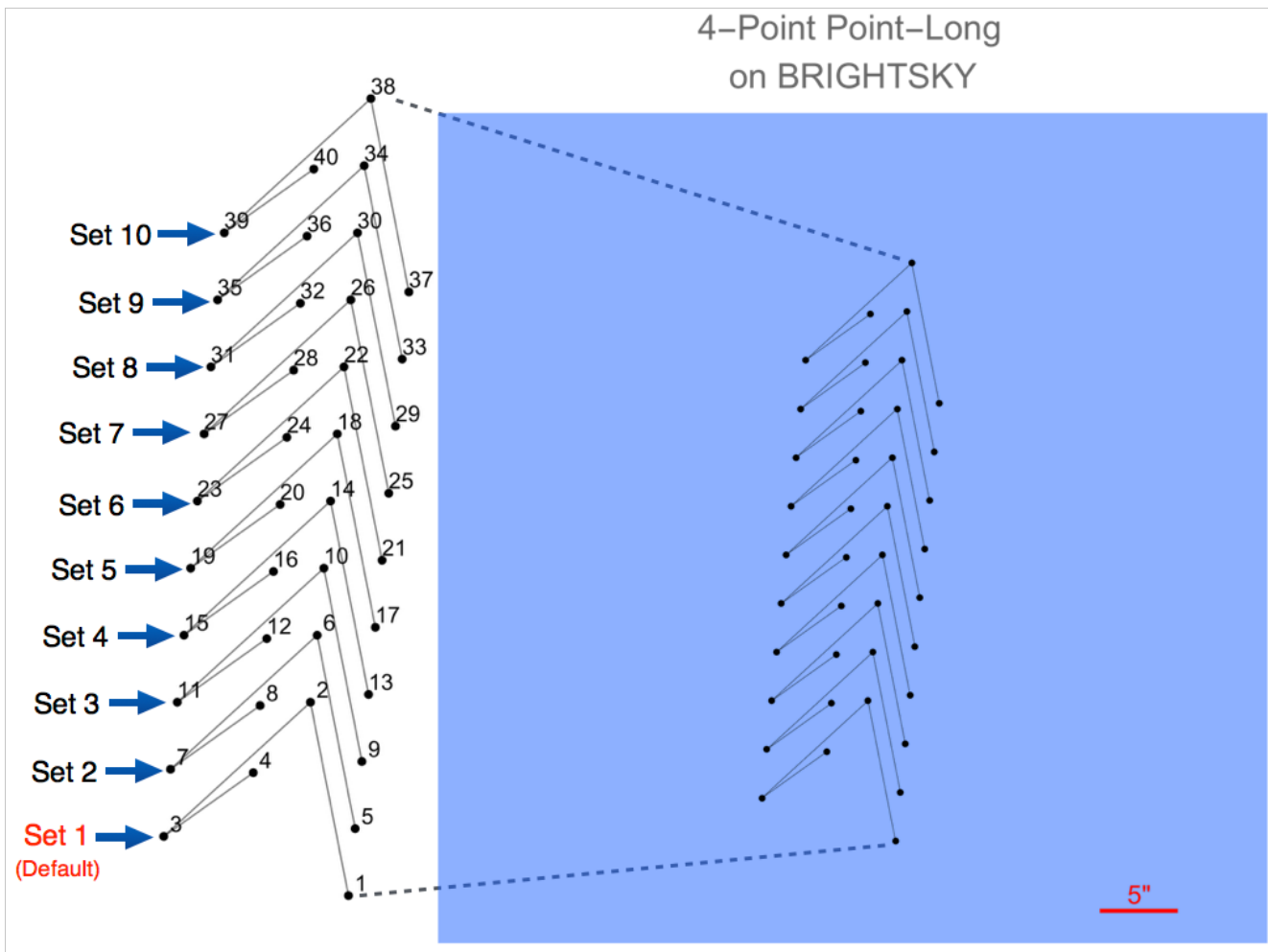
The 4-Point Sets dither patterns subsample the PSF, allow for simple background subtraction, and minimize the effects of bad rows or columns. For observations using [BRIGHTSKY](#) and [FULL arrays](#), users can select between 1-10 repeating sets of 4-point patterns with the Number of Sets parameter in APT. There is also a mirror parity option in APT, Direction, that moves the pattern from the bottom right to upper left if the option NEGATIVE is selected; the default option for Direction is POSITIVE which is illustrated in figure 1. Note the first set (Set 1 in figures 1 and 3) starts near the bottom of the subarray; this set is the default Starting Set in APT. For all other subarrays, only one 4-point set is allowed.

4-point point source patterns

Depending on the wavelength of the observation, APT will automatically select a 4-point pattern optimized for shorter (5.6–11.3 microns) or longer wavelengths (12.8–25.5 microns). Figure 1 illustrates all 10 sets of the 4-point pattern on the BRIGHTSKY subarray for the long and short wavelength 4-point point source patterns.

Figure 1. Four-point point source dither pattern

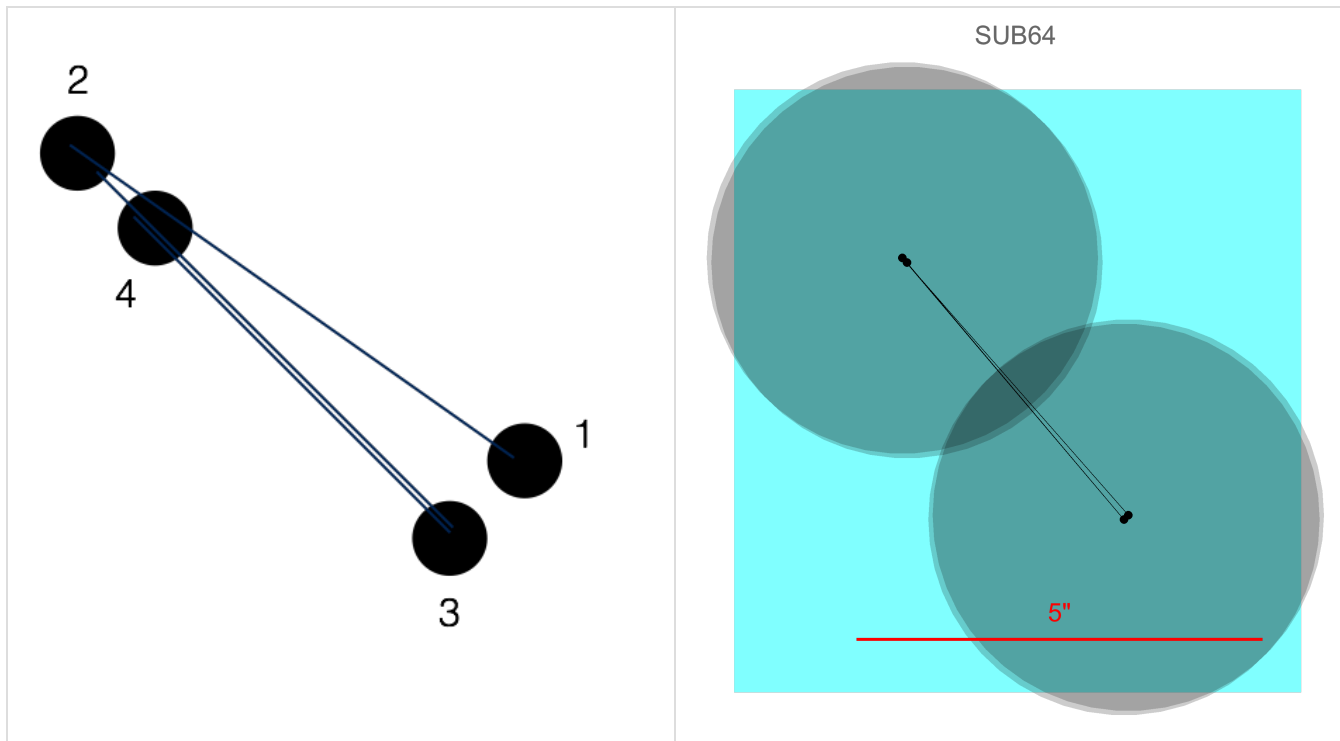




Top: four-point point source dither pattern for short wavelengths (5.6–11.3 microns)

Bottom: four-point point source dither pattern for long wavelengths (12.8–25.5 microns)

Due to the small size of the SUB64 array, a modified 4-point point-source pattern for long wavelengths ($\lambda \geq 12.8 \mu\text{m}$) is used. Note that because the SUB64 is so small, this pattern still does not entirely fit observations at 25.5 μm for PSF diameters at $6\lambda/D$ (see Figure 2 below).



Top: Four-Point Point-Long-64 pattern

Bottom Left: 4-Point Point-Long-64 pattern on the SUB64 array showing PSF diameters for 6/D at 21 m.

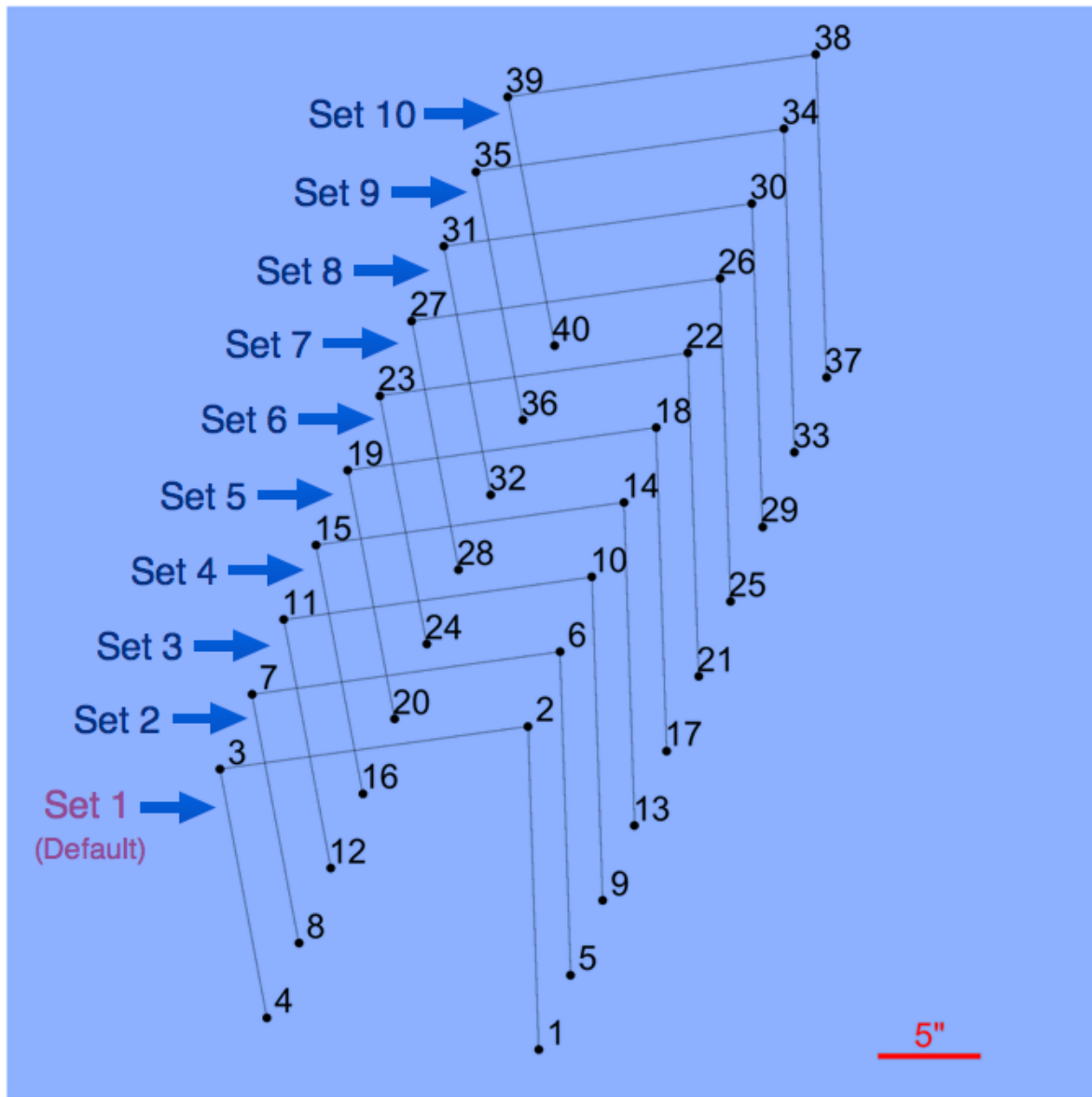
Bottom Right: 4-Point Point-Long-64 pattern on the SUB64 array showing PSF diameters for 6/D at 25.5 m. Note that the PSFs do not fit on the SUB64 at this wavelength.

Four-point extended source pattern

The 4-point Extended-Source pattern is optimized for moderately extended objects by maximizing the dither distance and minimizing slew time (keeping dithers to <20"). The figure below show what the four-point extended-source pattern looks like.

Figure 7A: Four-Point Extended-Source dither pattern

4–Point Extended on BRIGHTSKY



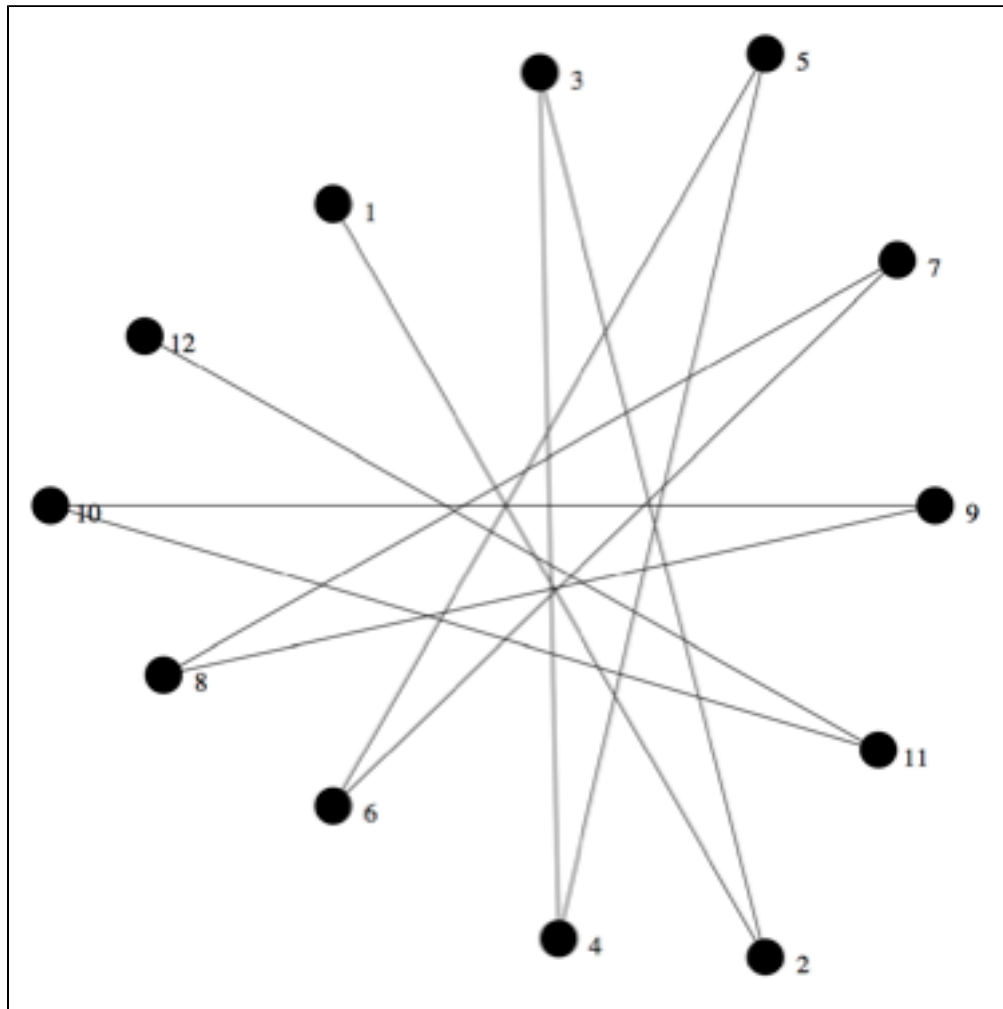
The Four-Point Extended-Source dither pattern.

REULEAUX

The 12-point REULEAUX triangle dither pattern is suitable for observing unresolved (or barely resolved) sources. The triangle is constructed by connecting the vertices of an equilateral triangle with circular arcs,

which maximizes the distance and minimizes the slew time between consecutive pointings. This pattern minimizes the number of exposures that place the peak of the point spread function (PSF) along same row or column of the detector and minimizes the effects of persistence from bright sources.

Figure 8. 12-point REULEAUX pattern showing the order of the offsets



Each REULEAUX pattern is constrained by competing requirements to:

1. Fit the pattern on the subarray
2. Ensure that the distance between successive pointings is $\geq 6\lambda/D$
3. Account for the observatory blind pointing uncertainty of 1" (1σ , each axis)

Recommended wavelength use matrix for REULEAUX pattern for SUB128 and SUB64

The only restriction on the REULEAUX pattern in APT is that the LARGE REULEAUX cannot be performed on the SUB64 array, as the pattern does not physically fit on the subarray. Otherwise, the user can select any size REULEAUX pattern for any subarray at any wavelength.

However, it is important to note that the SUB128 and SUB64 subarrays may not be able to contain observations at longer wavelengths (see Figure 9 showing the MEDIUM size REULEAUX pattern on the SUB64 array in the top graphic, and, in the bottom graphic, the PSF diameters for $6\lambda/D$ at 25.5 μm).

Table 1 shows the matrix of patterns that fit for a given filter and subarray combination (note: "Large" indicates LARGE, MEDIUM, and SMALL patterns can fit, "Medium" indicates LARGE and MEDIUM patterns can fit, "Small" indicates only SMALL patterns can fit, and "None" indicates no REULEAUX pattern can fit for that given subarray/filter combo). Note the table contains columns that account for a 1σ and 3σ pointing error.

Table 1. Matrix of patterns that fit for a given filter and subarray combination

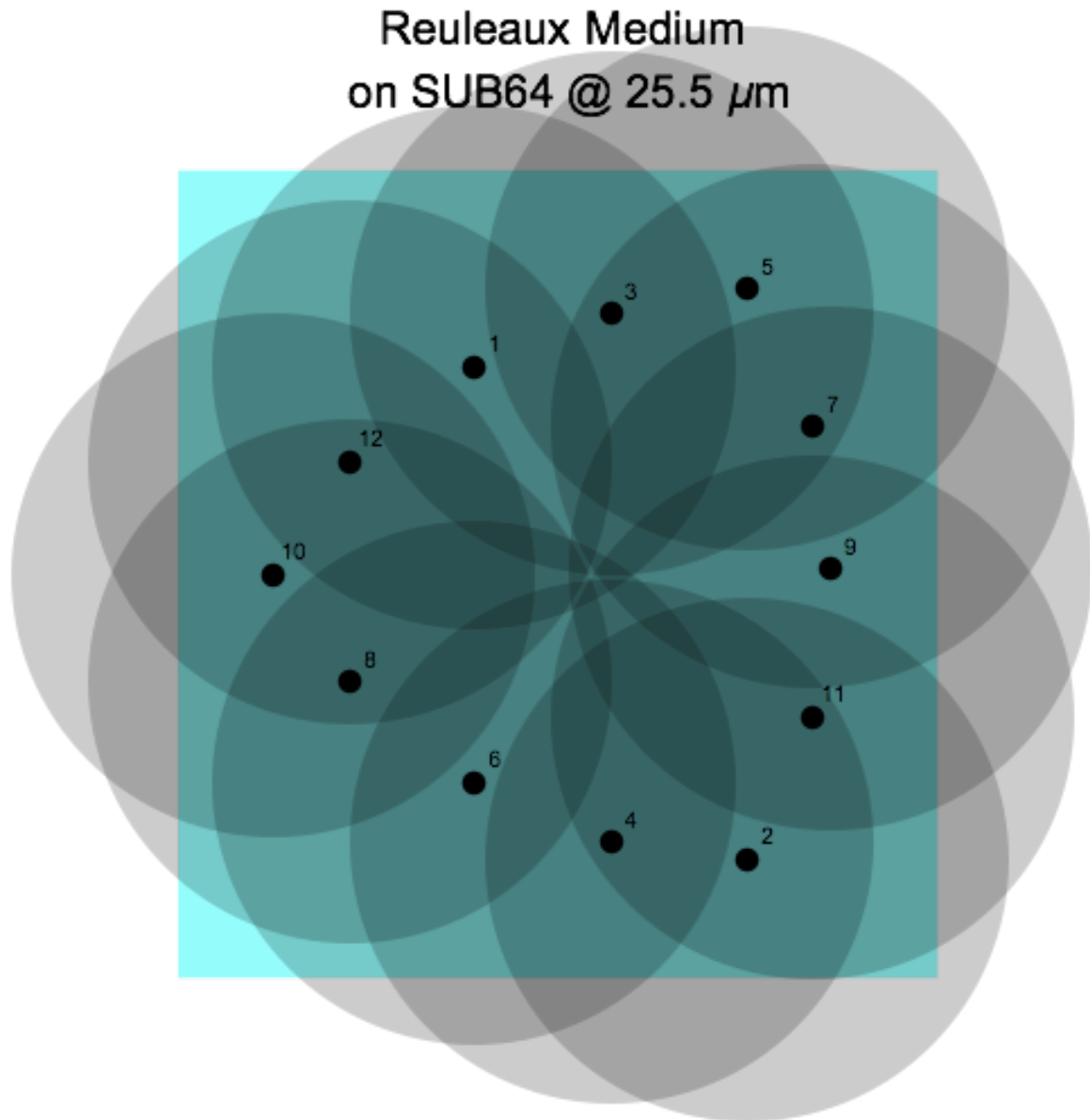
λ Central (μm)	PSF Diameter @ $6\lambda/D$ (pixels)	Sub 128	Sub 128 with 1σ Error	Sub 128 with 3σ Error	Sub 64	Sub 64 with 1σ Error	Sub 64 with 3σ Error
5.6	9.693	Large	Large	Medium	Medium	Small	Small
7.7	13.328	Large	Large	Medium	Medium	Small	Small
10	17.309	Large	Large	Medium	Small	Small	None
11.3	19.559	Large	Large	Medium	Small	Small	None
12.8	22.155	Large	Large	Medium	Small	Small	None
15	25.963	Large	Medium	Medium	Small	Small	None
18	31.156	Large	Medium	Medium	Small	Small	None
21	36.349	Medium	Medium	Medium	Small	None	None
25.5	44.138	Medium	Medium	Medium	None	None	None

Alternate Table 1. Matrix of patterns that fit for a given filter and subarray combination

Cycle 1 Call for Proposals

λ Central (μm)	PSF Diameter @ $6\lambda/D$ (pixels)	Sub 128	Sub 128 with 1σ Error	Sub 128 with 3σ Error	Sub 64	Sub 64 with 1σ Error	Sub 64 with 3σ Error
5.6	9.693	LARGE MEDIUM SMALL	LARGE MEDIUM SMALL	LARGE MEDIUM	LARGE MEDIUM	SMALL	SMALL
7.7	13.328	LARGE MEDIUM SMALL	LARGE MEDIUM SMALL	LARGE MEDIUM	LARGE MEDIUM	SMALL	SMALL
10	17.309	LARGE MEDIUM SMALL	LARGE MEDIUM SMALL	LARGE MEDIUM	SMALL	SMALL	None
11.3	19.559	LARGE MEDIUM SMALL	LARGE MEDIUM SMALL	LARGE MEDIUM	SMALL	SMALL	None
12.8	22.155	LARGE MEDIUM SMALL	LARGE MEDIUM SMALL	LARGE MEDIUM	SMALL	SMALL	None
15	25.963	LARGE MEDIUM SMALL	LARGE MEDIUM	LARGE MEDIUM	SMALL	SMALL	None
18	31.156	LARGE MEDIUM SMALL	LARGE MEDIUM	LARGE MEDIUM	SMALL	SMALL	None
21	36.349	LARGE MEDIUM	LARGE MEDIUM	LARGE MEDIUM	SMALL	None	None
25.5	44.138	LARGE MEDIUM	LARGE MEDIUM	LARGE MEDIUM	SMALL	None	None

Figure 9. MEDIUM size REULEAUX pattern on the SUB64 array showing PSF diameters



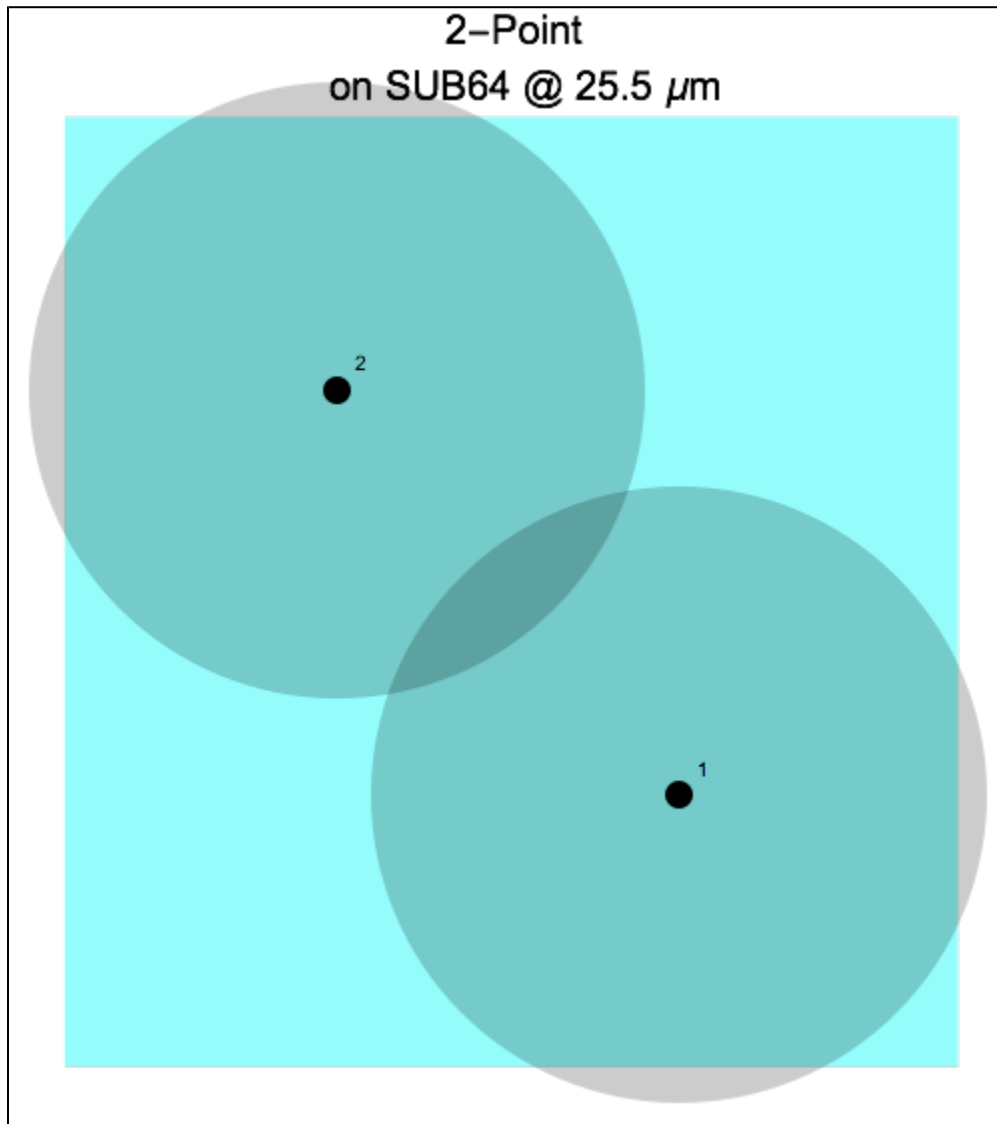
Top: MEDIUM size REULEAUX pattern on the SUB64 array showing PSF diameters for 6/D at 25.5 m. Note that the PSFs do not fit on the SUB64 at this wavelength.

Bottom: Same figure as above, but showing PSF diameters for 6/D at 7.7 m—the longest wavelength that fits entirely on the SUB64 at 6/D.

2-Point

The 2-Point dither option provides two exposures separated on the array and avoids placing the peak of the PSF along the same row or column. This pattern (1) allows for simple background subtraction and (2) minimizes the effects of bad pixels, rows, and columns. The two points for this dither are recorded in the [MIRI_Imaging_Dithers.csv](#) file.

Figure 10. Two types of *2-Point* dither patterns for the *SUB64* arrays



2-point pattern on the SUB64 array showing PSF diameters for 6/D at 25.5 m. Note that the PSFs do not fit on the SUB64 at this wavelength.

SPARSE-CYCLING

This limited access pattern, enables the observer to specify (consecutive) positions from the cycling lookup table using a list.

For example, the observer will be able to enter a string like this:

“1,3,6-10,23, 29-55”

This limited access pattern requires strong justification in the proposal, and pre-approval prior to use in APT.

NO DITHER

No dithering is only allowed for [time-series observations \(TSOs\)](#) and otherwise has limited access which will require strong justification in the proposal, and pre-approval prior to use in APT.

MIRI imaging dithers .csv file

The file [MIRI_Imaging_Dithers.csv](#) is a compilation of all dithers. Each list of points is the set of offset positions from a fiducial point that satisfy various sampling requirements. These fiducials are typically the center of the array or subarray as specified in the Science Instrument Aperture File (SIAF).

MIRI Coronagraph Imaging Dithering

Dithering is not allowed for JWST MIRI coronagraphic observations.

MIRI LRS Dithering

The JWST MIRI [low-resolution spectroscopy](#) mode provides dither templates for both point and extended sources.

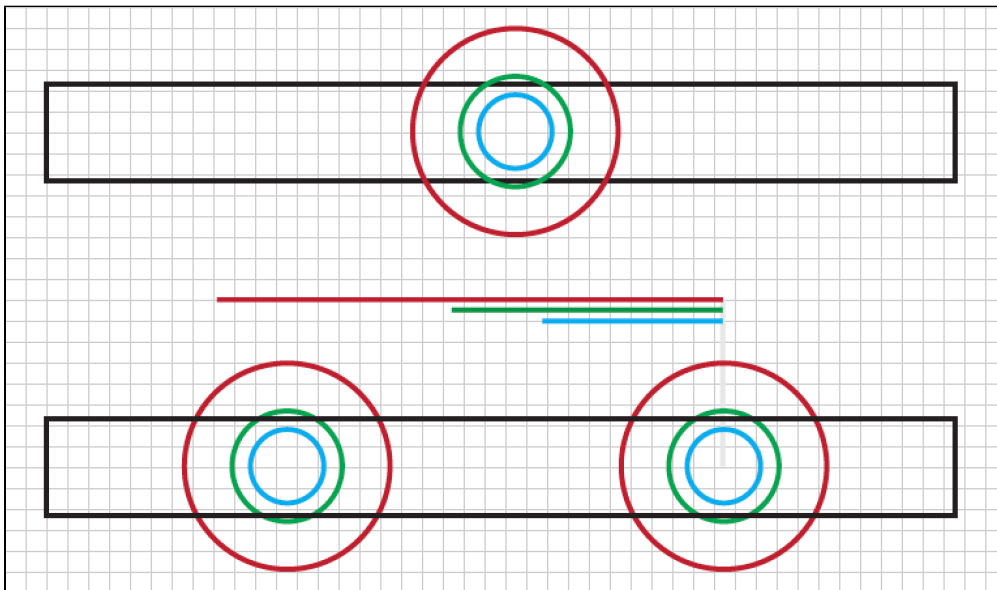
Dithering is possible for MIRI [low-resolution spectroscopy \(LRS\)](#) slit observations only. (It is disabled in the [slitless mode](#)). Dithers can mitigate the effects of bad pixels, and obtain sub-pixel sampling and background observations.

[JWST dithering](#) allows for moves specific to MIRI LRS. Dither patterns for observations are implemented in the [Astronomer's Proposal Tool \(APT\)](#) using the [JWST APT MIRI LRS template](#).

Two dither patterns will be offered in this mode:

1. **ALONG SLIT NOD**¹ is designed for compact sources, and uses a 2-point "nod" where a point source is dithered between positions that are located approximately one-third and two-thirds of the way along the slit direction.
2. **MAPPING** has a customizable number of slit positions and offsets in the slit-parallel and slit-perpendicular directions, allowing users to ensure that a source is well-mapped and that sufficient background data is obtained.

Figure 1. MIRI LRS dither patterns for *MAPPING* and *ALONG SLIT NOD* modes



Top: In MAPPING mode, the source is centered in the slit and an observer can specify a regular grid of slit positions (including the number of positions and their offsets) around the central pointing.

Bottom: In Along Slit Nod mode, the source is observed at 2 positions in the slit: at 15 pixels and 30.5 pixels from the edge of the slit. Blue, green and red circles indicate the first dark Airy ring for 5, 7.7 and 14 μm , respectively. Blue, green and red lines indicate the radius of the 4th dark Airy ring for 5, 7.7 and 14 μm , respectively.

¹ Bold italic font style indicates parameters, parameter values, and special requirements that are set in the APT GUI.

References

[Gordon , K. et al. 2015, PASP, 127, 953](#)

The Mid-Infrared Instrument for the James Webb Space Telescope, X: Operations and Data Reduction

[JWST technical documents](#)

MIRI MRS Dithering

JWST's Mid-Infrared Instrument ([MIRI](#)) medium-resolution spectrometer ([MRS](#)) has dithering options available in 2- and 4-point patterns for both point sources and extended sources, with options for channel-specific optimization.

Introduction

See also: [MIRI Medium Resolution Spectroscopy](#)

The MIRI medium-resolution spectrometer (MRS) is spatially undersampled at all wavelengths, particularly at the shortest wavelengths within each channel (see [Figure 1](#)). Ideal sampling of a point spread function (PSF) should provide at least 2 samples per spatial resolution element in order to avoid loss of information.

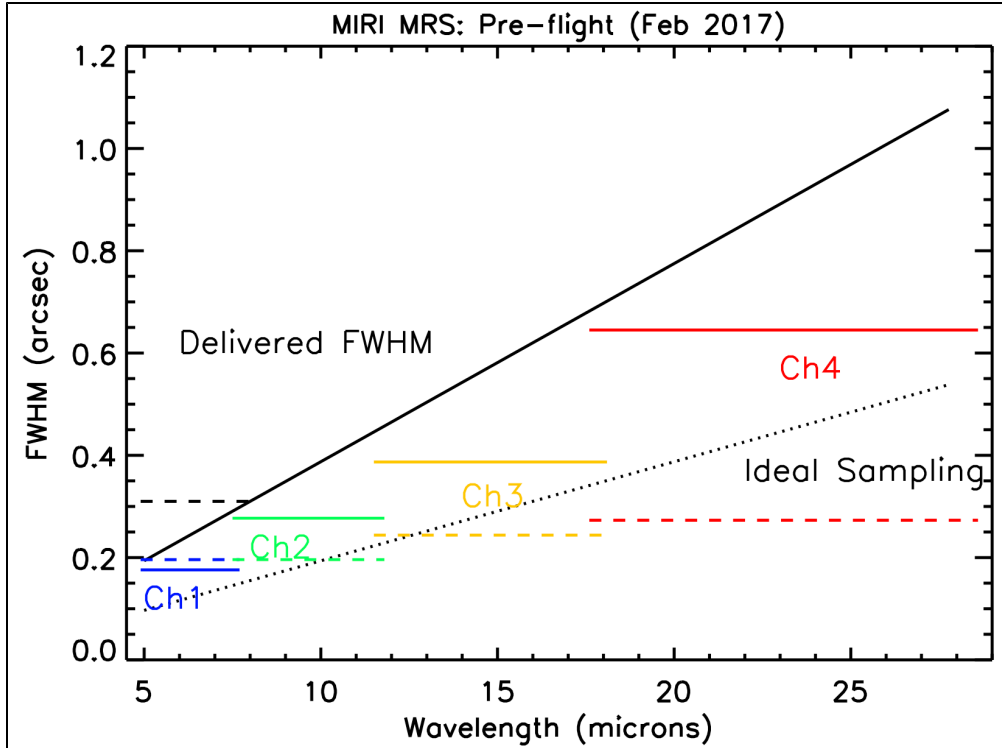
Dithering is therefore necessary to (1) improve this spatial sampling, (2) mitigate bad pixels by sampling the image with redundant detector locations, and (3) allow for sufficient PSF separation that pairs of exposures can be used as background exposures for each other.

The MRS consists of [4 separate IFUs](#), each with their own pixel size and slice width (see [Table 1 on the MRS main page](#)), that observe a scene simultaneously. These sizes have been chosen so that specific offsets can be applied to the telescope pointing that will simultaneously produce half-integer changes in the sampling for all 4 channels. An offset in the across-slice direction of 0.968" for instance corresponds to a move of 5.5, 3.5, 2.5, and 1.5 slices, respectively, in channels 1-4. Similarly, offsets in the along-slice direction of 2.058" correspond to nearly half-integer offsets of 10.50, 10.50, 8.43, and 7.54 pixels, respectively, in channels 1-4.

Note

January 2018: As of APT version 25.4.2, only the point source patterns and the extended source ALL pattern described below are available. The extended source patterns optimized for specific channels will be available in an upcoming release of APT.

Figure 1. MRS spatial resolution and ideal vs. actual sampling as a function of wavelength



Spatial FWHM of an isolated point source as a function of wavelength based on simulations and ground tests data. The solid black line indicates the FWHM measured from reconstructed data cubes; the dashed black line illustrates that the reconstructed FWHM in the along-slice direction is constant and approximately equal to 0.31'' shortward of 8 m. The dotted black line represents the ideal sampling, defined as one half the nominal FWHM. The solid and dashed colored lines illustrate the actual sampling of the MRS optics in the across-slice and along-slice directions respectively in each of the 4 channels (blue, green, yellow, red lines). MRS is roughly a factor of 2 undersampled at the shortest wavelengths in each channel.

Available dither patterns

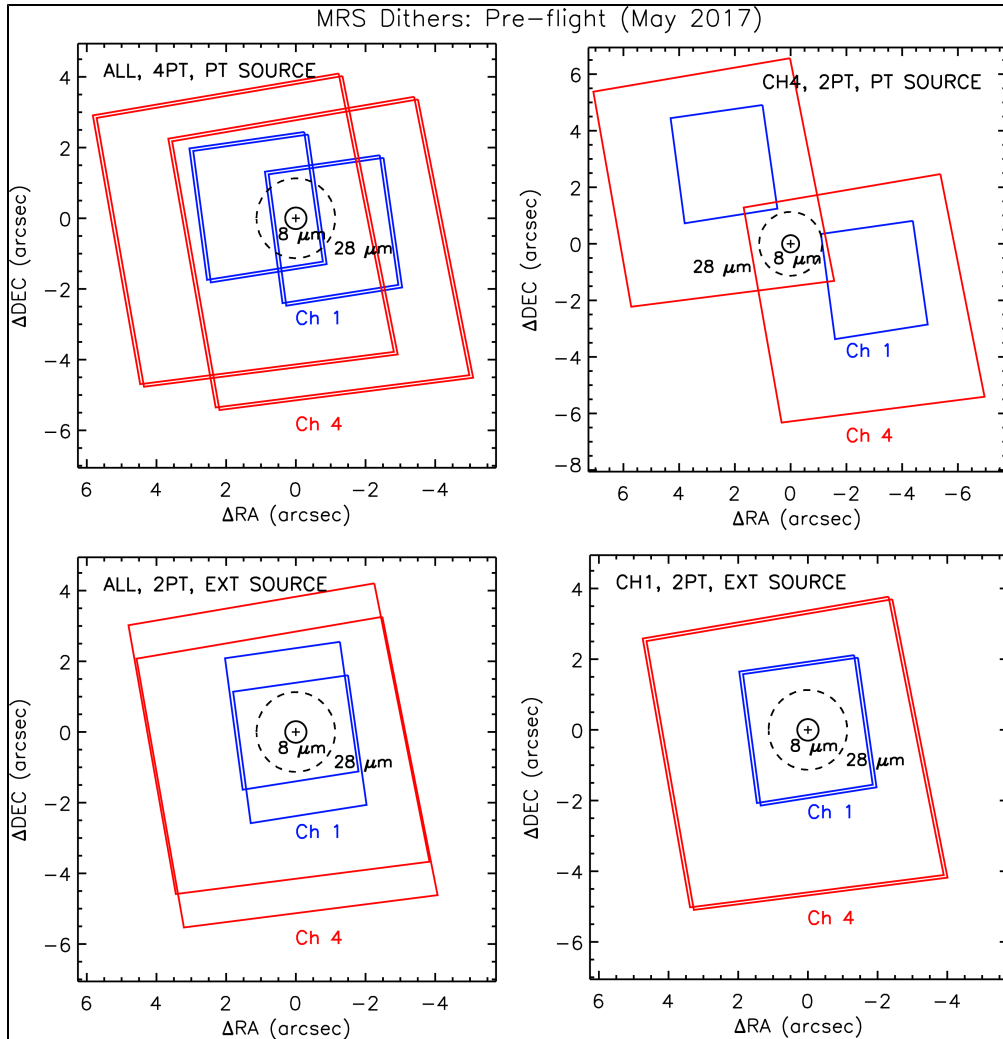
JWST dithering allows for moves specific to MIRI MRS. Dither patterns for the observation can be implemented in the [Astronomers Proposal Tool \(APT\)](#) with the [JWST APT MIRI MRS template](#). A dither pattern is defined as a sequence of small (less than 5" in the case of the MRS) moves from the starting position near the center of the MRS field of view. The sequence is fully specified in APT by choosing:

1. Either a 2-Point ¹ or a 4-Point pattern
2. Whether the pattern is optimized for a specific wavelength channel or for all channels (specified by the Primary Channel), and whether the optimization is for point sources (Channel 1, Channel 2, Channel 3, Channel 4, or ALL) or Extended Sources
3. The Direction of the pattern on the sky

There are two kinds of dither patterns available for MRS; patterns optimized for point source observations, and

patterns optimized for extended source (or mosaicked) observations. These two kinds of patterns differ in the size and purpose of their dither offsets; point source optimized patterns maximize the offset distance to provide large point source separation at the cost of decreased common field of view, whereas extended source optimized patterns minimize the offset distance to provide the greatest common field of view at the cost of decreased point source separation. Both sets of patterns provide improved spatial sampling and detector pixel redundancy.

Figure 2. Field coverage of MRS dither patterns



Example field coverage plots for various MRS dither patterns.

Top left panel: 4-Point pattern optimized for point source observations in all channels.

Top right panel: 2-Point pattern optimized for point source observations in channel 4 (note that the channel 1 fields no longer overlap with the science target).

Bottom left panel: 2-Point pattern optimized for extended source observations in all channels.

Bottom right panel: 2-Point pattern optimized for extended source observations in channel 1. In all panels the blue/red boxes illustrate the locations of the dithered MRS fields of view in channels 1/4, respectively. The solid/dashed black circles indicate the PSF FWHM at 8/28 μm respectively.

¹ Bold italics font style indicates parameters, parameter values, and special requirements that are set in the

APT GUI.

Dither patterns optimized for point sources

The default dither pattern for MRS is a 4-Point pattern that is optimized for point source observations at all wavelengths. As such, it provides an offset, which is large enough to separate channel 4 images, for accurate background subtraction (offset ~ 3 times the FWHM of a point source in channel 4) while keeping the channel 1 images comfortably within the field of view (channel 4 has larger field of view than channel 1). This pattern is illustrated in [Figure 2](#) (top left panel).

For observers who wish to increase the separation between the point source locations in successive exposures, variations on this basic pattern are provided that further increase the separation distance. These variations are channel-specific, in the sense that they achieve the greatest separation in a particular wavelength channel at the cost of poorer spatial sampling and smaller common field of view in other channels. The pattern optimized for channel 1 is identical to the default pattern. In contrast, the pattern optimized for channel 4, for instance, achieves a point source separation of 8 times the FWHM in channel 4 at the cost of moving the target entirely out of the field of view in channel 1 (see [Figure 2](#), top right panel).

Additionally, point source dither patterns can be specified with either of two Directions on the sky. The "positive" orientation repeats the pattern of the default "negative" orientation but with the offset directions swapped in order to rotate the movement on the sky by 43° , giving some flexibility in accommodating source geometry.

Dither patterns optimized for extended sources

In cases where the science target is larger than about an arcsecond in size (or when mosaicking large areas of sky), the point source optimized pattern may be undesirable since a portion of the target will fall outside the common field of view of the dithered observations. The all-wavelength extended source dither pattern therefore provides an offset that is large enough to provide half-integer sampling in all wavelength bands, but small enough to maximize the common field of view of each band (see [Figure 2](#), lower left panel).

Note that when using an extended source optimized pattern, a [dedicated sky exposure](#) must be declared within APT in order to provide a reference background image free of source contamination.

The largest possible common fields of view for dithered MRS observations can only be achieved at specific wavelength channels by sacrificing sampling and detector pixel redundancy in the other channels. Such channel-specific extended source patterns are therefore available for science cases that wish to maximize areal coverage at specific wavelength of interest at the expense of data quality at other wavelengths. As an example, the extended source pattern optimized for channel 1 provides ~ 12 arcsec 2 common field and good sampling for channel 1 at the expense of poor sampling and pixel redundancy in channel 4 (see [Fig. 2](#), lower right panel).

Since the offsets of the extended source patterns are substantially smaller than the point source optimized patterns, the Direction of these patterns need not be specified as both are identical.

2-Point vs 4-Point dithers

As described above, the MRS slice widths and pixel scales are designed such that a simple 2-Point dither pattern will nominally allow the MRS to achieve half-integer sampling in all 4 channels. In practice, however, optical distortions and discontinuities in the mapping of adjacent optical slices to detector pixels (see [Figure 1 on the MRS main page](#)) means that this half-integer sampling is not achieved for all locations within the MRS field.

The final image will therefore be both better and more uniformly sampled if the 2-Point pattern is repeated with a small ($\sim 0.1''$) offset to minimize the impact of field-dependent distortion. This 4-Point variation is available for both the point source and extended source optimized dither patterns.

The level of impact on the resulting image quality of poor spatial sampling due to 2- vs 4-point dithering is still under study, as are the impacts of no dithering (which may be desirable for certain science cases). In the worst case, (e.g., an undithered observations of a point source that falls at the boundary between adjacent slices), however, the reconstructed profile of a point source may be distorted by as much as 50% in the along-slice direction, the across-slice direction, or both.

Which pattern should I use?

The best dither pattern to use for a given set of observations depends strongly on the science case. [Figure 3](#) summarizes the advantages and disadvantages of each of the available MRS dither patterns as they affect the point source separation, common field of view, and image sampling quality ([Figure 4](#)) in each wavelength band.

In the majority of cases, programs observing either point sources or compact sources (less than about an arcsec in extent) should use the point source optimized, 4-Point ALL dither pattern. This provides robust performance at all wavelengths and adequate point source separation in all channels such that dedicated background observations are not required. In cases where additional PSF separation is desired at longer wavelengths (due to a particularly bright source, or some extended structure surrounding the source), channel-specific options may be used at the cost of no longer having the source in the field at short wavelengths. If image quality is not a priority, a 2-Point pattern may be used instead of a 4-Point pattern in order to reduce observing overheads (particularly for deep exposures where long individual exposure times are necessary in order to reduce detector noise).

Similarly, most programs observing extended sources or using the MRS to mosaic large areas of sky should use the extended source optimized, 4-Point ALL dither pattern. Although this has the least common field of view of any of the extended source patterns, it is the only pattern that simultaneously achieves ideal half-integer sampling at all wavelengths. If a particular science program wishes to prioritize field of view at

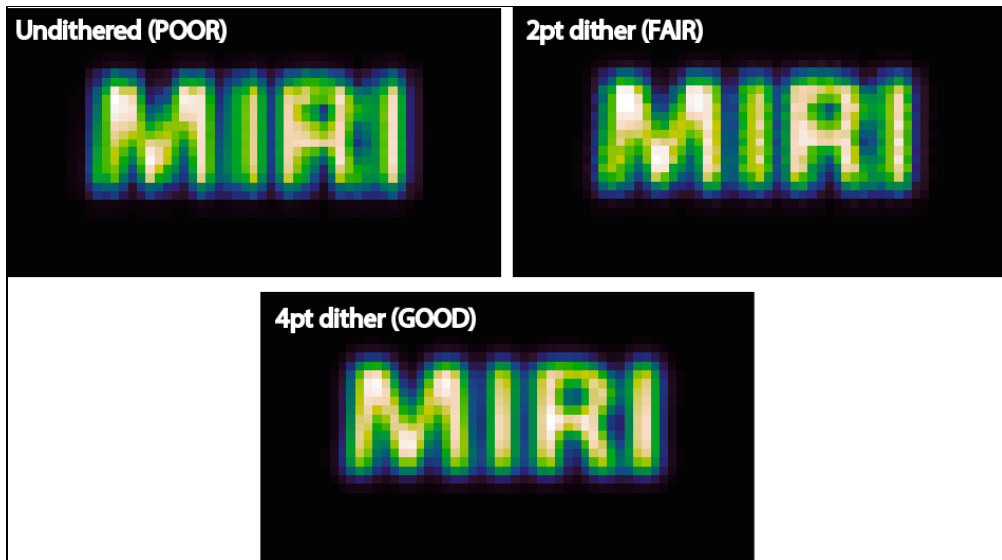
one wavelength at the expense of other wavelengths (e.g., mapping an emission line region with a specific spectral line), channel-specific options may be used at the cost of spatial sampling and/or detector pixel redundancy at other wavelengths. Likewise, if image quality is not a priority, a 2-Point pattern may be used instead of a 4-Point pattern in order to reduce observing overheads.

Figure 3. Expected relative performance of MRS dither patterns (pre-flight)

CH	Opt	#	PSF Sep. (FWHM)				Field Overlap (arcsec2)				Sampling			
			1	2	3	4	1	2	3	4	1	2	3	4
Point-Source Optimized Patterns														
ALL	PT	2	7.3	6.6	4.3	2.8	3.9	8.8	20.7	38.2	FAIR	FAIR	GOOD	GOOD
		4	7.7	6.9	4.5	2.9	3.5	8.2	19.8	37.1	GOOD	GOOD	GOOD	GOOD
1	PT	2	7.3	6.6	4.3	2.8	3.9	8.8	20.7	38.2	FAIR	FAIR	GOOD	GOOD
		4	7.7	6.9	4.5	2.9	3.5	8.2	19.8	37.1	GOOD	GOOD	GOOD	GOOD
2	PT	2	11.4	10.3	6.7	4.3	1.1	4.4	13.1	28.2	FAIR	FAIR	GOOD	GOOD
		4	12.0	10.8	7.0	4.5	0.9	3.9	12.2	27.0	GOOD	GOOD	GOOD	GOOD
3	PT	2	15.9	14.3	9.3	6.0	0.0	0.7	6.5	18.5	POOR	FAIR	FAIR	FAIR
		4	16.6	14.9	9.7	6.3	0.0	0.4	5.8	17.2	POOR	GOOD	GOOD	GOOD
4	PT	2	21.9	19.6	12.8	8.3	0.0	0.0	1.6	9.3	POOR	POOR	FAIR	FAIR
		4	22.9	20.6	13.4	8.7	0.0	0.0	1.1	8.0	POOR	POOR	GOOD	GOOD
Extended Source Optimized Patterns														
ALL	EXT	2	3.1	2.8	1.8	1.2	9.3	16.1	30.7	51.4	FAIR	FAIR	GOOD	GOOD
		4	3.1	2.8	1.8	1.2	9.2	15.9	30.5	50.6	GOOD	GOOD	GOOD	GOOD
1	EXT	2	0.4	0.4	0.2	0.2	12.3	19.8	36.2	57.8	FAIR	FAIR	FAIR	POOR
		4	0.4	0.4	0.2	0.2	12.3	19.8	36.1	57.6	GOOD	FAIR	FAIR	POOR
2	EXT	2	0.5	0.5	0.3	0.2	12.1	19.6	35.9	57.4	FAIR	FAIR	FAIR	FAIR
		4	0.5	0.5	0.3	0.2	12.1	19.5	35.8	57.2	FAIR	GOOD	FAIR	FAIR
3	EXT	2	0.7	0.7	0.4	0.3	11.9	19.3	35.4	56.9	POOR	FAIR	GOOD	FAIR
		4	0.7	0.7	0.4	0.3	11.8	19.2	35.3	56.6	POOR	FAIR	GOOD	FAIR
4	EXT	2	1.1	1.0	0.7	0.4	11.4	18.7	34.6	55.9	POOR	POOR	POOR	GOOD
		4	1.1	1.0	0.7	0.4	11.3	18.5	34.3	55.4	POOR	POOR	POOR	GOOD

Relative performance of the MIRI MRS dither patterns as a function of their source type (point vs extended source), optimization channel (ALL, 1, 2, 3, or 4) and number of points (2 or 4). Note that as of APT 25.4.2 the extended source patterns optimized for specific channels are not yet available. The table gives the image separation between exposures in units of the channels 1, 2, 3, 4 PSF FWHM, the common field overlap of the exposures in each channel, and the quality of the spatial sampling in each channel. Spatial sampling marked as ‘GOOD’ indicates half-integer sampling throughout the common field of view, ‘POOR’ indicates near-integer sampling, and ‘FAIR’ is intermediate between the two.

Figure 4. Typical image quality expected from dither patterns



Mock images illustrating the impact of incomplete dithering on reconstructed image quality.

References

Gordon , K. et al. 2015, PASP, 127, 953

The Mid-Infrared Instrument for the James Webb Space Telescope, X: Operations and Data Reduction

[JWST technical documents](#)

MIRI MRS Dedicated Sky Observations

Dedicated sky observations for the JWST [MIRI](#)'s medium-resolution spectrometer (MRS) will obtain a reference sky [background](#) in cases that require larger offsets than possible with [standard MRS dithering](#).

Introduction

See also: [MIRI Medium Resolution Spectroscopy](#)

Depending on the science target, it may be necessary to get a reference sky observation with the [medium-resolution spectrometer \(MRS\)](#) in a location further away from the science target than possible with [standard MRS dithering](#). For example, if an extended object or group of objects filled the entire MRS field of view, an offset sky observation would be necessary in order to reliably measure the [background signal](#). Similarly, if an [extended source dither pattern](#) was specified it would be necessary to observe a dedicated sky pointing since the total dither offset will be insufficient for pairwise background subtraction.

Obtaining a sky background

There are two options for obtaining a sky background: (1) use the offset background option in the [Astronomer's Proposal Tool \(APT\)](#) or (2) create a hand-built [mosaic](#).

Use the offset background option

The checkbox on the [APT MRS template](#) within APT (in the Fixed Targets form) is used to specify that the object requires a companion background observation and allows the user to select a sky target from the target list. This sky target may be created in the usual manner as if it were an astronomical object, and should have an observation of its own (note that the no-Target Acquisition option should be used for dedicated background observations).

In the Special Requirements section of the science target observation form, the science target and background target observations may then be linked together as a non-interruptible sequence by grouping the observation timings so that the background is obtained as soon as possible after the last exposure on the target. A to-be-determined upper limit will be imposed on the maximum allowable offset between the science and background targets.

Hand-built mosaic

The template allows an $N \times N$ mosaic to be specified. A 2-position mosaic, one position on the target and one on the background sky, can also satisfy the background requirement. However, using the offset background option is preferable since it more clearly indicates which of the mosaic tiles is the science target and which is the background.

MIRI Mosaics Overview

Mosaicking with the JWST [Mid-Infrared Instrument \(MIRI\)](#) is accomplished with larger pointing offsets for each tile than are available for dithering.

Mosaics with [JWST](#) using [MIRI](#) are accomplished with larger pointing offsets for each tile than are available for dithering; however, a dither pattern may be executed at each mosaic pointing. MIRI-specific mosaic patterns can be implemented using the [Astronomer's Proposal Tool \(APT\)](#). In general, mosaics are defined with some overlap to provide full coverage, but this is not a requirement.

[Dithers](#) and mosaics are distinct in terms of operational ordering. All dither positions must be executed before filter changes are executed. All [filter](#) changes are executed before proceeding to the next tile in a mosaic.

MIRI offers:

- [Imaging mosaics](#)
- [Medium-resolution spectrometer \(MRS\) mosaics](#)
- [Low-resolution spectrometer \(LRS\) mosaics](#)

MIRI Imaging Mosaics

The [imaging mode](#) for JWST's [Mid-Infrared Instrument \(MIRI\)](#) offers a mosaicking option for coverage of larger fields of view (FOV) that extend beyond a single pointing.

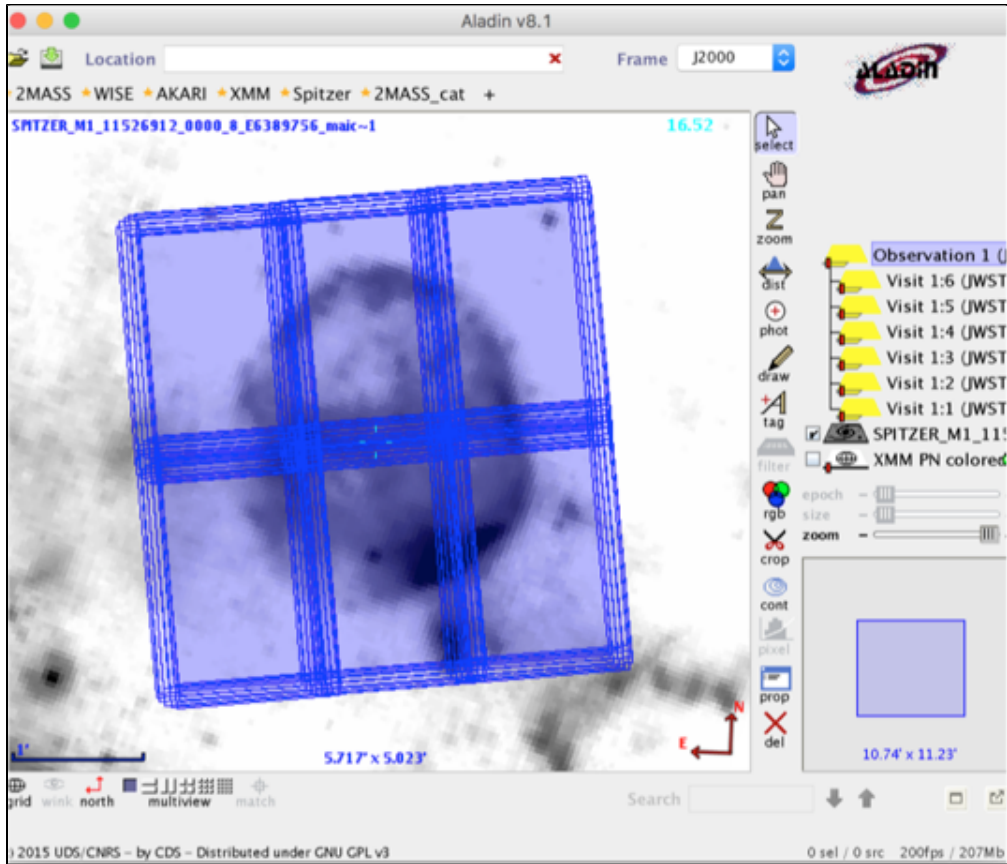
JWST mosaics allows for moves specific to [MIRI imaging. Mosaics](#) for an observation can be implemented in the [Astronomer's Proposal Tool \(APT\)](#) with the [JWST APT MIRI imaging template](#). These mosaics provide coverage of larger fields of view (FOV) that extend beyond a single pointing.

As with single-pointing MIRI imaging observations, the user first selects the desired imaging [subarray](#), [dither pattern](#), [readout mode](#), and [filters](#). The parameters that define the footprint of the MIRI imaging mosaic are the center coordinates, number of rows and columns of the individual pointings (or tiles), the mosaic orientation angle, percentage of overlap region between the tiles, and the amount of row and/or column shift that can be used to skew the tiled pattern. For example, Figure 1 shows the footprint of a 2×3 mosaic of [FULL¹](#) array tiles, with a 10% tile overlap and no row and/or column shifts. Figure 2 shows the same mosaic, but with 20% overlap between tiles and a row and column shift of 10. The footprints of the 12-point [REULEAUX](#) dither pattern are evident in both panels, while the blue shading reflects the level of exposure coverage as a function of position.

Starting with the first tile in the mosaic, the exposures are carried out at each dither step, and the filter changed once the dither pattern has been completed. Once all the user-specified filters have been rotated through for a single tile, the sequence is repeated for the next tile, and so on.

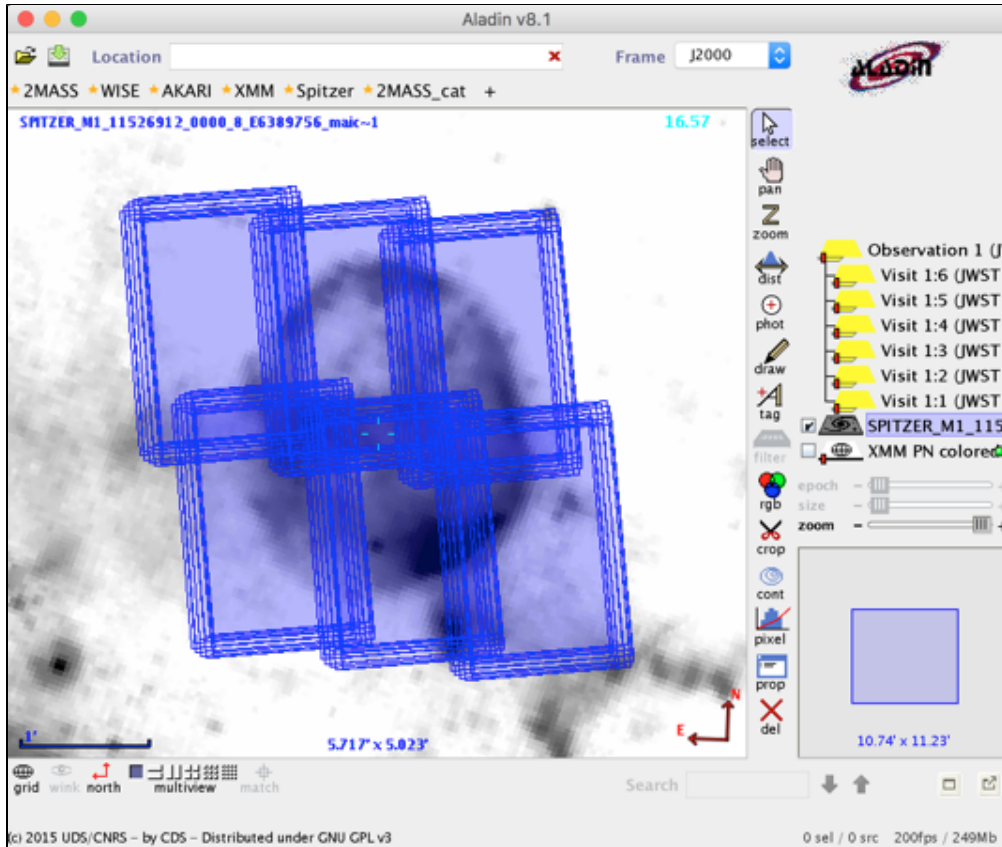
For MIRI imaging mosaics, each tile will usually be a separate visit that requires its own guide star. This depends both on the overlap region between the tiles and the visit splitting distance calculated by the APT. If the entire mosaic cannot be scheduled simultaneously due to missing guide stars, it maybe necessary to split one or multiple tiles into a separate associated observation.

Figure 1. 2×3 MIRI imaging mosaic with 10% tile overlap, no row or column shifts



Footprint of a 2×3 MIRI imaging mosaic using FULL array tiles, with a 10% tile overlap and no row and/or column shifts.

Figure 2. 2×3 MIRI imaging mosaic with 20% tile overlap, 10 pixel row and column shifts



The same mosaic as in Figure 1, but with 20% overlap between tiles, and a row and column shift of 10. The footprints of the 12-point REULEAUX dither pattern are evident in both figures, while the blue shading reflects the level of exposure time coverage.

¹ Bold italics font style indicates parameters, parameter values, and special requirements that are set in the APT GUI.

MIRI LRS Mosaics

The [low-resolution spectroscopy mode](#) for JWST's [Mid-Infrared Instrument \(MIRI\)](#) offers a mosaicking option for coverage of larger fields of view (FOV) that extend beyond a single pointing.

[Mosaics](#) for an LRS observation can be implemented in the [Astronomer's Proposal Tool \(APT\)](#) with the [JWST APT MIRI Low Resolution Spectroscopy template](#). These mosaics provide coverage of larger fields of view (FOV) that extend beyond a single pointing.

Mosaics are only supported for observations with the LRS slit; the slitless LRS mode is dedicated to single-pointing time series observations. As in a regular observation, the user should select exposure settings for the observation, and pick the FULL subarray setting for slit spectroscopy observations.

Two methods are available for defining the mosaic pattern. By choosing the MAPPING option in the Dither Type drop-down list, the user can specify a number of spatial and spectral offset steps around the slit center position, with the offset provided in arcseconds. Alternatively, with the number of spatial and spectral steps set to 1, a pointing pattern can be defined in the Mosaic Properties tab of the observations template. Here the pattern is defined in rows, columns, and percentage overlap between the pointings. Combining the two methods, or selecting the "along slit nod" dither option together with a Mosic, allows the user to define a dither pattern at each mosaic pointing location.

The user should always check the defined pattern using the [APT Aladin visualization functionality](#), which shows the slit footprints superimposed on the target. The user should also consider using the [MIRI Medium-Resolution Spectrometer](#), which provides integral field spectroscopy at higher spectral resolution than the LRS from \sim 5 to 28.5 μm , albeit without continuous spectral coverage.

MIRI MRS Mosaics

The JWST MIRI medium-resolution spectrometer (MRS) offers a mosaicking option to cover larger fields of view that extend beyond a single pointing. The mosaics have been optimized for each channel.

Introduction

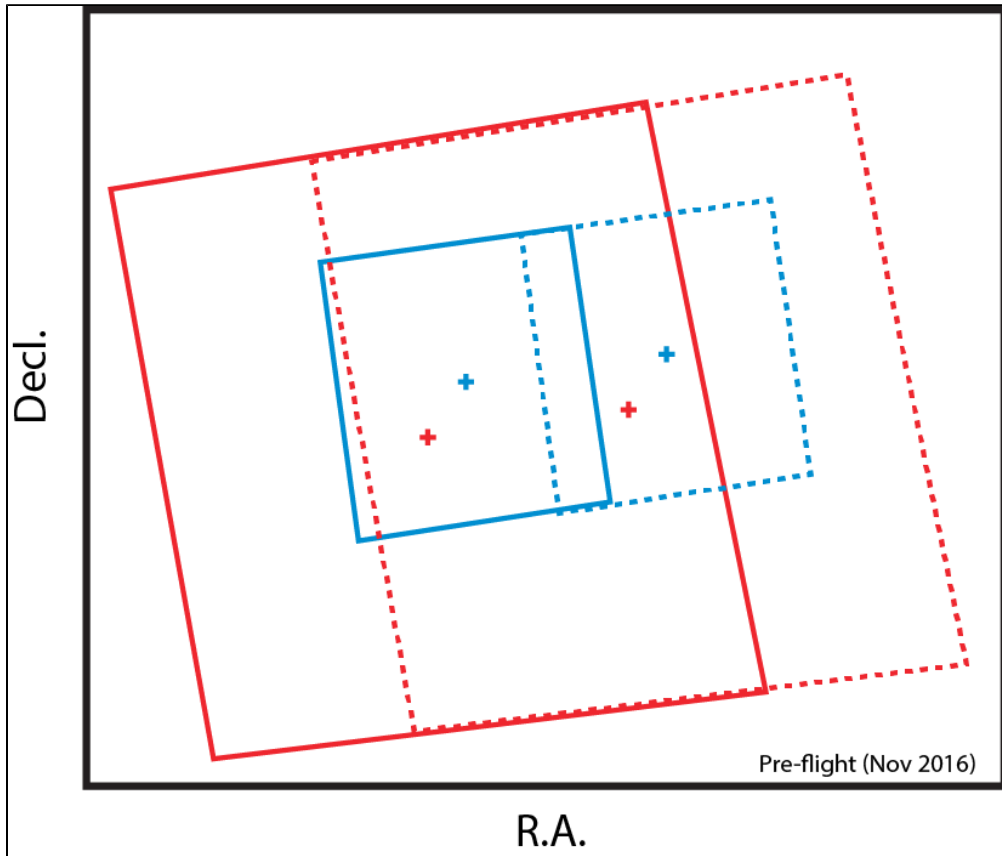
JWST mosaics can be constructed for the [MIRI medium-resolution spectrometer \(MRS\)](#) and implemented in the [Astronomer's Proposal Tool \(APT\)](#) with the [JWST APT MIRI MRS template](#). These mosaics provide coverage of larger fields of view (FOV) that extend beyond a single pointing, and can be constructed using any of the 4 channels as the primary field of view.

Primary channel selection and mosaics

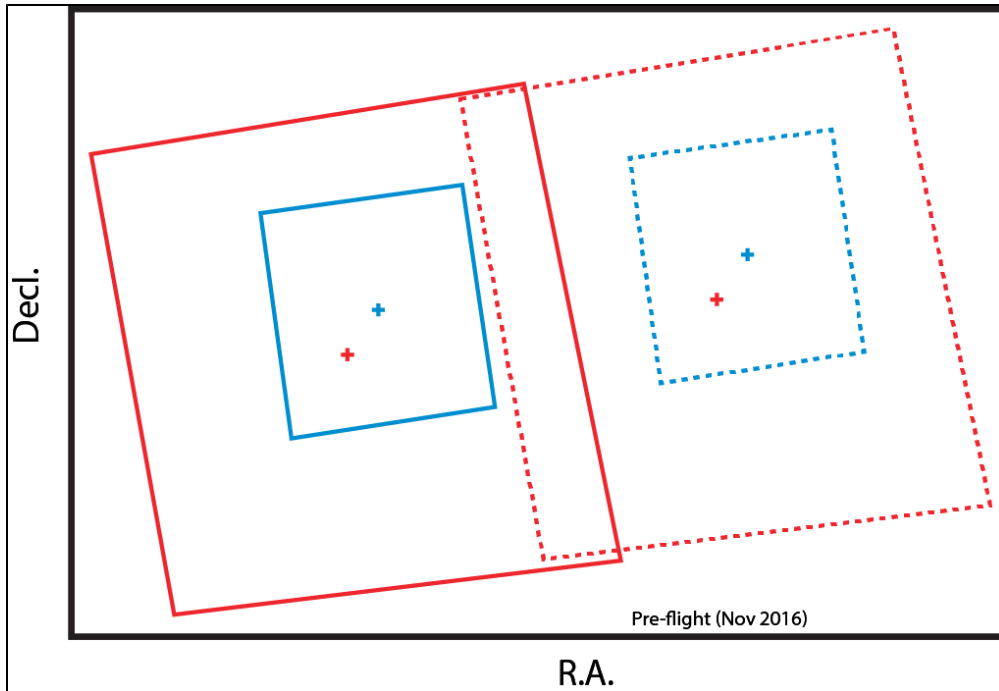
Choosing Channel 1 (or ALL¹) in APT places the target at the [pointing origin](#) of the channel 1A (i.e., Channel 1, SHORT(A)) field of view, and the boundaries of this field will be used to determine the effective footprint for purposes of determining mosaic tile boundaries and overlaps. Similarly, choosing channel 4 will place the target at the [pointing origin](#) of the channel 4A field of view, and the boundaries of this field will be used for determining mosaic tile positions. Since the channel 4 field of view is much larger than that of channel 1, the mosaic tile offsets will be commensurately larger. With channel 1 (or ALL) as the primary channel, each channel 1 tile will overlap the others to a specified percentage, while each channel 4 tile will overlap the next more substantially ([Figure 1](#)). If channel 4 is selected as the primary channel, each channel 4 tile will overlap the others to the specified percentage, while there will be gaps between the channel 1 tiles ([Figure 2](#)).

Note that tiles generated by APT are produced symmetrically about the astronomical target. Therefore, for an even number of tiles, the astronomical target will be centered between two tiles, while for an odd number of tiles it will be centered in a tile.

Figure 1. Mosaicing with channel 1 (or ALL) as the primary channel



The blue/red rectangles illustrate locations of the channels 1 and 4 fields of view in the first and second tiles (solid and dotted lines respectively). The crosses represent the center of the fields for each tile. The tiles are shown undithered for visual illustration purposes.

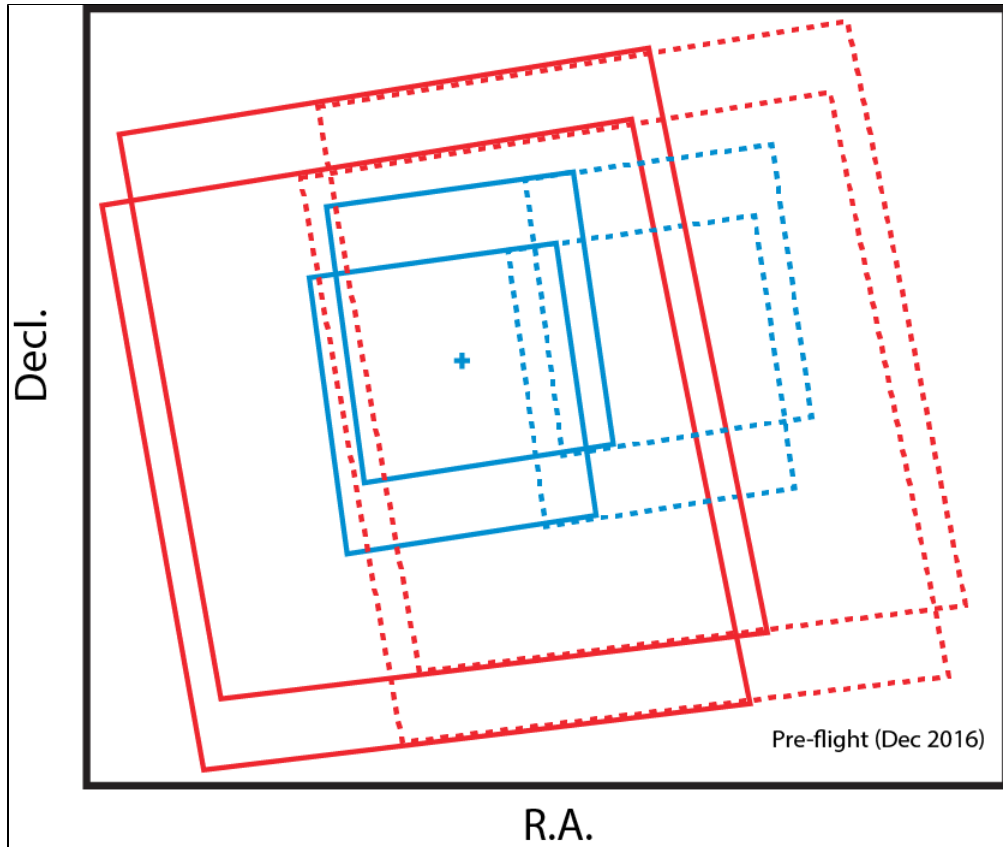
Figure 2. Mosaicing with channel 4 as the primary channel

Same as Figure 1, but with channel 4 as the primary channel. The crosses represent the center of the fields for each tile. Note the gap between the channel 1 fields (blue boxes). The tiles are shown undithered for visual illustration purposes.

Dithering and Mosaics

Note that although the figures above only show a single pointing for each mosaic tile, these tiles should also be dithered in order to optimize spatial and spectral sampling throughout the field of view (e.g., [Figure 3](#)). The [extended source dither patterns](#) described on the MRS dithering page are best suited for this purpose as they are designed to optimize spatial sampling while maximizing common field overlap area. Usage of such a pattern will require additional specification of a [dedicated sky exposure](#).

Figure 3. Mosaicing with standard 2-point extended dithering at each mosaic location



Same as [Figure 1](#), but with the 2-Point extended dithering pattern at each mosaic location. The blue cross denotes the (undithered) central location of channel 1 in the first mosaic tile.

¹ Bold italics font style indicates parameters, parameter values, and special requirements that are set in the APT GUI.

MIRI Time Series Observations

The JWST [Mid-Infrared Instrument \(MIRI\)](#) currently has full support for time-series observations (TSOs) with the [low-resolution spectrometer \(LRS\)](#), and limited support with the Imager.

The stability of the JWST observatory enables very precise spectro- and imaging photometry of time-variable objects. Such time-series observations (TSOs) will be useful for characterizing transiting exoplanets, but will also be used for other sources such as eclipsing binaries and cataclysmic variables.

The JWST [MIRI](#) currently allows for TSO observations in the following modes:

- [Low-resolution spectroscopy TSOs](#)
- [Imaging TSOs](#)

MIRI Imaging TSOs

JWST MIRI currently has limited support for time-series observations (TSOs) with the imager.

Introduction

The MIRI imager has limited support for high precision imaging photometry in time-series observations (TSOs). Available capabilities and limitations for such observations are described below.

Sensitivity and saturation

Sensitivities and saturation limits are available in the description of [MIRI Predicted Performance](#).

Users should always refer to the [Exposure Time Calculator](#) for the most accurate signal-to-noise calculations.

Dithering

Contrary to regular imaging observations, TSOs should be carried out without dithering to maintain target position on the same pixels throughout the observation.

Imaging observations with Dither set to None are currently available as a standard option only for the SUB64 subarray. Non-dithered imaging for the FULL array and other subarrays are a limited access option in APT that can only be selected by checking the Allow Restricted box in the Proposal Information form. Note that use of limited access options requires justification in the proposal text.

Filters and subarrays

All filters available for general [MIRI imaging](#) observations can be selected for TSOs.

Target acquisition

Target acquisition with the MIRI imager, whilst recommended for TSOs, is not currently supported. It is expected to become available in the future.

Exposure time limitations

For regular (non-TSO) observations, an exposure time limit of 10,000 seconds for a single exposure is applied. For TSOs this limitation can be waived, allow observations of long time-variable phenomena in a single exposure, which is optimal for stability and photometric precision. Selecting Time Series Observation in the [Special Requirements](#) pane in APT enables this waiver.

Imaging TSOs in APT

Observing proposals for TSOs with MIRI Imaging should use the standard [MIRI imaging template](#), then select the Time Series Observation and No Parallel special requirements to enable the optimal TSO functionality. This will enable the No dither option for the SUB64 subarray, and waive the exposure time limit.

Support for imaging TSOs with MIRI in APT is currently still under development.

MIRI LRS TSOs

Time-series observations (TSOs), which are typically very precise spectrophotometric observations of time-variable objects, are allowed for the JWST [MIRI low-resolution spectrometer \(LRS\)](#).

Introduction

A typical problem with spectroscopic observations using a narrow (relative to the PSF) slit is throughput variations due to telescope pointing uncertainties and drifts. The natural solution, therefore, to reach higher spectrophotometric precision is to operate the [MIRI LRS](#) in a slitless mode, thus preventing any pointing-induced throughput variations. The LRS slitless subarray (SLITLESSPRISM) further offers the optimal solution between the requirement for fast readout times and a large enough detector area to get a proper spectral image. This mode will be particularly useful for characterizing transiting exoplanets, but may also be used for other sources such as eclipsing binaries and cataclysmic variables.

Slit vs. slitless spectroscopy

Main article: [MIRI Low-Resolution Spectroscopy](#)

The expected light loss from the slit mask is significant when compared with slitless spectroscopy, particularly at longer wavelengths ($\lambda > 9 \mu\text{m}$). In addition, there are considerable increases in achievable precision over a long baseline. There are, however, two main limitations to slitless spectroscopy:

- The sensitivity is around a factor 10× lower than the LRS in slit mode. The absence of the slit leads to a higher background in the slitless subarray, effectively reducing the signal to noise. Observers should keep this in mind when considering fainter targets.
- The dispersion profile of the LRS turns over below 4.5 μm , i.e., for a limited wavelength range around 4.5–5 μm , different wavelengths are dispersed onto the same detector pixels. As a result, the wavelength and absolute flux calibrations in this region are not as reliable as for LRS slit observations. For slit observations, a dedicated filter is mounted on the slit mask structure to block the radiation below 4.5 μm .

TSO mode in APT

Time-series observations of bright targets require fast read times to avoid detector saturation. To this end, observations may be carried out with fewer than the recommended [NGROUPS](#) = 5. The minimum [NGROUPS](#) required is 2. However ground testing indicates that the accuracy of the detector calibration worsens significantly as read out ramps are shortened. Observations for which absolute calibration is important are advised against selecting [NGROUPS](#) < 5.

Slitless spectroscopy mode is selected from the [MIRI LRS template](#) in the [Astronomer's Proposal Tool \(APT\)](#), by choosing the **SLITLESSPRISM¹** [subarray](#). Low-resolution spectroscopic TSO observations must use the slitless option. Selecting the slitless mode for LRS will automatically add Time Series Observation and No Parallel to the Special Requirements pane in APT. This creates a waiver for the usual exposure time limit of 10,000 s to allow longer time-series monitoring.

Selection of slitless LRS spectroscopy results in several unique settings:

- Disables dithering for optimal stability and repeatability
- Defaults to FAST read mode
- Waives the 10,000 s exposure time limit
- Makes target acquisition mandatory

¹ Bold italics font style indicates parameters, parameter values, and special requirements that are set in the APT GUI.

Performance

Users should always refer to the [JWST Exposure Time Calculator](#) for the most up to date sensitivity numbers and bright limits.

Pages in the MIRI [performance section](#) provide information about the sensitivities and bright limits for the MIRI LRS modes.

MIRI Predicted Performance

The performance of JWST's [Mid-Infrared Instrument \(MIRI\)](#) is predicted by a model that uses a number of parameters derived from laboratory measurements.

The performance of MIRI has been studied in detail by [Glasse et al. \(2015\)](#) and [Boccaletti et al. \(2015\)](#). These studies bring together performance metrics from laboratory testing with a sensitivity model formulated by Swinyard et al. (2004). These models have been adapted by the [Exposure Time Calculator \(ETC\)](#). [Operational overheads \(Gordon et al. 2014\)](#), including target acquisition, small angle maneuvers to allow efficient background subtraction, time spent moving MIRI mechanisms, or taking calibration observations are incorporated and included in the final time calculated by the [Astronomer's Proposal Tool \(APT\)](#).

Users should ultimately use the [ETC](#) for all sensitivity calculations.

Available JWST [Mid-Infrared Instrument \(MIRI\)](#) performance articles are listed below:

- [MIRI Bright Source Limits](#)
- [MIRI Sensitivity](#)

More articles will be released in the near future.

References

[Boccaletti, A. et al. 2015, PASP, 127, 633](#)

The Mid-Infrared Instrument for the James Webb Space Telescope, V: Predicted Performance of the MIRI Coronagraphs

[Glasse, A. et al., 2015, PASP, 127, 686](#)

The Mid-Infrared Instrument for the James Webb Space Telescope, IX: Predicted Sensitivity
Updated version

[Gordon, K. D. et al., 2014, PASP, 127, 696](#)

The Mid-Infrared Instrument for the James Webb Space Telescope, X: Operations and Data Reduction

[JWST technical documents](#)

MIRI Bright Source Limits

The bright source limits of JWST's [Mid-Infrared Instrument \(MIRI\)](#) are predicted by a saturation model that uses measurements obtained during ground testing.

Introduction

The performance of MIRI has been measured directly at both the component and system level using the fully assembled MIRI flight model in a flight-like radiative environment with a well characterized radiometric source ([Glasse et al. 2015](#)). Results of these JWST throughput measurements have been integrated into a sensitivity model, which includes the following components: (1) background, (2) photon conversion efficiency (PCD), (3) encircled energy, and (4) detector performance ([Pontoppidan 2016](#)).

Users should ultimately use the [Exposure Time Calculator \(ETC\)](#) for all bright limit calculations.

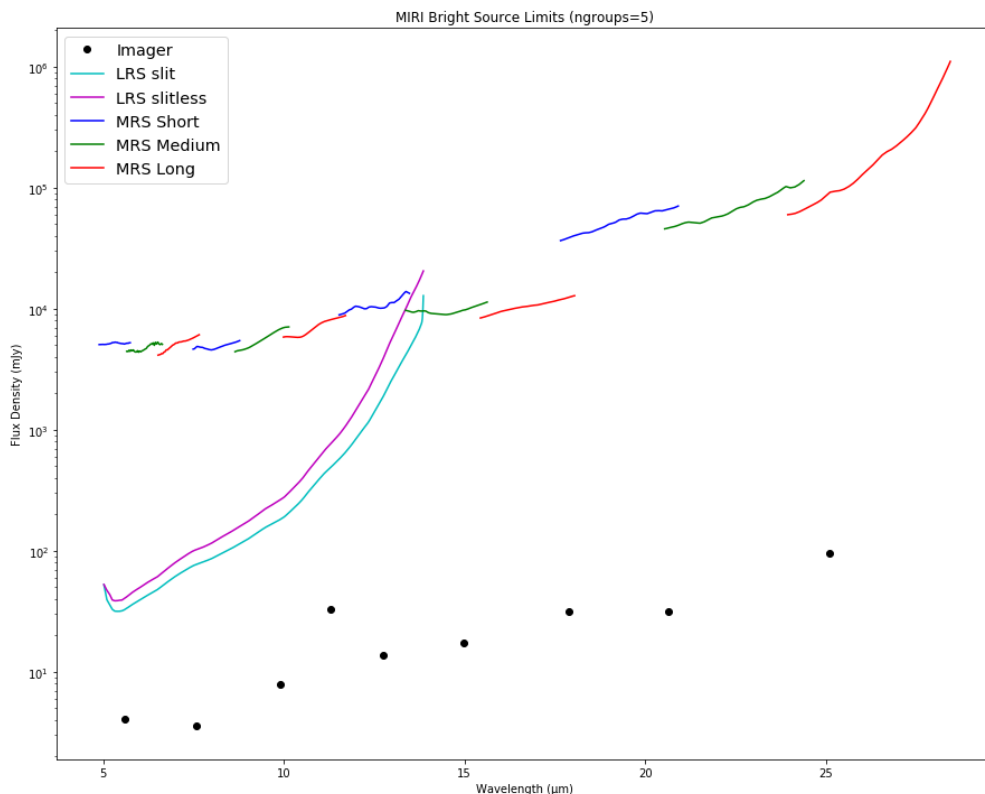
Values

The tables and figures below show bright source limits assuming a 5-group integration. The values shown represent the fluxes at which the detector reaches 70% of the pixels' full-well capacity.

Imager

Table 1. MIRI imager bright source limits (for ngroups=5)

Filter	Bright source limit (mJy) full frame	Bright source limit (mJy) 64×64 subarray
F560W	4.1	134
F770W	3.6	118
F1000W	7.8	255
F1130W	33	1077
F1280W	13.6	444
F1500W	17.6	575
F1800W	31.7	1035
F2100W	31.8	1038
F2550W	95.3	3112

Figure 1. MIRI bright source limits (for ngroups = 5)

MIRI imager bright source limits for all modes, assuming FULL frame.

¹ Bold italics font style indicates parameters, parameter values, and special requirements that are set in the APT GUI.

References

[Glasse, A. et al. 2015, PASP, 127, 686](#)

The Mid-Infrared Instrument for the James Webb Space Telescope, IX: Predicted Sensitivity

[Pontoppidan, K. 2016, Proc of SPIE, 9910, 16](#)

Pandeia: a multi-mission exposure time calculator for JWST and WFIRST

[JWST technical documents](#)

MIRI Sensitivity

The sensitivity model for JWST's [Mid-Infrared Instrument \(MIRI\)](#) incorporates ground testing measurements to model parameters such as [background](#), photon conversion efficiency, encircled energy, and detector performance.

Introduction

The performance of JWST has been measured directly at both the component and system level using the fully assembled MIRI flight model in a flight-like radiative environment with a well-characterized radiometric source ([Glasse et al. 2015](#)). The results of the JWST throughput measurements have been integrated into a sensitivity model that includes the following components: (1) [background](#), (2) photon conversion efficiency (PCE), (3) encircled energy, and (4) detector performance ([Pontoppidan 2016](#)).

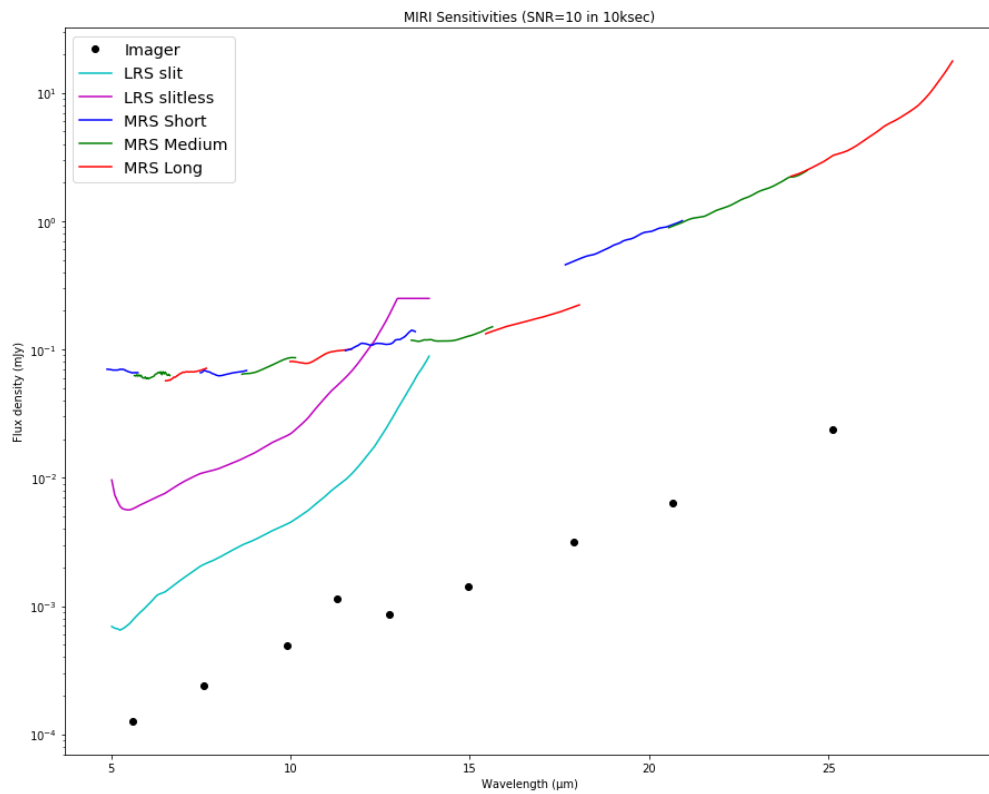
Values

Users should ultimately use the [Exposure Time Calculator \(ETC\)](#) for all sensitivity calculations.

The tables and figures below show sensitivity values for a 10,000 second observation to S/N = 10.

Table 1. S/N = 10 in 10^4 s for MIRI imaging filters assuming FULL array

Filter	Low-background detection limit (μJy)
F560W	0.12
F770W	0.24
F1000W	0.50
F1130W	1.15
F1280W	0.87
F1500W	1.42
F1800W	3.14
F2100W	6.32
F2550W	24.02

Figure 1. Expected sensitivity for the various MIRI instrument modes

MIRI sensitivity plot for the medium-resolution spectrometer (MRS), low-resolution spectrometer (LRS), and imager (in circles) configurations, corresponding to $S/N = 10$, 10^4 s on-source integration time. For spectroscopic modes the numbers represent continuum sensitivities, with S/N calculated per spectral pixel.

References

[Glasse, A., et al., 2015, PASP, 127, 686](#)

The Mid-Infrared Instrument for the James Webb Space Telescope, IX: Predicted Sensitivity

[Pontoppidan, K. 2016, Proc of SPIE, 9910, 16](#)

Pandeia: a multi-mission exposure time calculator for JWST and WFIRST

[JWST technical documents](#)